

Optimization and characterization of D-peptides for treatment of Alzheimer's disease

Inaugural-Dissertation

zur Erlangung des Doktorgrades
der Mathematisch-Naturwissenschaftlichen Fakultät
der Heinrich-Heine-Universität Düsseldorf

vorgelegt von

Daniel Frenzel
aus Lutherstadt Wittenberg

Jülich, November 2014

List of contents

ABBREVIATIONS	4
1. INTRODUCTION	5
1.1 HISTORY OF THE PERCEPTION OF DEMENTIA	5
1.1.1 ANCIENT TIMES	5
1.1.1 MEDIEVAL TIMES	6
1.1.2 TO THE 19 TH CENTURY	6
1.1.3 THE 19 TH CENTURY	7
1.2 RECENT PROGRESS IN NEURODEGENERATION	9
1.2.1 CHRONIC INFLAMMATION: ACTIVATION OF THE IMMUNE SYSTEM	9
1.2.2 INFLUENCE OF SENESENCE IN NEURODEGENERATION	11
1.3 THE LIMITS OF THE IMMUNE SYSTEM HYPOTHESIS	11
1.4 GENETIC RISK FACTORS OF ALZHEIMER'S DISEASE	11
1.4.1 EARLY-ONSET ALZHEIMER'S DISEASE:	12
1.4.2 LATE ONSET ALZHEIMER'S DISEASE:	12
1.4.3 ENDOCYTOSIS	13
1.5 HYPOTHESIS OF AB-INDUCED CYTOTOXICITY	14
1.5.1 MICROTUBULE-ASSOCIATED PROTEIN TAU	15
1.5.2 AB INDUCED TAU HYPERPHOSPHORYLATION	16
1.5.3 CASPASE-3 AND GSK-3 TRIGGERED TAU HYPERPHOSPHORYLATION	16
1.5.4 NMDAR ENDOCYTOSIS	17
1.5.5 MGLUR5 ACTIVATION	17
1.5.6 PYROGLUTAMYLATED AB (pE3-AB)	17
1.5.7 INTERACTION OF AB WITH PRP	17
1.5.8 AB CAUSES OXIDATIVE STRESS BY DISTURBING MEMBRANE FUNCTION	18
1.5.9 CONSEQUENCES	18
1.6 PEPTIDE DRUGS FOR ALZHEIMER THERAPY	19
1.6.1 ADVANTAGES OF PEPTIDES AS DRUGS	19
1.6.2 DISADVANTAGES OF PEPTIDES AS DRUGS	19
1.6.3 GENERAL OPTIMIZATION OF PEPTIDE BASED DRUG CANDIDATES	19
2. AIM OF THIS WORK	21
3. THEORY	22
3.1 ONE TO ONE INTERACTION KINETICS	22
3.1.1 INTERACTION KINETICS	22
3.1.2 APPLICATION OF INTERACTION KINETICS FOR OPTICAL BIOSENSORS	23
3.1.3 APPLICATION OF INTEGRATED RATE LAWS	23
3.1.4 MULTIVALENCY AND AVIDITY	24
3.2 SURFACE PLASMON RESONANCE	25
3.2.1 HISTORY OF SURFACE PLASMON RESONANCE	25
3.2.2 TOTAL INTERNAL REFLECTION	26
3.2.3 MOMENTUM RESONANCE	27
3.2.4 SPECTROMETER TYPES	27
3.2.5 PROTEIN INTERACTIONS WITH SPR	27
3.3 BIOLAYER INTERFEROMETRY	28
3. MATERIAL AND METHODS	30

3.1 MATERIAL:	30
3.2 METHODS:	31
3.2.1 EXPRESSION OF AB(1-16)-GB1	31
3.2.2. PURIFICATION OF AB(1-16)-GB1	31
3.2.3 CREATION OF AN AB (1-16)-GB1 AFFINITY PURIFICATION SEPHAROSE	32
3.2.4 EXPRESSION OF THE scFv-IC16	33
3.2.5 PURIFICATION OF scFv-IC16	33
3.2.6 PREPARATION OF AB(1-42) MONOMERS AND SEC OLIGOMERS	34
3.2.7 DENSITY GRADIENT CENTRIFUGATION (DGC)	35
3.2.8 PREPARATION OF AB(1-42) ASSEMBLY STATES BY DGC	35
3.2.9 IMMOBILIZATION VIA SA-COUPLING FOR SPR-SPECTROSCOPY	36
3.2.10 BINDING KINETICS OF scFv-IC16 WITH SPR-SPECTROSCOPY	37
3.2.11 BINDING KINETICS OF FAB FRAGMENTS WITH SPR-SPECTROSCOPY	37
3.2.12 BINDING KINETICS OF D-PEPTIDES WITH SPR-SPECTROSCOPY	38
3.2.13 PREPARATION OF CM7 CHIPS FOR THERMODYNAMICS WITH SPR	38
3.2.14 THERMODYNAMICS WITH SPR-SPECTROSCOPY	38
3.2.15 IMMOBILIZATION OF AB(1-42) ON SUPER SA-BIOSENSORS FOR BLI	39
3.2.16 PARALLEL SENSOR KINETICS OF scFv-IC16 WITH BLI	39
3.2.17 KINETIC TITRATION SERIES OF THE scFv-IC16 WITH BLI	40
3.2.18 SAMPLE PREPARATION FOR TEM AND EVALUATION	40
3.2.19 ATOMIC FORCE MICROSCOPY OF AB FIBRILS	40
3.2.20 DYNAMIC LIGHT SCATTERING	41
 4 RESULTS	 42
 4.1 CHARACTERIZATION OF AB(1-42) WITH TEM	 42
4.2 TIME DEPENDENCY OF AB AGGREGATION	44
4.3 CHARACTERIZATION OF AB(1-42) WITH AFM	45
4.4 CHARACTERIZATION OF AB(1-42) WITH SPR	46
4.5 CHARACTERIZATION OF AB MONOMERS WITH SPR	47
4.6 CHARACTERIZATION OF AB OLIGOMERS WITH SPR	48
4.7 CHARACTERIZATION OF AB FIBRILS WITH SPR	49
4.8 CHARACTERIZATION OF AB MONOMERS WITH BLI	50
4.9 PE3-AB OLIGOMER PREPARATION	53
4.10 CHARACTERIZATION OF D-PEPTIDES	53
4.10.1 AFFINITY ESTIMATION OF DIRECT D3-DERIVATIVES	53
4.10.2 SINGLE AMINO ACID SUBSTITUTIONS	55
4.10.3 COMBINATION WITH THE AB BINDING SITE D7	57
4.10.4 CHARACTERIZATION OF CYCLIC D3-DERIVATIVES	60
4.10.5 INTERACTION OF D3 WITH PE3-AB OLIGOMERS AND FIBRILS	63
4.10.6 THERMODYNAMICS OF CYCLIC D3-DERIVATIVES	63
4.10.7 AFFINITY PREDICTION OF MULTIVALENT D3-DERIVATIVES	66
 5. DISCUSSION	 68
 5.1 SURFACE CHARACTERIZATION WITH scFv-IC16	 68
5.2 MECHANISM FOR THE INTERACTION BETWEEN D3 AND AB(1-42)	69
5.3 WHY DOES RD2 HAVE A HIGHER AFFINITY THAN D3?	69
5.4 HOW IS D3 OVERCOMING THE PLASMA MEMBRANE?	70
5.5 MULTIVALENCY IN D-PEPTIDES	71
5.6 COMBINATIONS WITH THE AB BINDING SITE D7	71
5.7 CYCLISATION OF D-PEPTIDES	73
5.8 PEPTIDES AS DRUGS AND OPTIMIZATION STRATEGIES FOR D3	73
5.8.1 IS ADDING BINDING SITES USEFUL?	73
5.8.2 HOW TO ENHANCE THE PLASMA HALF-LIFE TIME?	74

5.9 FUTURE PERSPECTIVE OF PEPTIDE DESIGN	74
<u>6. SUMMARY</u>	<u>76</u>
<u>7. ZUSAMMENFASSUNG</u>	<u>77</u>
<u>8. LITERATURE</u>	<u>78</u>
<u>9. SUPPORTING INFORMATION</u>	<u>86</u>
<u>PUBLICATIONS AND PRESENTATIONS</u>	<u>89</u>
ACCEPTED PAPERS:	89
POSTER PRESENTATIONS:	89
<u>DANKSAGUNG</u>	<u>90</u>
<u>EIDESSTATTLICHE ERKLÄRUNG</u>	<u>91</u>
<u>CURRICULUM VITAE</u>	<u>92</u>

Abbreviations

2YT	Yeast tryptone medium	LDH	Lactate dehydrogenase
AA	Amino acid	LOAD	Late onset Alzheimer's disease
ABCA	ATP binding cassette	MAPT	Tau proteins
AD	Alzheimer's disease	mGluR5	Metabotropic glutamate receptor 5
AFM	Atomic force microscopy	MHC	Major histocompatibility complex
AGC	A kinase group	MWCO	Molecular weight cut-off
APOE	Apolipoprotein E	NaOH	Sodium hydroxide
			N-Methyl-D-aspartic acid or N-Methyl-D-
APP	Amyloid precursor protein	NMDA	aspartate
Aβ	Amyloid-beta	NSB	Non specific binding
BLI	Biolayer interferometry	OD	Optical density
	Calmodulin-dependent		
CAMK	protein kinase	PAGE	Polyacrylamide gel electrophoresis
CK1/2	Casein kinase 1/2	PAMP	Pathogen-associated molecular pattern
CLU	Clusterin	PBS	Phosphate buffered saline
CMGC	A kinase group	PrP	Prion protein
CNS	Central nervous system	PSEN	Presenilin
CR1	Complement receptor type 1	RNA	Ribonucleic acid
CV	Column volume	ROS	Reactive oxygen species
	Density gradient		
DGC	centrifugation	RT	Room temperature
DNA	Deoxyribonucleic acid	scFv	Single-chain variable fragment
	Early onset Alzheimer's		
EOAD	disease	SDS	Sodium dodecyl sulfate
GB1	Protein G domain B1	SEC	Size exclusion
HCl	Hydrochloric acid	SPR	Surface plasmon resonance
	Isopropyl β -D-1-		
IPTG	thiogalactopyranoside	TEM	Transmission electron microscopy
LB	Lysogeny broth	TIR	Total internal reflection

1. Introduction

1.1 History of the perception of dementia

1.1.1 Ancient times

The awareness of mental decay as we age is nearly as old as our culture. The great Greek physician of the 7th century B.C. Pythagoras divided the human life into five stages. The last two stages were designated to the “old age” (> 63 years), mainly characterized by a decline of physical and psychological abilities¹. There is evidence that these changes were frequently observed, because it was taken seriously by the lawmaker of that time. E.g. the Greek judge Solon took age into account while revising the laws associated with drafting wills^{2,3}.

It is unclear what Hippocrates was thinking when describing age related diseases. According to one source¹, Hippocrates included the term “paranoia” into his classification of mental diseases, which were described as deterioration of mental abilities as a person grew older¹. On the other hand, another source claimed, that “although incompetent behavior was recognized in the elderly, Hippocrates did not include it among his mental disorders”. Indicating that mental deterioration with age was observed as a normal, unlucky but inevitable process. Comments of Plato and Aristotle reveal similar beliefs¹. Aristotle presented the view that old people are useless for high administrative posts. Interestingly, in his notes, he never mentions the possibility of exceptions. So it is likely that he also shared the belief that mental decay is an inevitable process connected to aging³.

In contrast, the Roman philosopher Cicero wrote that “senile debility” was not a characteristic of all men, but only of those who are weak¹. He suggested an active mental life would prevent or at least postpone mental decline⁴. However, Aristotle’s medical influence for centuries vanquished any opposing thought and so the philosophy of Cicero did not take root.

On the other side, if comparing these thoughts with medical compilations of that time “*De Re Medica*; 30 A.D.”, it is noticeable, that mental decline as a person ages is not mentioned that often⁴. The first author to include age-related mental decay “morosis” in his encyclopedia was the Roman physician Galen (150–200 A.D.)⁵. Interestingly, his texts suggested that old age was a disease state³: “old age is not natural in the same way that feeding and growing are; the latter two can be considered as natural processes, while the former is not, being instead an inevitable infection of the body”.

1.1.1 Medieval times

As the power of the church increased after the fall of the Roman Empire, ancient dogmas were taken as unquestionable and theological doctrines prohibited scientific progress by learning through observation and research⁶. Commentaries of mental decline faded after Galen till the 16th century. Roger Bacon gave one of the few references about senile dementia from that time and was later nearly convicted to be a heretic for his work in science⁷. Remarkably, in his work “Methods of Preventing the Appearance of Senility” he describes, that oblivion and memory are localized to specific parts of the brain. His work was based mainly on theories of Arabian Galenists³.



Figure I1: Woodcut located in the Wellcome Institute Library, London. With the rising power of the catholic church after the fall of the roman empire the progress in science diminished. People started to believe that sickness is a punishment of god for sins. Every person with mental problems or other diseases may be a potential sinner.

1.1.2 To the 19th century

The concept of dementia underwent gradual refinement till the 19th century and the awareness of dementia was not restricted to the medical society and even mentioned in literacy descriptions. For example, Shakespeare made numerous descriptions of dementia or senile diseases through his characters in his plays⁸.

In the 16th century, the interest in mental sicknesses grew in the medical community. Barrough published in 1583 a textbook about cognitive disorders, which was based on Galen's classification⁹. However, there was still little known about the reasons of the diseases and no base for diagnoses. Although Barrough indicates abnormalities in the brain as a source of certain mental diseases, these changes were mainly seen as body fluid imbalances. This concept indicates the Hippocratic roots.

In the 17th century distinct types of dementia became better characterized behaviorally. When dissection of the human body became more tolerated, there was an increasing trend in the search of physiological changes in the brain. Thomas Willis published in "Practice of Physick" a characterization of dementia which was based on clinical and anatomical knowledge. He attributed e.g. "Stupidity or morosis or foolishness ... signifies a defect of the intellect and judgment, yet it is not improperly reckoned among the Diseases of the head or brain" as caused by: 1) congenital factors, 2) age, 3) head injury, 4) alcohol or drug abuse, 5) disease and 6) prolonged epilepsy. Other anatomists tried to find correlates of mental diseases in the brain. Torack wrote that a majority of mental diseases do not show an evident anatomical correlate³.

Towards the 18th century, people began to feel a need to replace the theories of Aristotle and Hippocrates by modern concepts that were based on disturbed nervous function. William Cullen proceeded to reclassify all diseases into four classes. One of those was entitled "Neurosis" and it was the first time that senile dementia was classified as a medical entity¹⁰.

1.1.3 The 19th century

The 19th century was characterized by progress regarding all mental disorders and the way society dealt with the beings suffering from one. It was widely accepted to treat people with mental disorders like criminals. Phillippe Pinel, consulting physician of Napoleon, was condemned for his book entitled "Treatise on Insanity" because of the way he believed society failed to for the patient: "abandoned the patient to his melancholy fate, as an untamable being, to be immured in solitary durance, loaded with chains, or otherwise treated with extreme severity, until the natural close of a life so wretched shall rescue him from misery". In the end, he succeeded with his trial to establish that insanity is a disease and not a crime^{3,11}. As a consequence, institutions for more human care were funded. It was also Pinel who introduced scientific principles based on objective observation into the clinical setting. These reforms resulted in widespread clinical/pathological descriptions of mental disorders and a detailed classification later by his student Esquirol. Esquirol also made specific refinements of the categories of dementia¹⁰. He distinguished between "dementia" and

“amentia”. “Dementia” is the loss of mental faculties by disease, whereas patients with “amentia” were never able to acquire knowledge¹⁰.

Continuing the trend of anatomists to study brains that began at the end of the 17th century, in 1860 there was a general appreciation of the idea that a loss of brain weight accompanies dementias¹². It was Wilks, who provided a first description of the term atrophy as a loss of substance in the brain. He observed that the sulci of the brain were greatly increased in comparison to healthy individuals³. Many of these features have also been recognized in individuals suffering from later stages of Syphilis (general paresis). One characteristic of that disease state was a reduction in the diameter of blood vasculature due to swelling and proliferation of endothelial cells. In addition to afflicting the peripheral vasculature, this pathology was visible in the cerebrovasculature³. As a consequence, much attention was spent on examining cerebrovascular changes as a hallmark of dementia. Degeneration of blood vessels followed by a stroke was a common explanation for the observed substance loss in senile brain atrophy and senile dementia, and both, Alois Alzheimer and Otto Binswanger extensively described this arteriosclerotic brain atrophy in the 1890s^{3,13-16}. The development of histochemical techniques like the carmine stain allowed the reconsideration of the pathological changes in dementia. Blocq and Marinesco described for the first time an accumulation of an unidentified substance into plaques in the brain of an elderly epileptic patient. Later the same was observed in patients with senile dementia¹⁷. Following the discovery of the Golgi by silver staining (1873), Bielschowsky was able to clearly visualize cellular components for the first time and was able to identify thread-like structures within neurons (he called them neurofibrils)¹⁸. In 1907, Alois Alzheimer used this stain for describing the pathology in the brain of a deceased woman that developed dementia at an early of 51³. He was able to identify the mentioned thread-like structures inside the cells and widespread plaque pathology between the cells. Together with other disease observations, like the fast progression and the exceptionally early onset, Alzheimer was able to distinguish this disease presentation from the majority of predominantly described dementias caused by neurosyphilis. This is why Alzheimer decided to create an initial disease description as a unique disease entity. In the next 5 years following this initial description, 11 similar cases of pre-senile (before age 65) dementia were described with the same pathological properties, namely plaques and neurofibrillary tangles. Endorsement of Alzheimer’s disease as a unique type of dementia was mainly pushed by Emil Kraepelin, the foremost psychiatrist at the time. Although it seems that Emil Kraepelin was not entirely sure about the status of Alzheimer’s disease as a unique subtype of dementia, he included it into his “Textbook of Psychiatry” published at 1910³.

1.2 Recent progress in neurodegeneration

Today we know the field of neurodegenerative diseases is diverse. Nevertheless, all known chronic neurodegenerative diseases show at some point a degenerative process that leads to the decay of certain types of neurons, and neurodegeneration is often associated with immune activation¹⁹. The central nervous system is known to be an immune-privileged area; although, innate and (to a lower degree) adaptive immune responses take place to prevent viral or bacterial infections, stop tumor growth and remove necrotic cells, to prevent the tissue from further damage.

Both, macrophages and microglia cells are able to clear debris as a result of brain injury by phagocytosis to promote regeneration. If, for example, phagocytosis is impaired the regeneration process is delayed. Interestingly changes in the immune response and activation of microglia cells have been discovered in the majority of known neurodegenerative disorders¹⁹.

1.2.1 Chronic inflammation: Activation of the immune system

In most neurodegenerative diseases, proteins like A β , tau, alpha-synuclein, TDP-43 and other aggregation prone proteins are found in an abnormal structural conformation, so called amyloid like plaques. Often these proteins form fibrillar structures by interaction of β -sheets and co-aggregate²⁰. Many studies with the aim to evaluate genetic factors influencing disease progression, identified genes that are able to alter the likelihood of these proteins to form amyloid like plaques.

Chorea Huntington is one of the most famous examples of malign protein aggregation. The number of “CAG”-repeats in the gene for Huntingtin is directly related to the onset of the disease and the likelihood of the Huntingtin-fragments to go into amyloid like aggregates. In the case of A β , significant effort has been spent on trying to identify numerous isoforms that are less aggregation prone²¹. For tau, one identified certain mutations that can lead to the development of fronto-temporal lobar degeneration (FTLD) and enhance the chance of tau to aggregate to amyloid like structures. In some cases of FTLD, amyotrophic lateral sclerosis (ALS) and certain types of muscle dystrophy, amyloid like aggregates containing TDP-43 have been observed. At least 29 missense-mutations have been identified which influence the likelihood of TDP-43 to aggregate and alter cytotoxicity²². For hereditary types of Parkinson’s disease, mutations have been identified that alter the chance of alpha-synuclein to form so called Lewy-bodies (LB)²³.

There are hypotheses how aggregation prone proteins lead to cytotoxicity. If the aggregation occurs intracellular: i) Loss of function²⁴, because of depletion of soluble protein into the

aggregates, ii) gain of function²⁵ because of delocalization into aggregates or post-processing of the protein by co-factors (kinases, proteases) and iii) ER stress²⁶. If protein aggregates accumulate in the extracellular space, iv) an inflammation/immune response can be observed because these proteins are now subjected to recognition by the immune system¹⁹.

Aggregated proteins can resemble pathogen associated molecular patterns (PAMPs) and thymus independent type 2 (TI-2) antigens²⁷⁻³⁰. PAMPs can be proteins, polysaccharides or nucleotides and can be recognized by pattern recognition receptors (PRRs), which are evolutionary conserved and may initiate immune signaling. Ideally these receptors act against pathogen associated contents, including bacterial polysaccharides, flagellum proteins, peptidoglycans and virus-associated particles like double stranded RNA²⁰. TI-2 antigens are typically polymeric molecules that are activating B-cells directly to secrete IgMs²⁰. Both PAMPs and TI-2-associated antigen patterns are high molecular sizes, contain repetitive epitopes and features can often be found in amyloid like aggregates³¹.

In contrast to the innate immune system, the response of the adaptive immune system is expected to be limited by two factors. Firstly the expression of the major histocompatibility complex (MHC) is reduced in the CNS³². MHC binds small peptides that are cleaved from larger proteins, thereby making these peptides accessible for T-lymphocytes. The immune system then responds when the presented peptide is identified as non-self. Secondly, the concentration of T-lymphocytes is low in the CNS. Often a chronic inflammation can be observed in patients suffering from proteinopathies. A hallmark of extracellular amyloid like aggregates is their high resistance to degradation³¹. Different studies on mice showed that A β aggregates remain stable, even if expression is terminated³³⁻³⁵. Conversely, it was shown that intra-cellular aggregates, e.g., polyglutamine disorders, can be reduced or entirely removed if production is stopped or the proteasome activity enhanced³⁶⁻³⁹. Nevertheless it appears that both intracellular and extracellular protein aggregates are able to activate the innate immune response according to the “danger theory of immune activation”⁴⁰. This theory postulates that intracellular stress, such as protein aggregation or a virus infection generates a signal for the immune system. The observation that inflammatory markers are often the earliest signs of disease pathology in neurodegenerative diseases may be explained by such a signaling mechanism. Finally intra- and extracellular protein aggregates acting as PAMPs will lead to a chronic inflammatory condition²⁰. In Alzheimer’s disease, histopathological, biochemical and molecular studies show that the brain is subject to chronic inflammation even in the earliest disease stages. Activation of the innate immune system is reflected by gliosis, increased levels of numerous inflammatory factors, including chemokines, cytokines and acute phase reactants, in the absence of overt lymphocytic or mononuclear infiltrates.

1.2.2 Influence of senescence in neurodegeneration

Replicative senescence was first described by Hayflick who defined the term “Hayflick-Limit”. The Hayflick-Limit is the number of divisions a (eukaryotic) cell is able to perform before apoptosis occurs because of the continued decrease in length of the chromosomes telomeres. Typically senescent cell cultures show altered morphology and become unresponsive to growth factors. Overcoming the Hayflick-Limit is a precondition for tumor development, and the influence of the Hayflick-Limit on life expectancy has been a controversial discussion point^{20,41}.

Senescence of cells of the CNS, including neurons or glia cells, remains poorly understood. For neurons, replicative senescence is considered to not play a major role, as neurons are terminally differentiated and not expected to undergo senescence⁴². However, there are physiological changes (not just protein aggregates) in aging neurons, which potentially lead to senescence-like conditions, e.g., i) oxidative stress damages the mitochondrial genome and leads to impaired oxidative metabolism, which is devastating for a cell type that is highly dependent energy production via this route⁴³, and ii) mutations accumulate in the nucleus, but especially in mitochondrial DNA⁴⁴. These changes combined may decrease the responsiveness of neurons to growth factors or disturb the receptor-transmitter balance, because the expression of receptors is reduced (due to DNA damage) or the vesicle-dependent transport of neuro-transmitters is impaired (mainly dependent on mitochondria). In such an environment it is possible that other cell types change their behavior towards a disease state²⁰.

1.3 The limits of the immune system hypothesis

The immune system is involved in pathogenesis. However some aspects of AD-pathogenesis can hardly be explained with this model alone. The tau symptomatic is such an example. As explained, intracellular tangles have been found very early in the history of AD. However, the reasons for their appearance and the connections with A β are not well understood. Moreover, in addition to some of the causative genes, a number of risk alleles were found that increase the risk to develop an AD-symptomatic. For most of these risk alleles a clear pathway is unknown.

1.4 Genetic risk factors of Alzheimer’s disease

Several genes are known that either increase the risk or possess a full penetrance for developing Alzheimer’s disease. There are two types of AD defined: early-onset AD (EOAD) and late-onset AD (LOAD). Each type has a unique set of disease modifying gene variants.

EOAD genes are primarily known for their property to induce AD, whereas LOAD genes mainly increase the chance to develop AD⁴⁵.

1.4.1 Early-onset Alzheimer's disease:

EOAD begins before age 65 with an incidence rate between 6–7 %⁴⁶. At least three gene mutations cause EOAD: amyloid-beta (A4) precursor protein (APP), presenilin 1 (PSEN1) and presenilin 2 (PSEN2). Most of these mutations are dominantly inherited, but not fully penetrant. Fewer than 13 % of EOAD cases showed full penetration over multiple generations⁴⁵.

Amyloid-beta (A4) precursor protein

APP is located within chromosome 21 and it was one of the first causal genes identified for AD. However, the role of APP for cellular function is not fully defined. Currently, 25 pathogenic mutations in or adjacent to the A β domain have been identified^{45,47,48}. The Arctic mutation seems to be dominantly inherited and fully penetrant. The average age of onset is ~57 years of age. This mutation lowers the total A β (1-40)- or A β (1-42)-levels and promotes protofibril formation. The Swedish mutation is a double mutation before the A β domain and increases the total A β production and changes intracellular A β localization. The London mutation is localized after the A β domain and increases A β (1-42) production⁴⁵.

Presenilin 1

PSEN1 is a component of the γ -secretase and located on chromosome 14. Changes in the function of γ -secretase can alter the production of A β . Already 185 mutations have been discovered that may induce AD. EOAD because of PSEN1 is completely penetrant, which results in a high variation in disease onset. However the allele is dominantly inherited^{45,48}.

Presenilin 2

Although the function of PSEN2 is not fully understood, it is thought to function in a similar manner to PSEN1. PSEN2 is located at chromosome 1 and 12 pathogenic mutations have been identified⁴⁸. However, in comparison to PSEN1 the onset is delayed (mean 53.7 vs. 45.5 years of age) and the survival time after diagnosis is longer (10.6 vs. 8.4 years)⁴⁵.

1.4.2 Late onset Alzheimer's disease:

For the sporadic type of Alzheimer's disease, numerous risk factors have been identified, but no causative gene has been found. The observation that for many alleles the role in AD disease progression is unknown makes evaluations even harder.

Apolipoprotein E

There are three APOE alleles: $\epsilon 2$ (rs429358, population frequency: 6.4 %), $\epsilon 3$ (wild-type, population frequency: 78.3 %) and $\epsilon 4$ (rs7412, population frequency: 14.5 %), which differ by substitutions at position 112 or 158 of the processed protein⁴⁵. Studies indicate the $\epsilon 4$ -allele is the greatest known genetic risk factor for LOAD, whereas $\epsilon 2$ seems to lower the risk. Despite the fact that the $\epsilon 4$ -allele increases the risk to develop LOAD, it is non-causative and some individuals that are homozygotes never develop AD. It is hypothesized that APOE may be involved in $A\beta(1-42)$ -clearance via proteolysis and astrocyte mediated degradation. The amount of $A\beta(1-42)$ -depositions appears to be correlated with the number of $\epsilon 4$ -alleles.

Clusterin

Clusterin also known as apolipoprotein J (CLU) and is located on chromosome 8 and is suggested to be involved in $A\beta(1-42)$ -clearance. Studies indicate that it increases the toxicity of $A\beta(1-42)$. Furthermore, individuals with AD have increased levels of clusterin and the concentration of clusterin seems to be correlated with mental decline. A single allele (rs11136000) is known to have a protective function by lowering $A\beta(1-42)$ -levels⁴⁵.

ATP-binding cassette, subfamily A (ABC1), member 7

ATP-binding cassette, subfamily A (ABC1), member 7 (ABCA7) is an ATP-binding cassette transporter and functions to maintain lipid homeostasis. Interfering ABCA7 functions decreases phagocytosis. Lipid dysfunction, changes in lipid homeostasis, and modifications of neuronal membrane homeostasis can all cause numerous diseases, including AD. Based on this theory, the allele variant rs3764560 of ABCA7 is known to increase the risk of the development of AD, because of a disturbed lipid homeostasis and phagocytosis⁴⁵.

1.4.3 Endocytosis

Endocytosis is necessary for transport of molecules across cell membranes. APP is processed within endosomes^{49,50}. The endosomal transport is regulated via clathrin-coated pits⁵¹. Consequently, inhibiting clathrin mediated transport lowers the $A\beta(1-42)$ levels and several other genes regulating endocytosis seem to effect AD⁵².

Bridging integrator 1

Bridging integrator 1 (BIN1) is located on chromosome 2 and has multiple functions, these include synaptic vesicle endocytosis, which decreases the formation of clathrin-coated vesicles. Likely, allele variants which reduce the effect of BIN1 on synaptic vesicle endocytosis would be protective in the case of AD, because the efficiency of APP-processing

would be reduced. In contrast, allele variants that interfere with the role of BIN1 in inhibiting clathrin-coated vesicle formation would increase the risk of AD, because A β (1-42) production from APP will be enhanced⁴⁵.

Phosphatidylinositol binding clathrin assembly protein

Phosphatidylinositol binding clathrin assembly protein (PICALM) is located on chromosome 11 and is responsible for binding the clathrin-assembly complex, protein trafficking and synaptic endocytosis. PICALM has four isoforms and one (rs3851179) was identified to increase the risk of the development of AD by decreasing clathrin-coated vesicle formation⁴⁵.

Complement component (3b/4b) receptor 1

Complement component (3b/4b) receptor 1 (CR1) is located at chromosome 1 and has two different isoforms. It is suggested, that CR1 is involved in A β -clearance and endocytosis. A risk allele rs3818361 has been identified, but an exact role in pathogenesis is not known⁴⁵.

CD2-associated protein

CD2-associated protein (CD2AP) is located on chromosome 6 and regulates the function of the actin-cytoskeleton and receptor mediated endocytosis. CD2AP may regulate APP processing and lipid homeostasis, which are both crucial for AD pathogenesis⁴⁵.

1.5 Hypothesis of A β -induced cytotoxicity

Currently, many hypotheses about the cytotoxicity of A β or certain A β assembly states (oligomers, protofibrils) and the various possible pathways involved exist. In many cases, reviews reveal contradictions in the proposed models or the proposed hypotheses are not able to explain the full AD-symptomatic, which results in a *complicated* AD model, inheriting a large number of partial descriptions.

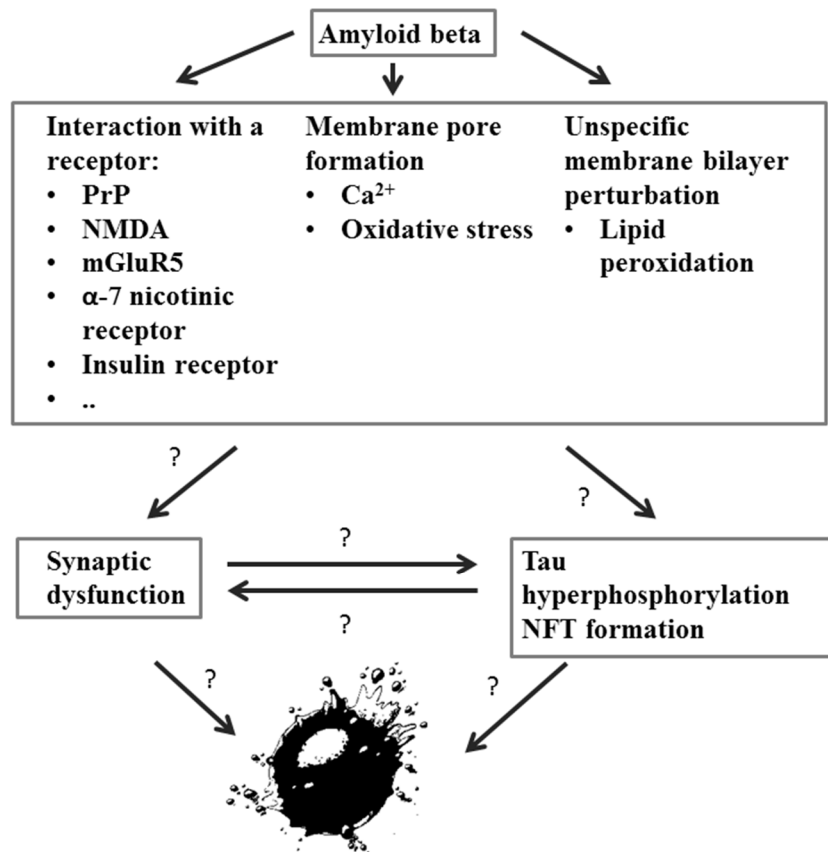


Figure I2: Current hypothesis of the cytotoxicity of Aβ. The relationship between synaptic dysfunction, tau hyperphosphorylation and cell death is not resolved. Often the mechanisms, which lead to certain observations, are not resolved or contradicting with other observations.

1.5.1 Microtubule-associated protein tau

Tau (MAPT) is a microtubule-associated protein (MAP) and highly expressed in neuronal cells to stabilize microtubules by interacting with tubulin. In other cells the expression is lower (e.g., astrocytes or oligodendrocytes). This stabilization is critical for neurons, because they build long cell extensions (axons) and use microtubule associated transport mechanisms for vesicle transport (containing neurotransmitters). On the other hand, tau competes with the motor protein kinesin and reduces transport capacity.

In humans there are six different tau splice products, differing in the number of tubulin binding domains. In case of $\tau 3L$, $\tau 3S$, or $\tau 3$ there are three binding domains and four in the case of $\tau 4L$, $\tau 4S$ and $\tau 4$. All tau isoforms seem to become prone for self-aggregation into filaments after hyperphosphorylation. Hyperphosphorylation seems to be a response to oxidative stress⁵³, such as lipid peroxidation after treatment with, e.g. 4-hydroxy-2-nonenal. Specific mutations in MAPT are linked to inherited cases of frontotemporal dementia with parkinsonism-17 (FTDP-17) and Pick's disease.

1.5.2 A β induced tau hyperphosphorylation

Some studies indicate tau phosphorylation can be induced by A β ⁵⁴. Unfortunately, there is a paucity of information to enable the construction of a detailed pathway of the A β -triggered tau hyperphosphorylation. Phosphorylation is an abundant process in cells. The *overwhelming majority* of kinases are promiscuous (see “phosphonetnetworks.org”).

The most popular example describing A β -dependent tau-phosphorylation would be Glycogen Synthase Kinase-3 (GSK-3), which has more than 100 *known* substrates⁵⁵. Additionally, phosphorylation can be triggered by a multitude of factors, such as: oxidative stress response^{56,57}, nutrition triggered autophagy⁵⁸, cell cycle control⁵⁹, radiation response⁶⁰, cell proliferation and apoptosis⁶¹. In addition to these, the activation (direct, indirect) of these kinases by A β remains an enigma. In addition to GSK-3, there are > 24 other kinases involved in tau phosphorylation. These kinases are divided into the families CMGC, CAMK, CK1/CK2 and AGC⁶².

1.5.3 Caspase-3 and GSK-3 triggered tau hyperphosphorylation

Caspase-3 plays a critical role in the execution of apoptosis in mammalian cells. Caspases are initially inactive (procaspase) and can be activated by cleavage of other caspases. This mechanism, once triggered, results in an activation-cascade “caspases cascade”, which is irreversible. Caspase-3 seems to be crucial for apoptotic chromatin condensation and DNA fragmentation⁶³.

In rats and mice, activation of caspase-3 by A β -oligomers⁶⁴ with resulting cleavage of Akt1 and activation of GSK-3, has been reported. GSK-3 was found to phosphorylate tau⁶⁵. On the other hand, the role of GSK-3 in many other processes, including apoptosis, is not well understood⁶⁶. Activation of GSK-3 together with caspases-3 activation is expected to make the cell more susceptible to intrinsic-triggered apoptosis, thus leading to cell death before intra-cellular tau-aggregates can form. Conclusively, at least one process must delay or stop apoptosis. This is why hyperphosphorylated tau has been suggested to antagonize apoptosis^{67,68}. However, there are contradictory reports from groups suggesting an opposite effect⁶⁹⁻⁷¹. Further studies related to caspase-3-activation by the A β -fragment-(25-35) are also contradictory. One study claims that caspase-3 is activated when cells are exposed to A β (25-35) for 48 h. However, this effect seems to be transient because after 72-96 h the caspase-3 levels recover to the level of the controls⁷². Another study tried a similar approach, but used LDH to quantify apoptosis⁷³. Unfortunately, LDH is not selective for apoptosis.

1.5.4 NMDAR endocytosis

NMDA receptors are critical for synaptic plasticity in neurons. Studies indicate⁷⁴, that A β (1-42) promotes endocytosis of NMDA receptors in cortical neurons. Reducing A β by treating neurons with a gamma-secretase inhibitor restored surface expression of NMDA receptors. The supplied model, involves the need of an alpha-7 nicotinic receptor to promote endocytosis. However, other studies indicate that a loss of alpha-7 nicotinic receptor promotes cognitive decline, which seems to contradict with the proposed model⁷⁵.

1.5.5 mGluR5 activation

mGluR5 activation seems to counter-act apoptosis⁷⁶. Thus, activation of mGluR5 can enhance cell survival caused by treatment with toxic A β species. Other studies indicate that A β -oligomers are able to bind and over-activate mGluR5 receptors⁷⁷. Here, the opposite: over-activation of the receptor should yield a mechanistic explanation of synaptic failure and AD-symptomatic. Unfortunately, if AD could be explained by an increase in receptor binding then treatment with mGluR5 receptor antagonists should reduce AD symptomatic. The fragile X-syndrome is also suspected to be caused by overly activated mGluR5 receptors. In a mice model, receptor antagonists reversed the symptoms⁷⁸. Unfortunately, no studies involving treatment of AD with mGluR5 receptor antagonists have been reported.

1.5.6 Pyroglutamylated A β (pE3-A β)

Some studies examining pE3-A β are based on Glabe *et al.*⁷⁹. An evaluation of the A β -preparation protocol suggests that the toxic effects may be a combination of A β and HFIP, and thus pathogenicity arises from the method rather than a true cytotoxicity. A publication working without HFIP found no difference in toxicity⁸⁰. One statistical analysis found that A β (1-42) correlates stronger with cognitive impairment⁸¹. Experiments in mice found that pE3-A β (3-42) is able to induce neurodegeneration⁸² and that electrical activity of pyramidal cells decreases⁸³. Moreover, the treatment with a cyclase inhibitor reduced the decline pyramidal cell activity, which seems convenient with another study, which was evaluating the expression of glutaminy cyclase in the human cortex⁸⁴. The expression of glutaminy cyclase correlated with the concentration of insoluble pE3-A β ⁸⁴. In this study the correlation of the elevation pE3-A β with cognitive decline was stronger in comparison with unmodified A β ⁸⁴.

1.5.7 Interaction of A β with PrP

A study found that PrP may mediate binding to A β , thereby leading to impairment of synaptic plasticity⁸⁵. The conclusion of this hypothesis is that a PrP-knockout or blocking of PrP by

IgGs should yield milder AD-symptoms. Unfortunately, this could not be replicated. Cell cultures of hippocampal cells and cognition tests on mice showed no difference when treated with A β -oligomers⁸⁶. To obtain a final proof, expression of the arctic mutant of A β in PrP-knockout strains seems necessary. Other studies indicate high specificity of PrP for oligomeric A β ⁸⁷. However, this dataset is problematic because of the following reasons: i) no positive control with an PrP-binding IgG for validating correct immobilization, ii) A β was used as the analyte, but concentration determination of high molecular assembly states was unknown and moreover, the solubility of the assembly states used was also unknown, iii) no other methods like co-(immuno-) precipitation were applied for comparison.

1.5.8 A β causes oxidative stress by disturbing membrane function

There are theories that A β may disturb the mitochondrial membrane potential⁸⁸ and form membrane-pores^{89,90}. Similar was reported for pE3-A β , which seems to increase the permeability of an artificial plasma membrane for certain ions and small molecules⁹¹. Disturbing the cell or mitochondrial membrane homeostasis causes oxidative stress⁸⁸. This observation is congruent with many genetic risk factors for LOAD, which highlights the importance of membrane homeostasis. Furthermore, oxidative stress is a common hallmark for many other chronic neurodegenerative diseases like Chorea Huntington and Parkinson. Additionally, this theory connects tau hyperphosphorylation with AD-pathogenesis in a straightforward way⁵⁶. The mitochondrial genome accumulates damage over time⁹². This increases the chance of mitochondrial failure, which usually leads to oxidative stress due to ROS production. This effect can be synergistic with other stressors and may explain why the on-set age of many neurodegenerative diseases grows sigmoidal with age. The biggest problem of this theory is that the evidence of pore formation is negligible⁸⁹. Immunogold labeling would be an option for TEM to prove that pores consisting of A β exist. Although no pathway exists, an extension of this theory may be that A β promotes pore formation indirectly by interaction with other proteins.

1.5.9 Consequences

The smallest known common denominator of all these theories is the evidence that A β acts in different ways cytotoxic or initiates pathways that lead to cytotoxicity. Because of this simple fact, it seems feasible to find and characterize agents that can interfere with the mechanism of A β induced cytotoxicity. A current target of research is oligomer and protofibril formation. Even if the mechanism is not known, the pure existence of these cytotoxic A β -species seems to have an effect and may cause harm.

To characterize binding affinities to such assembly states, techniques like biolayer interferometry (BLI) and surface plasmon resonance (SPR) Spectroscopy have been applied to characterize the interaction of possible peptide based drug candidates.

1.6 Peptide drugs for Alzheimer therapy

The gap from peptides to proteins is fluent. Like proteins, peptides fulfill versatile tasks. In fungi they may act as antibiotics. In higher organisms, peptides can function as signal molecules like neurotransmitters or hormones. Well-known examples with medical and economic impact are the peptide hormones insulin and glucagon. The market of peptide based drugs for treating diabetes, cancer, cardiovascular diseases, inflammation is growing⁹³.

1.6.1 Advantages of peptides as drugs

Although traditional small molecules are easy to produce and can show high metabolic stability, they frequently lack specificity, which causes side-effects. In contrast, peptides can possess a high substrate specificity and affinity, and thus reduce the drug dose. Unlike small molecules, degradation of peptides via the proteasome leads to non-toxic products. In contrast to proteins, peptides are significantly smaller and can be synthesized chemically, which makes the production task scalable and economical. This may be a reason why the market for peptide drugs is growing. Many peptides have in comparison to proteins a higher chance to pass plasma membranes. This makes them appropriate for application in neurodegeneration.

1.6.2 Disadvantages of peptides as drugs

A drawback of peptide drugs is their relatively low bioavailability because of degradation by enzymes in the intestines, blood or cell plasma. Depending on their size, peptides possess relatively low half-life times in the organism because of the clearance by kidneys or liver. Because of this, clearance times in the range of minutes have been reported, which must be considered in peptide design and application. Furthermore, in direct comparison to small molecules, the production costs are still high.

1.6.3 General optimization of peptide based drug candidates

Many approaches have been developed in industry and nature to modify the properties of the peptide and the bioavailability. In summary, there are three major paths: i) addition or removal of functional groups at the level of the amino acids, ii) usage of non-canonical amino acids or D-enantiomeric amino acids, and iii) the cyclisation of the peptide.

Regarding point i), functional groups can change hydrophobicity, substrate specificity and the affinity. Moreover, functional groups can be used to remove net charges, and thus to enhance

the ability to pass membranes⁹⁴. A common approach is to replace the free carboxylic group by an ester. To enhance the resistance to carboxypeptidases, oxazolidinone can be used to mask the C-terminus from the enzyme. Sometimes the ability to pass membranes has to be optimized. A solution to this potential problem is the use of the triglyceride system. In the case of the opioid peptide deltorphin, the local concentration on the membrane was greatly enhanced. Other approaches exploit the possibility that certain peptidases process a prodrug in a way that the result is the biological active compound⁹⁴.

Although their conformation is mirrored, D-peptides or D-proteins have the same structure and properties as their L-counterparts. Usage of D-enantiomeric amino acids ii) is a very effective way to enhance the resistance of D-peptides to degradation, because most enzymes have substrate specificity for L-peptides or L-proteins. This allows oral application of D-peptides. Furthermore D-peptides cause a lower immunogenic response⁹⁵. Currently there are two design approaches for D-peptides. If there is a known L-peptide binder, it is possible to inverse its sequence (L-peptide: N-Asp-Gly-Thr-C to D-peptide: N-Thr-Gly-Asp-C). The result is a D-peptide with a similar primary structure, but inversed N-/C-termini (see Fig. I3).

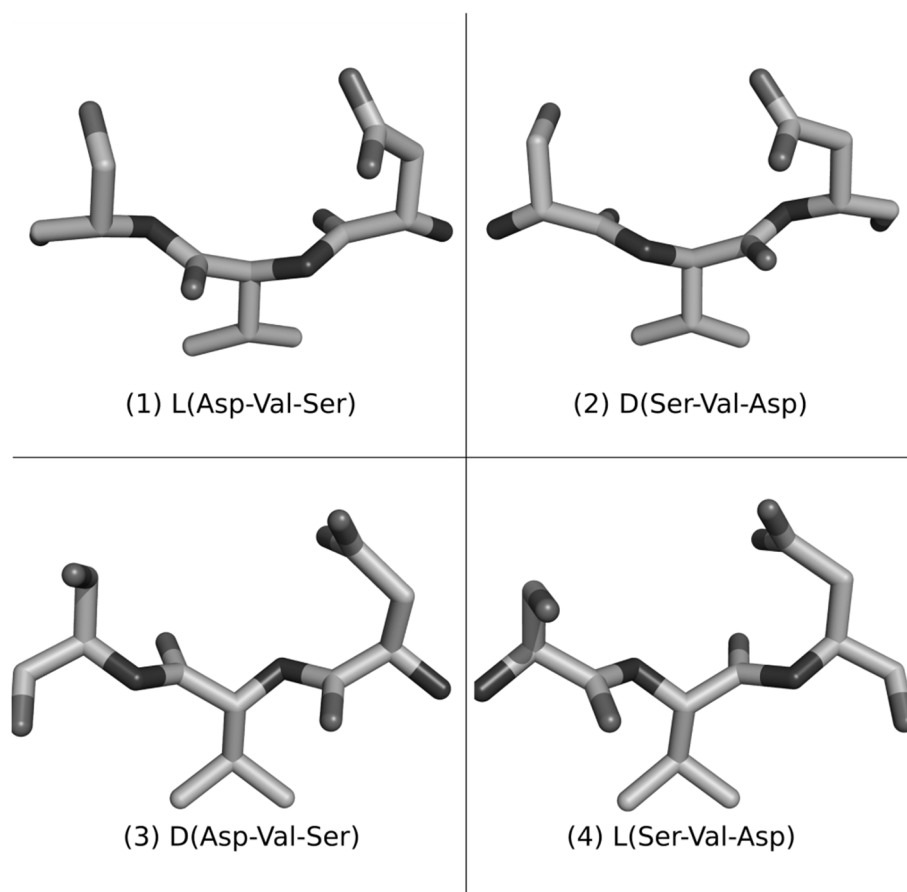


Figure I3: L-peptide and its analogues. L-peptide (1), D-enantiomer (3) with the same sequence, retro-inverso peptide (2) with inverted sequence and D-amino acids, and the retro L-peptide (4) with inverted sequence and L-amino acids. Source: Gainza⁹⁶

If the task is to find a yet unknown D-peptide for an epitope, then the use of mirror-image phage display represents a suitable approach to identify a peptide⁹⁷. Here, a selection of phages is presented to a D- enantiomeric version of the epitope. Phages that are able to bind the epitope are selected and used for further iteration steps of this procedure. The result is an enrichment of L-peptide sequences that can bind the epitope efficiently. These sequences can directly be used for the production of D-peptides, which is able to bind the L-epitope.

In nature there is a wide spectrum of cyclic peptides, even in combination with D-amino acids. The spectrum includes peptides acting as antibiotic to peptides functioning as hormones, such as oxytocin. Cyclisation iii) of peptides can enhance resistance to digestion. Furthermore, cyclisation reduces the amount of possible conformations and thus enhances rigidity^{98,99}. This is why a reduction of the entropic penalty has been reported for some peptide binders⁹⁸.

2. Aim of this work

The possibilities of peptides are nearly unlimited and offer potential for treatment of AD. For characterization of D-peptides, sensitivity is essential, because peptide based drugs possess a typically a low molecular weight. SPR spectroscopy is the method of choice to estimate binding affinities, because it possesses unmatched sensitivity for small agents and allows real-time recordings of label-free kinetic interactions. For characterization of the interaction of D-peptides with different A β assembly states such as A β monomers, oligomers and fibrils, a SPR-based assay has to be implemented. For this, the preparation, purification and immobilization of A β monomers, oligomers and fibrils must be evaluated on a simple (e.g. monovalent analyte) model system. The implemented assay will be applied for the estimation and comparison of the binding kinetics of certain D-peptides. Additionally, the results may be used to find a mechanistic explanation of the interaction of the evaluated D-peptides with A β . This may assist peptide design and optimization in down-stream optimization steps. Possible access points for D-peptide optimization, which will be evaluated and discussed in this work, are: sequence alterations, multiplication of binding sites with the aim to design tandem peptides, structural changes such as peptide cyclisation, and possibilities to enhance the half-life time of drugs in the organism. All these points may enhance the performance of the potential drug candidate for AD therapy.

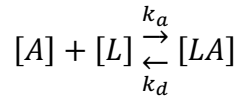
3. Theory

3.1 One to one interaction kinetics

The interaction kinetics describes the interaction of at least two interactants and can be separated into three phases: i) association, ii) steady state and iii) dissociation. In i) two or more components bind each other, in ii) the amount of molecules binding is equal to the amount of molecules dissociating. Finally, iii) is determined by the breaking of the interactions. Each of the phases contains information about the kinetics.

3.1.1 Interaction kinetics

Binding between a ligand L and an Analyte A occurs when analyte and ligand come in contact by diffusion and when both have correct orientation and energy. Afterwards the complex LA might dissociate again. The velocity of the forward (k_a) and backward reaction (k_d) shifts the equilibrium. This formula describes the reaction:



The association rate, as the number of binding events per unit of time, can be described by the following term:

$$\text{i.} \quad k_a = \frac{[LA]}{[L][A]}$$

After association and some time, the interactions may be disrupted. The rate, as the number of dissociation events per unit of time, can be described by:

$$\text{ii.} \quad k_d = \frac{[L][A]}{[LA]}$$

Taken together, the reaction of analyte and ligand is an equilibrium reaction of association and dissociation and can be described by:

$$\text{iii.} \quad k_a[L][A] = k_d[LA]$$

Conclusively, the net rate of the created complex $\Delta[LA]$ per time unit Δt is determined as the sum of complex production and complex dissociation.

$$\text{iv.} \quad \frac{d[LA]}{dt} = k_a[L][A] - k_d[LA]$$

So the equilibrium constants can be defined as:

$$\text{v.} \quad K_A = \frac{k_a}{k_d} = \frac{[AL]}{[A][L]}$$

$$\text{vi.} \quad K_D = \frac{k_d}{k_a} = \frac{[A][L]}{[LA]}$$

3.1.2 Application of interaction kinetics for optical biosensors

The device can measure the concentration of complex $[LA]$ formed on the surface as response “R” in “RU” or other units like “nm” in the case of BLI. The unit is irrelevant as long as the dependency to the concentration is linear. The concentration of the analyte is ideally known at the moment of interaction. However, the estimated concentration of free ligand has to be determined indirectly. The maximum binding capacity “ R_{\max} ” can be assumed as the maximum response. Assuming R_{\max} is correct, the concentration of free ligand would be $[R_{\max} - R]$. So the modified rate equation is:

$$\text{vii.} \quad \frac{dR}{dt} = k_a[R_{\max} - R][A] - k_d[R]$$

$$\text{vii.} \quad \frac{dR}{dt} = k_a R_{\max} [A] - k_a [R][A] - k_d [R]$$

$$\text{vii.} \quad \frac{dR}{dt} = k_a R_{\max} [A] - (k_a [A] + k_d) [R]$$

3.1.3 Application of integrated rate laws

A regular function is a relation of numbers and variables. A differential equation is a relation of a function(s) to its derivate function(s). A simple example that fits in this context would be a possible solution of the differential equation: $F(x) = f(x) = f'(x) = e^x$, because the derivation of e^x is e^x .

The rate equations i) - iv) relate the change of complex formation (concentration) to the concentration of the analyte and the ligand. However, to find a theoretical description of the measured data (fitting), a formula that relates the concentration of the complex to time is required.

Based on the integrated rate law, the common rate formula: $r = -\frac{d[C]}{dt} = k * [C]$ has the integration formula: $[C] = [C_0] * e^{-k*t}$. In the case of the rate equation vii), the integrated rate formula is¹⁰⁰:

$$\text{viii.} \quad R = \frac{k_a R_{\max} [A]}{k_a [A] + k_d} (1 - e^{-(k_a [A] + k_d) * t})$$

For the dissociation term: $\frac{d[R]}{dt} = -k_d * [R]$, the integration is easy to solve:

$$\text{ix.} \quad R = R_0 * e^{-k_d * t} + R_{t \rightarrow \infty}$$

Because the decay of the complex is ideally infinitely long, the *optional* term $R_{t \rightarrow \infty}$ can be added as an offset, to describe a finite dissociation phase.

3.1.4 Multivalency and avidity

Multivalency is defined as the operation of multiple molecular interaction events which occur simultaneously between two entities (e.g. analyte and ligand). Multivalency is a design principle that can convert agents of low affinity to agents of high affinity¹⁰¹. Theoretically one can distinguish between homo-multivalency and hetero-multivalency, dependent on whether the agent consists of identical (homo) or non-identical (hetero) binding sites. Antibodies are typically homo-multivalent binders, because both binding sites are identical¹⁰². In contrast, some of the bivalent peptides, discussed in this work, belong to the hetero-multivalent agents.

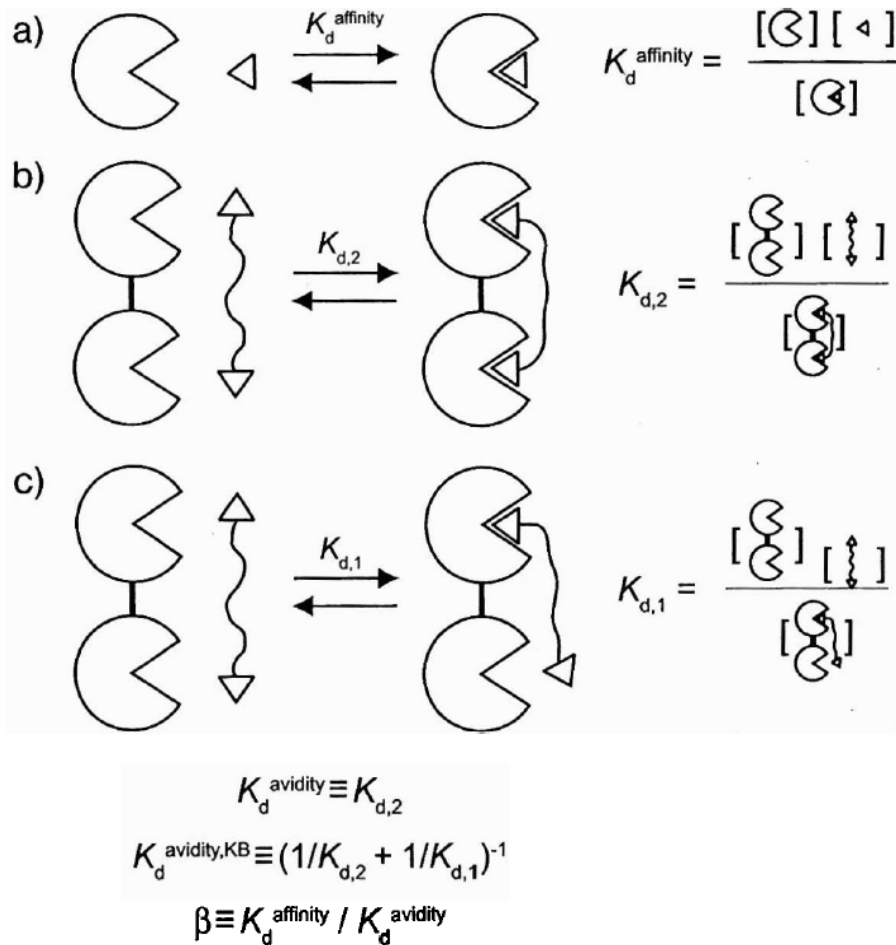


Figure I4: Illustration of avidity according to “Multivalency in ligand design”. a) is the interaction of a monovalent agent, b) and c) show the two binding states of a bivalent agent. The K_D calculation of both binding states are illustrated on the right side and the formula for the affinity below. Source: Krishnamurthy, et al.¹⁰¹

For both types, the calculation of the theoretical total K_D works the same and is illustrated in Fig. I4. In case of a multivalent agent, the total K_D is always smaller than the single K_D s of each binding site and can be calculated by the following equation:

$$x. \quad \frac{1}{K_D} = \sum_{i=1}^{\infty} \frac{1}{K_{Di}}$$

It is possible to visualize the development of the K_D with increasing number of binding sites. In Fig. I5 the multiplication of a hypothetical binding site with a K_D of 10^{-6} M is illustrated.

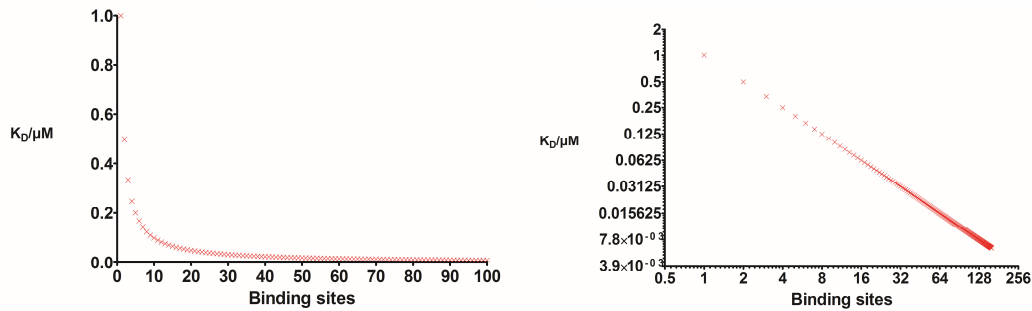


Figure I5: Relationship of affinity and the number of binding sites. The affinity increases with the amount of binding sites and anneals to zero.

The K_D anneals to zero with increasing number of binding sites (Fig. I5). For a 2-, 4-, or 8-fold increase in affinity (means: $1/2^{\text{th}}$, $1/4^{\text{th}}$, or $1/8^{\text{th}}$ of the initial K_D), one needs 2-, 4-, or 8-times more binding sites.

3.2 Surface plasmon resonance

Surface plasmon resonance spectroscopy developed to a technique for biological interaction studies. In the following, there is a brief description of the method and the theoretical background of binding kinetics.

3.2.1 History of surface plasmon resonance

R. M. Wood discovered between 1902 and 1912 the SPR-phenomenon when he observed an unusual reflected light pattern after he shone polarized light at a metal layer^{103,104}. Later Pines and Bohm found that the observed energy loss in the reflected light is caused by excitation of the conducting electrons, resulting in plasma oscillations¹⁰⁵⁻¹⁰⁸. Subsequently, it was found that the electric field of these plasma oscillations could be extended beyond the boundaries of the sample¹⁰⁹. This important fact has a consequence; that plasma oscillations can be affected by any contamination on the surface of the sample. Later this method was described as “excitation of the evanescent field” and used to study ultra-thin metal films or coatings.

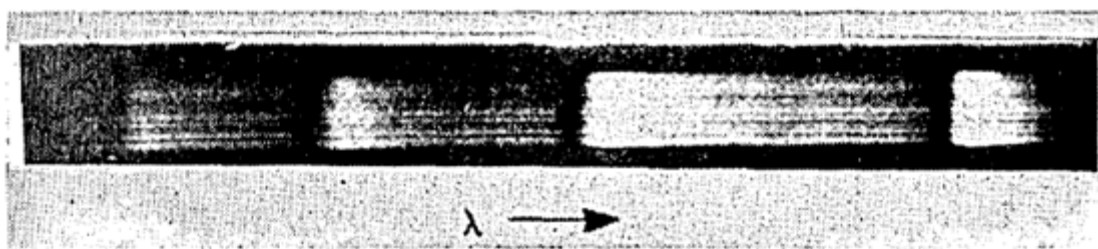


Figure I6: A spectrogram exhibiting Wood's anomalies. This is a reproduction from Wood ¹⁰³. It shows the reflected light pattern he observed.

Kretschman and Otto demonstrated an optical method based on the attenuation of the totally reflected light¹¹⁰⁻¹¹² (Fig. I6). Since the 1980s SPR-spectroscopy has been used to study thin films of chemical and biological samples¹¹³⁻¹¹⁶. The main advantage was to study the interaction of an immobilized interactant (ligand) and another interactant in solution (analyte) in real time.

3.2.2 Total internal reflection

SPR is a physical phenomenon that can occur when plane-polarized light is beamed onto a metal film under total internal reflection conditions. When light hits a half circular prism it is bent toward the plane of the interface, if the optical density of the prism is higher than that at the interface. If the incident angle θ is small enough, a percentage of the light is refracted. Changing θ above a critical value has the consequence that all the light is reflected within the prism. This is called “total internal reflection” (TIR) and illustrated in Fig. I7. The electrical field of the photons extends about a quarter of the wavelength beyond the reflecting surface and it is possible to quantize the reflected light, because there is no loss of intensity due to diffraction.

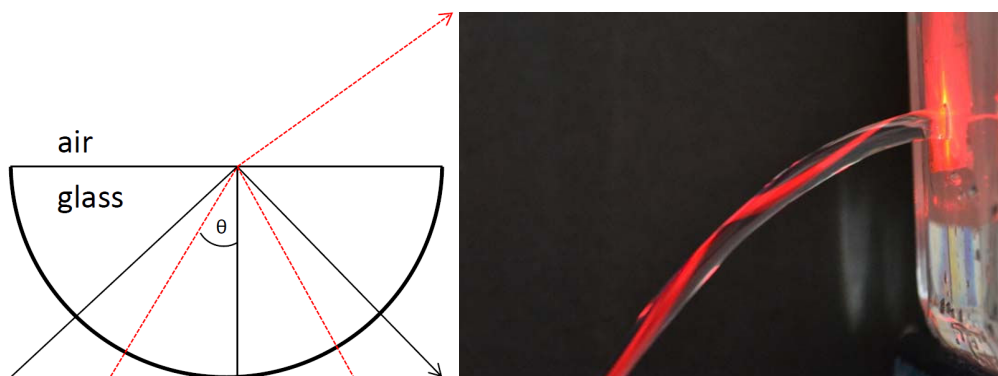


Figure I7: Illustration of total internal reflection (TIR). If the angle of the incident light (black) is greater than the bias angle θ , the light is nearly reflected without diffraction (compare black and red). The photo on the right shows TIR on the example of water which is poured from a hole on the side of a bottle. Since the refractive index of air is 1.00 and water is 1.33, the laser beam travels through the stream. Source: Freeberg ¹¹⁷.

3.2.3 Momentum resonance

For SPR, the prism can be coated with a layer of a noble metal such as gold. Then, the photons electric field can interact with the free (conducting) electrons on the gold surface. The energy of the photons is then transferred to the electrons, which convert into surface plasmons. Both, the plasmons and the photons have a momentum, and resonance only occurs if the momentum of the photons matches the momentum of the plasmons (momentum resonance).

3.2.4 Spectrometer types

When using a thin film, both the photons electric field and the plasmons act on the other side of the film. The width of the field, which is useful to know for measurements, is approximately 300 nm. Changes in the composition of the medium will change the momentum of the plasmons. Consequently, the angle of momentum resonance also changes. The angular change can be measured relatively easily by a diode array of the resulting dark band and SPR spectrometers based on this technique are commercially available (angular SPR; illustrated in Fig. I8)¹¹⁸. An alternative to this technique would be to use a constant angle and change the wavelength until resonance occurs (wavelength SPR)¹¹⁹. This technique is not used widely.

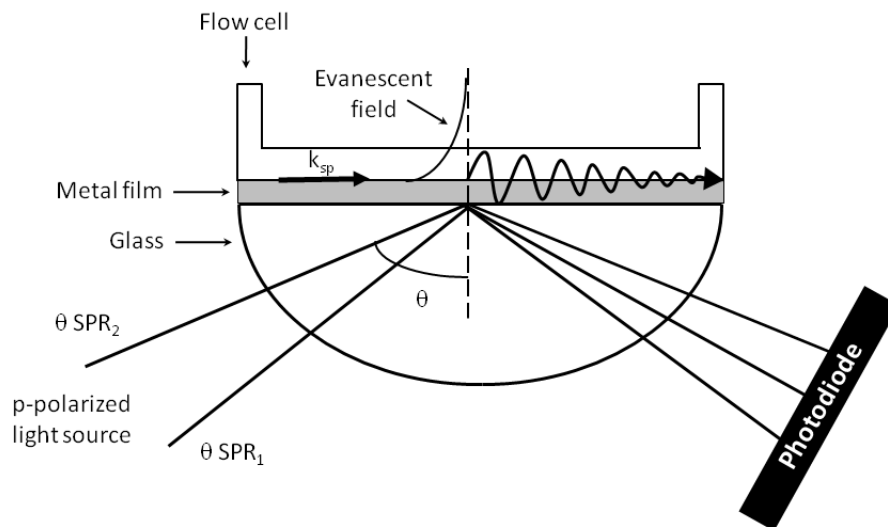


Figure I8: Principle of an angular based SPR spectroscopy. P-polarized light is beamed onto a thin metal layer. If the angle of incident light is adapted to achieve momentum resonance, the intensity of the reflected light is minimal. This is because the energy is transferred to the electrons in the conducting layer of the metal surface. Source: Andrade, *et al.*¹²⁰.

3.2.5 Protein interactions with SPR

SPR mainly depends on the conducting metal film, the wavelength of the incident light and the refractive index of the medium on the metal film. The metal film must contain conducting

electrons, which are able to resonate with the incoming light at an appropriate wavelength. Examples which fulfill this are silver, gold, copper, aluminium, sodium and indium. Secondly, the metal should be chemically inert and must be free of oxides or sulphides. This is why gold became practical for SPR experiments. The refractive index, on the other hand, is dependent on the temperature, because it influences the density of the medium.

The binding of molecules results in a change of the refractive index and thus changes the resonance angle of the photons (Fig. I9). There is a linear correlation of the change in the refractive index and the number of molecules on the surface, at least in the case of proteins. This observation simplified a broad introduction of SPR-spectroscopy for interaction studies in life sciences.

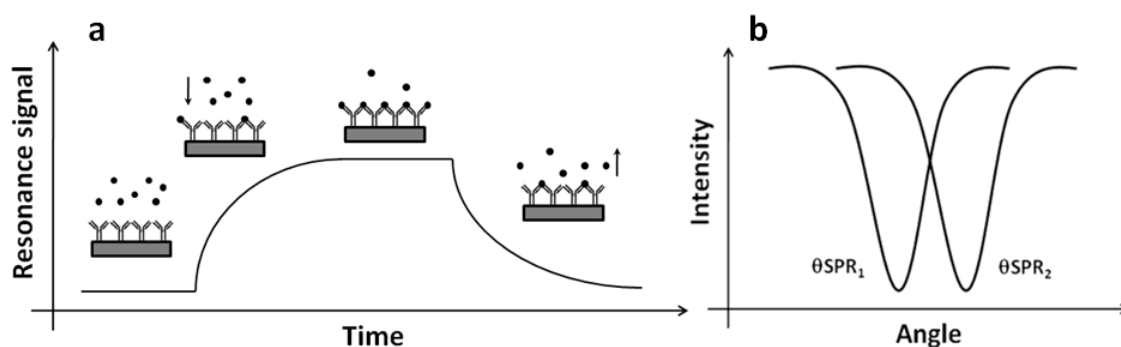


Figure I9: Illustration of SPR with biological samples¹²⁰. If the free analyte is binding to the immobilized ligand, the mass on the surface and thus the refractive index changes. This has the consequence that the angle of momentum resonance is shifted b). When the angle in real-time is plotted, a sensorgram with an increasing signal is obtained a). If the analyte is dissociating again, the sensorgram shows a decreasing signal a). Both are necessary for estimating the binding velocities and the affinity of the interaction. Source: Andrade, *et al.*¹²⁰

3.3 Biolayer interferometry

In principle, the technique of optical interferometry is simpler than exploiting the SPR-phenomenon. If two light waves of the same wavelength are in phase the amplitude of the waves is the sum of both. In contrast, if both waves are completely out of phase, the amplitudes sum to zero.

The Octet system from ForteBio applies a single-use sensor with a biocompatible matrix for ligand immobilization. These sensors contain a semi-reflective layer below the layer containing the ligand. A part of the incoming white light is reflected back and used as reference. A small percentage of the residual light is reflected back at the layer containing the ligand. Dependent on the refractive index there is a phase shift. A simple spectrometer is used to measure the phase shift based on the light intensity. Unfortunately, there is no published

information about how the signals of the different wavelength are combined to give the final phase shift signal read out by the software.

3. Material and Methods

3.1 Material:

Tris/Tricine gel electrophoresis

Resolving gel	16.5 % (v/v) Acrylamide, 30 % (v/v) gel buffer, 10.6 % (v/v) glycerol, 0.33 % (v/v) APS, 0.016 % (v/v) TEMED
Spacer gel	10 % (v/v) Acrylamide, 33 % (v/v) gel buffer, 1 % (v/v) APS, 0.05 % (v/v) TEMED
Stacking gel	4 % (v/v) Acrylamide, 24.8 % (v/v) gel buffer, 0.67 % (v/v) APS, 0.033 % (v/v) TEMED
Buffer for gels	1 M Tris-HCl pH 8.45, 0.1 % SDS (w/v)
Buffer for cathode	0.1 M Tris-HCl pH 8.25, 0.1 M Tricin, 0.1 % SDS (w/v)
Buffer for anode	0.2 M Tris-HCl pH 8.9

Standard gel electrophoresis

Stacking gel	5 % (v/v) Acrylamide, 125 mM Tris-HCl pH 6.8, 0.1 % (w/v) SDS, 0.06 % (v/v) APS, 0.06 % (v/v) TEMED
Resolving gel	15 % (v/v) Acrylamide, 375 mM Tris-HCl pH 8.8, 0.1 % (w/v) SDS, 0.1 % (v/v) APS, 0.04 % TEMED
Running buffer	50 mM Tris-HCl pH 8.3, 385 mM glycine, 0.1 % (w/v) SDS

Culture media

Lysogeny broth (LB)	5 g l ⁻¹ Yeast extract, 10 g l ⁻¹ Tryptone, 10 g l ⁻¹ NaCl, 10 ml l ⁻¹ 20 % Dextrose, 5 ml l ⁻¹ 2 M MgCl ₂ , pH 7.4
2X Yeast extract and Tryptone (2YT)	10 g l ⁻¹ Yeast extract, 16 g l ⁻¹ Tryptone, 5 g l ⁻¹ NaCl, 10 ml l ⁻¹ 20 % Dextrose, 5 ml l ⁻¹ 2 M MgCl ₂ , pH 7.4

Buffers for amine coupling

Wash buffer for amine coupling i)	0.1 M Tris-HCl, pH 9.0, adjusted with HCl
Wash buffer for amine coupling ii)	0.1 M sodium acetate, 0.5 M NaCl, pH 4.0, adjusted with acetic acid
Column binding buffer	0.2 M NaHCO ₃ , 0.5 M NaCl, pH 8.3, adjusted with Na ₂ HCO ₃ /NaH ₂ CO ₃
Blocking buffer	0.5 M ethanolamine, 0.5 M NaCl, pH 8.3, adjusted with acetic acid

Buffers for protein purification

Suspension buffer for <i>E. coli</i>	50 mM Tris-HCl pH 8.0, 1 mM EDTA, 1 mg/ml Lysozyme
Chemical lysis buffer for <i>E. coli</i>	8.33 mM imidazole, 833 mM NaCl, 16.6 mM CaCl ₂ , 1 % Triton X-100
Denaturation buffer	8 M Urea, 50 mM Tris-HCl pH 7.2, 500 mM NaCl
Renaturation Buffer	50 mM Tris-HCl pH 7.2, 500 mM NaCl

Standard buffers

Density Gradient Centrifugation (DGC)	10 mM Na ₂ HPO ₄ /NaH ₂ PO ₄ , 5 % to 50 % Iodixanol, pH 7.4 adjusted with NaH ₂ PO ₄
Size Exclusion Chromatography (SEC)	50 mM Na ₂ HPO ₄ /NaH ₂ PO ₄ , 150 mM NaCl, 0.6 %

Phosphate Buffered Saline (PBS)	Tween 20, pH 7.4 adjusted with NaH ₂ PO ₄ 10 mM Na ₂ HPO ₄ /NaH ₂ PO ₄ , 137 mM NaCl, pH 7.4 adjusted with NaH ₂ PO ₄
4X-Laemmli sample buffer	40 % (v/v) Glycerol, 8 % (v/v) β -ME, 200 mM Tris-HCl pH 6.8, 3 g/l Bromophenol blue
Strain	Genotype
<i>E. coli</i> BL21(DE3)	F ⁻ ompT gal dcm lon hsdSB(rB ⁻ mB ⁻) λ (DE3 [lacI lacUV5-T7 gene 1 ind1 sam7 nin5])
<i>E. coli</i> Mach1	Δ recA1398 endA1 tonA Φ 80 Δ lacM15 Δ lacX74 hsdR(r _K ⁻ m _K ⁺)
<i>E. coli</i> OmniMAX2	F ['] (proAB ⁺ lacIq lacZ Δ M15 Tn10(TetR) Δ (ccdAB)) mcrA Δ (mrr-hsdRMS-mcrBC) Φ 80lacZ Δ M15 Δ (lacZYA- argF) U169 endA1 recA1 supE44 thi-1 gyrA96 relA1 tonA panD
Plasmid	Insert
pET-22b-A β 16-GB1	Fusion protein: A β (1-16)-GB1
pET-22b-scFv-IC16-His6	scFv-IC16 with His ₅ -Tag

3.2 Methods:

3.2.1 Expression of A β (1-16)-GB1

For recombinant production of A β (1-16)-GB1, *E. coli* BL21 DE3 pRARE2 was transformed with the expression vector pET22b-A β (1-16)-GB1. 1 l LB expression culture was inoculated with an aliquot of a 50 ml overnight LB culture (grown at 37 °C, 150 rpm) to a final OD₆₀₀ of ~0.1. Cells were grown at 37 °C (150 rpm) to an OD₆₀₀ of 0.6 until IPTG was added to a final concentration of 1.0 mM for induction of protein expression. Expression was carried out for 3 hours at 37 °C under gentle agitation (150 rpm). Cells were harvested by centrifugation (30 min, 4 °C, 4000 g), pellets washed with PBS and stored at -20 °C until further use.

3.2.2. Purification of A β (1-16)-GB1

Pellet was resuspended in 20 ml suspension buffer for *E. coli*, supplemented with protease inhibitors (Complete EDTA-free Protease Inhibitor Cocktail Tablets, Roche). For cell lysis, cells were pumped through a microfluidizer for three times at 25,000 Pa (HORIBA M-110P). After centrifugation for 30 min at 20,000 g the pellet was discarded. Supernatant containing A β (1-16)-GB1 was purified by affinity chromatography with IgG-Sepharose from Qiagen (CV: 3 ml) that was equilibrated with the suspension buffer for *E. coli*. Supernatant was loaded onto the column by gravity flow, followed by washing steps with two CVs of PBS. Elution was done with five CV 50 mM glycine buffer, pH 2.5. After purification A β (1-16)-GB1 was dialyzed against the column binding buffer for amine coupling for the subsequent

amine coupling procedure. Expression and purification was checked by SDS-PAGE (0.25 mA per cm²) with a tris/tricine gel (Fig. M1).

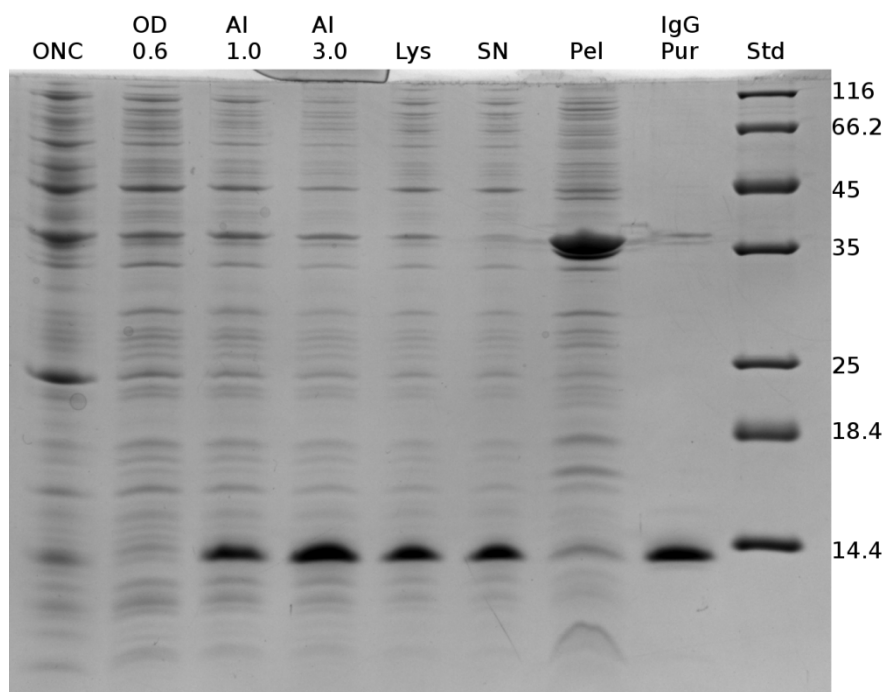


Figure M1: Expression of A β (1-16)-GB1 in *E. coli*. ONC: overnight culture, OD_{0.6}: immediately before induction at optical density at 600 nm of 0.6, AI1.0: 1 h after induction, AI3.0: 3 h after induction, Lys: cell lysate, SN: supernatant of the lysate, Pel: pellet of the lysate, IgG Pur: After IgG affinity purification, Std: marker

3.2.3 Creation of an A β (1-16)-GB1affinity purification sepharose

Prior to the coupling step, solutions have been cooled down (4°C) and the time intervals for all washing steps were minimized. Firstly, the NHS-activated Sepharose was washed with 10 CV 1 mM HCl. Then the pH was adjusted by washing with 3 CV column binding buffer for amine coupling. Coupling was done by incubating the column material with A β (1-16)-GB1 in the column binding buffer for amine coupling at RT for 4 hours. After coupling, the column was drained from the supernatant and any non-reacted groups were blocked by addition of column blocking buffer for amine coupling over night at 4°C. Then the column material was washed three times with each wash buffer for amine coupling (i and ii). Then the column material was transferred into a 20 % ethanol solution containing 0.01 % NaN₃ to prevent microbial growth.

3.2.4 Expression of the scFv-IC16

For recombinant production of scFv-IC16, *E. coli* BL21 DE3 pRARE2 was transformed with the expression vector pET22b-scFv-IC16-5His. Each 1 l 2YT expression culture was inoculated with an aliquot of a 50 ml overnight LB culture (grown at 37 °C, 150 rpm) to a final OD₆₀₀ of ~0.1. Cells were grown at 37 °C (150 rpm) to an OD₆₀₀ of 1.6-1.8. Subsequently, cultures were chilled for 1 hour at 4 °C until IPTG was added to a final concentration of 1.0 mM for induction of scFv-IC16 protein expression. Expression was carried out for 24 hours at 18 °C under gentle agitation (150 rpm). Cells were harvested by centrifugation (30 min, 4 °C, 3750 rpm), pellets washed with PBS and stored at –20 °C until further use (this step is the *critical*, as it renders further Ni²⁺ affinity purification unnecessary and thus enhances the amounts of yield; illustrated by the ~60 % purified pellet fraction in Fig. M2). Expression was checked by SDS-PAGE (0.4 mA per cm²; Fig. M2).

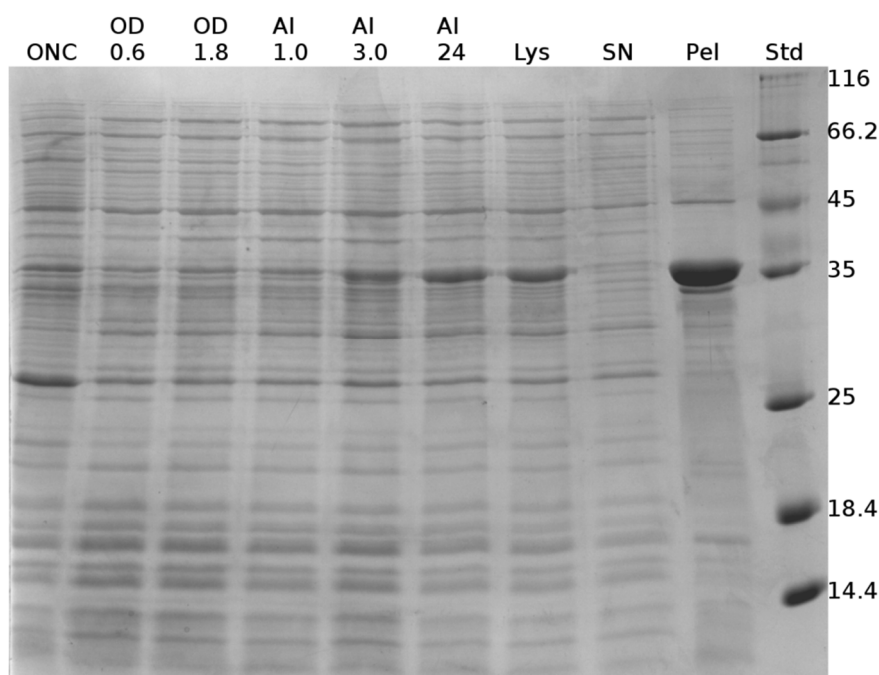


Figure M2: Expression of scFv-IC16 in *E. coli*. ONC: overnight culture, OD0.6: before induction at OD₆₀₀ 0.6, OD1.8: immediately before induction at OD₆₀₀ 1.8, AI1.0: 1.0 h after induction, AI3.0: 3.0 h after induction, AI24: 24 h after induction, Lys: cell lysate, SN: supernatant fraction of the lysate, Pel: pellet fraction of the lysate.

3.2.5 Purification of scFv-IC16

Bacterial pellets were resuspended in PBS supplemented with protease inhibitors (Complete EDTA-free Protease Inhibitor Cocktail Tablets, Roche). For cell lyses, cells were pumped through a microfluidizer (HORIBA M-110P) for three times at 25,000 Pa. Suspensions were gently centrifuged (45 min, 10,000 g) and the supernatant discarded. The pellet was washed

until it was white with ddH₂O (30 min, 10,000 g) and resolved in denaturation buffer. For refolding, renaturation buffer was added to elution fractions in a 10:1 ratio (v/v). Afterwards, an affinity chromatography purification was performed with A β (1-16) coupled NHS-sepharose (Pierce). After equilibration with a 10:1 mixture of renaturation buffer and denaturation buffer, fractions containing scFv-IC16 were loaded onto the column. A washing step with 10 CVs renaturation buffer removed non-bound material. Elution was achieved with 50 mM glycine, pH 2.5. Each elution fraction was immediately neutralized by addition of 50 μ l 2 M Tris-HCl, pH 8.0 per ml fraction volume and checked by SDS-PAGE (0.4 mA per cm²; Fig. M3). Fractions containing scFv-IC16 were pooled, dialyzed against PBS, and concentrated to a final concentration of 5 μ M with Vivaspin 20 columns from Sartorius Stedim (3000 MWCO PES).

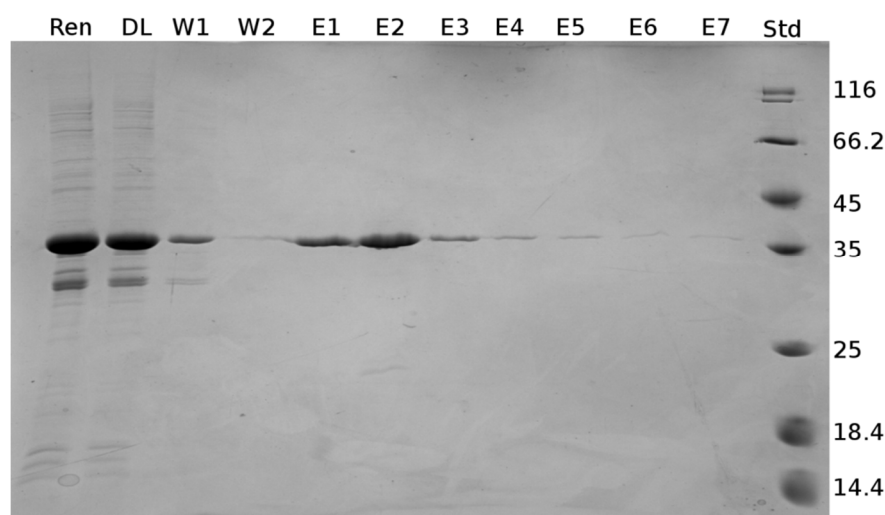


Figure M3: Purification of scFv-IC16 in *E. coli*. Ren: renaturated scFv-IC16, DL: flow through of affinity purification, W1-2: washing fractions 1-2, E1-E7: eluate fractions 1-7, Std: marker

3.2.6 Preparation of A β (1-42) monomers and SEC oligomers

The protocol used by Johansson, et al.¹²¹ was adapted for A β (1-42) monomer and oligomer preparation by SEC with minor modifications. Lyophilized stocks of A β (1-42) (Bachem), carboxy-terminally biotinylated A β (1-42) (Eurogentec) and amino-terminally biotinylated A β (1-42) (Anaspec) were separately dissolved in 100 % hexafluoroisopropanol (HFIP) and incubated overnight at RT. In the case of oligomer preparations, amino-terminally biotinylated A β (1-42) and non-biotinylated A β (1-42) were mixed in a 1:10 ratio. After incubation, solutions were divided into 125 μ g aliquots. HFIP was removed by evaporation in a Concentrator 5301 (Eppendorf). A β (1-42) was resolubilized in 100 μ l SEC-buffer and briefly centrifuged (30 s) at 15,000 g to sediment insoluble material immediately prior to

separation by SEC. Separation was performed with a Superdex 75 10/300 GL column operated at RT by an Äkta purifier system at a flow rate of 0.8 ml min⁻¹. For each single run ~100 µl of solubilized Aβ(1-42) was loaded onto the column. Monomers eluted at ~14 ml, whereas oligomers eluted close to the void volume (at ~8 ml). Samples were immediately used for immobilization on sensor chip surfaces. Initially, for establishment of the immobilization assay a BCA-assay was used to correlate the absorbance at 214 nm of the SEC fractions to the overall Aβ concentration. It was observed, that an A₂₁₄ = 250 mAU (oligomers) or A₂₁₄ = 150 mAU (monomers) in the size exclusion chromatogram correlates with ~1 µM total Aβ concentration derived from a BCA-assay. Omitting the BCA-assay step dramatically reduces the time between elution and immobilization. For immobilization of monomers and oligomers (10 % amino-terminally biotinylated) Aβ(1-42) concentrations of ~10 nM and ~100 nM, respectively, were used.

3.2.7 Density gradient centrifugation (DGC)

The gradient was prepared in thin-walled ultracentrifugation tubes (Ultra-Clear 11 x 34 mm, 2.2 ml from Beckman) by successively overlaying the following volumes of DGC-buffer solutions: 260 µl 50 %, 260 µl 40 %, 260 µl 30 %, 780 µl 20 %, 260 µl 10 % and 100 µl 5 % (v/v). After addition of 100 µl sample, the gradient was centrifuged (3 h, 4°C, 259,000 g, lowest acceleration/deceleration) using a TLS-55 rotor in a benchtop ultracentrifuge Optima TL-100 (Beckman-Coulter). From each gradient, 14 fractions of 140 µl were harvested from top to bottom. Monomers were harvested from fraction one, oligomers from fractions four to six and fibrils from fractions 11 to 13.

3.2.8 Preparation of Aβ(1-42) assembly states by DGC

The protocols used by Wood, et al.¹²² and Nagel-Steger, et al.¹²³ were adapted for Aβ(1-42) fibril preparation with minor modifications. Lyophilized aliquots of Aβ(1-42) and amino-terminally biotinylated Aβ(1-42) were dissolved separately in 100 % HFIP and incubated at RT overnight. For oligomer and fibril production, biotinylated Aβ(1-42) and non-biotinylated Aβ(1-42) in HFIP were mixed in a 1:10 ratio and subsequently divided into 72 µg aliquots. For creation of monomers, amino-terminally biotinylated Aβ(1-42) was dissolved in 100 % HFIP, incubated at RT overnight and subsequently divided into 72 µg aliquots. HFIP was removed by evaporation in a Concentrator 5301 (Eppendorf). Then, Aβ pellets were solubilized in 200 µl sodium phosphate buffer pH 7.4 (10 mM; yielding an 80 µM Aβ solution) and incubated for 3 hours (oligomers) or 24 hours (fibrils) at 25 °C (600 rpm). Samples for monomer production were not incubated.

3.2.9 Immobilization via SA-coupling for SPR-spectroscopy

For SPR experiments Series S Sensor Chips SA (GE Healthcare Life Sciences) in combination with a Biacore T200 system were used. Series S Sensor Chips SA are coated with streptavidin and allow ligand immobilization based on the biotin-streptavidin interaction. For our experiments PBS (filtered with 0.2 μm , PVDF) was used as running buffer. After docking a new sensor chip, the system was initiated with a “Prime” command and the detector normalized with 70 % glycerol (GE Healthcare Life Sciences). All flow cells were activated with three consecutive one minute injections of 1 M NaCl in 50 mM NaOH. For ligand immobilization the flow rate was adjusted to 5 $\mu\text{l min}^{-1}$ in order to minimize sample consumption. After immobilization the flow cells were stabilized by a constant flow overnight to remove unspecific bound material and detergent. To do so, the flow speed and temperature was set to 30 $\mu\text{l min}^{-1}$ and 25 $^{\circ}\text{C}$ respectively.

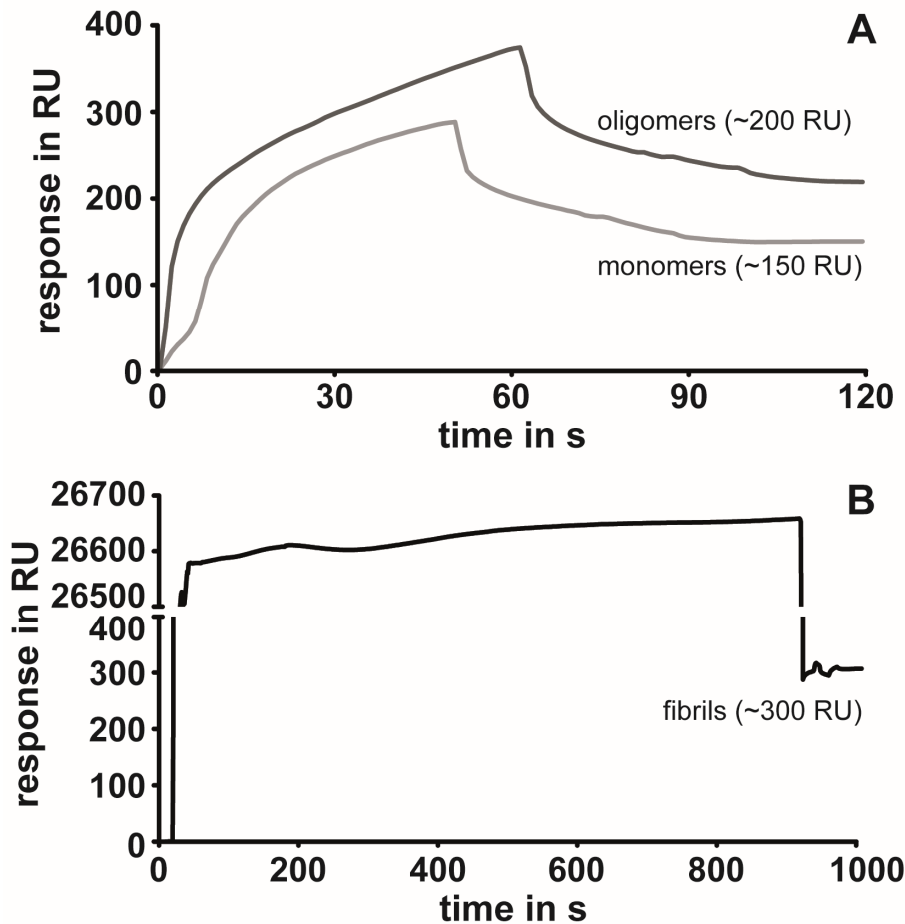


Figure M4: Illustration of an immobilization experiment. Immobilization of A β without (A) and with (B) iodixanol. Noticeable on the huge baseline jump because of the change of the refractive index at high iodixanol concentrations.

3.2.10 Binding kinetics of scFv-IC16 with SPR-spectroscopy

For SPR experiments Series S Sensor Chips SA (GE Healthcare Life Sciences) in combination with a Biacore T200 system were used. For interaction studies the flow speed and temperature were adjusted to 30 $\mu\text{l min}^{-1}$ and 25 °C respectively. All interaction studies were performed in the single-cycle kinetic mode ¹²⁴. Here, five different analyte concentrations were injected within a single cycle (contact time: 90 s, final dissociation time after the highest concentration: 1800 s) in order of increasing concentration. The applied analyte concentrations for scFv-IC16 were 312.5, 625, 1250, 2500 and 5000 nM. Binding studies with monoclonal antibody 6E10 were performed with concentrations of 0.32, 1.6, 8, 40 and 200 nM. All binding data were double referenced by collecting data in dual-channel mode with an untreated and therefore not A β (1-42) containing reference flow cell connected upstream of the flow cell with the respective A β (1-42) assembly state and by the subsequent subtraction of a blank buffer injection (1 \times PBS) from the obtained binding responses. Double referenced SPR data were evaluated with Biacore T200 Evaluation Software (version 1.0) using the available binding models. A β monomer data was fit to a 1:1 binding model, whereas sensorgrams of A β oligomers and fibrils were analyzed with a heterogeneous ligand binding model accounting for two separate ligand sites for analyte binding. Values for bulk refractive index (R_I) was manually set to zero, because double-referencing was applied and low amounts of ligand were immobilized.

3.2.11 Binding kinetics of Fab fragments with SPR-spectroscopy

For SPR experiments Series S Sensor Chips SA (GE Healthcare Life Sciences) in combination with a Biacore T200 system were used. For interaction studies the flow speed and temperature were adjusted to 30 $\mu\text{l min}^{-1}$ and 25 °C respectively. All interaction studies were performed in the single-cycle kinetic mode¹²⁴. Here, five different analyte concentrations were injected within a single cycle (contact time: 90 s, final dissociation time after the highest concentration: 1800 s) in order of increasing concentration. The applied analyte concentrations for Fab fragment 6 (Probiodrugs) were: 3.9, 15.6, 62.5, 250 and 1000 nM and for Fab fragment 17 (Probiodrugs) they were: 38.4, 96, 240, 600, 1500 nM. All binding data were double referenced by collecting data in dual-channel mode with an untreated reference flow cell connected upstream of the flow cell with the respective A β (1-42)/pE3-A β (3-40) assembly state and by the subsequent subtraction of a blank buffer injection (1 \times PBS) from the obtained binding responses. Double referenced SPR data were evaluated with Biacore T200 Evaluation Software (version 1.0) using the available binding models. A β monomer data was fit to a 1:1 binding model or a heterogeneous ligand model accounting for two

separate ligand sites for analyte binding. The value for bulk refractive index (R_I) was manually set to zero, because double-referencing was applied and low amounts of ligand were immobilized.

3.2.12 Binding kinetics of D-peptides with SPR-spectroscopy

For SPR experiments Series S Sensor Chips SA (GE Healthcare Life Sciences) in combination with a Biacore T200 system were used. All interaction studies were performed in the single-cycle kinetic mode¹²⁴. Here, five different analyte concentrations were injected within a single cycle (contact time: 90 s, final dissociation time after the highest concentration: 1800 s) in order of increasing concentration. The applied analyte concentrations for scFv-IC16 were 48.8, 195.3, 781.3, 3125 and 12500 nM. The other steps were according to the protocol used for the scFv interaction studies.

3.2.13 Preparation of CM7 chips for Thermodynamics with SPR

For thermodynamics the feasibility of Series S Sensor Chips CM7 (GE Healthcare Life Sciences) chips in combination with a Biacore T200 system were evaluated. These chips possess a higher surface capacity, which renders them useful for small analytes. Series S Sensor Chips CM7 were coated with 7500-8000 RU NeutrAvidin (from Pierce, dissolved in sodium acetate buffer pH 5.0, 50 $\mu\text{g ml}^{-1}$) with an amine-coupling procedure. For this, the flow cells were activated with 0.1 M NHS and 0.4 M EDC (10 min). After activation the ligand was injected into the flow cells. Finally the surface was washed with three 30 s pulses of 1 M ethanolamine (pH 8.0). Then, 2500 RU A β (1-42) monomers containing 100 % N-terminal biotinylated A β (1-42) were immobilized via biotin-SA coupling in the flow cells 2 and 4. Flow cells 1 and 3 were used as uncoated reference cells. For the experiments PBS (filtered with 0.2 μm , PVDF) was used as running buffer. After docking a new sensor chip, the system was initiated with a “Prime” command and the detector normalized with 70 % glycerol (GE Healthcare Life Sciences). After immobilization the flow cells were stabilized by a constant flow overnight to remove unspecific bound material and detergent. To do so, the flow speed and temperature was set to 30 $\mu\text{l min}^{-1}$ and 25 °C respectively.

3.2.14 Thermodynamics with SPR-spectroscopy

For interaction studies the flow speed and temperature were adjusted to 30 $\mu\text{l min}^{-1}$ and 4°C - 42°C respectively. All interaction studies were performed in the multi-cycle kinetic mode¹²⁴. Here, five different analyte concentrations were injected within a multiple cycles (contact time: 180 s, final dissociation time after the highest concentration: 600 s) in order of increasing concentration. The applied analyte concentrations for D-peptides were 390.6,

1562.5, 6250, 25000 and 100000 nM. The concentration of 6250 nM was injected two times to validate surface activity. The temperature measurement at 4°C was repeated once too. This was necessary to supervise the surface activity among the temperature iteration cycles. The surfaces were regenerated with 50 mM glycine buffer of pH 2.5. All binding data was double referenced by collecting data in dual-channel mode with an untreated and therefore not A β (1-42) containing reference flow cell connected upstream of the flow cell with the respective A β (1-42) assembly state and by the subsequent subtraction of a blank buffer injection (1× PBS) from the obtained binding responses. Double referenced SPR data were evaluated with Biacore T200 Evaluation Software (version 2.0) using the available binding models. A β monomer data was fit to a 1:1 Langmuir binding model. The value for bulk refractive index (R_I) was manually set to zero.

3.2.15 Immobilization of A β (1-42) on Super SA-biosensors for BLI

C-terminally biotinylated A β (1-42) (EUROGENTEC) was dissolved in 100 % HFIP and incubated at RT overnight. The stock solution was divided in 26.5 μ g aliquots. HFIP was removed by evaporation in a Concentrator 5301 (Eppendorf). A β was freshly solubilized in 550 μ l sodium phosphate buffer pH 7.4 (10 mM; yielding a 10 μ M A β solution). To separate the monomers from bigger particles, they were subjected to a density gradient centrifugation (DGC) as described in Frenzel *et al.* 2014. After centrifugation, fraction one (140 μ l) was used for immobilization of A β (1-42) monomers via standard Streptavidin-Biotin-coupling procedure with Super SA-sensors (ForteBio). It was planned to immobilize 0.15 nm, 0.25 nm and 0.75 nm of ligand on eight sensors respectively. Further eight sensors were used as reference and remained in phosphate buffer.

3.2.16 Parallel sensor kinetics of scFv-IC16 with BLI

Parallel sensor kinetics were performed in the interaction buffer (PBS with 0.5 % Polysorbate 20, 0.1 % BSA and 10 % NSB reducer from GE Healthcare). In total, five sensors were used to measure five different analyte concentrations in parallel, while one sensor was used to measure the buffer reference. Additional six sensors were used as sensor reference. All steps were performed at 25 °C with an agitation speed of 1000 rpm. 2.4 μ M scFv-IC16 was diluted four times with a dilution factor of two. To measure the interaction between A β (1-42) and scFv-IC16, the association and dissociation times were 270 and 90 s, respectively, for every analyte concentration. Data Analysis software: 8.0.0.35 was applied for measurements. The sensorgrams with the concentrations: 2400, 1200, 600, 300 and

150 nM were fitted with the BiaEvaluation software 4.1 from Biacore using a 1:1 binding model without R_i -term.

3.2.17 Kinetic titration series of the scFv-IC16 with BLI

To measure the affinity between scFv-IC16 and A β (1-42), the association and dissociation phases were recorded for 270 and 90 s, respectively, for every analyte concentration. Five sensors recorded the kinetic titration series, whereas one sensor recorded the buffer reference signal and six sensors were used as sensor reference. All steps were performed at 25 °C with an agitation speed of 1000 rpm. The other steps are comparable with section. Data Analysis software: 8.0.0.35 was applied for measurements. The sensorgrams with the concentrations: 2400, 1200, 600, 300, and 150 nM were fitted with the BiaEvaluation software 4.1 from Biacore with a 1:1 kinetic titration series model without a R_i -term.

3.2.18 Sample preparation for TEM and evaluation

Lyophilized stocks of A β (1-42) (Bachem), carboxy-terminally biotinylated A β (1-42) (Eurogentec) and amino-terminally biotinylated A β (1-42) (Anaspec) were separately dissolved in 100 % hexafluoroisopropanol (HFIP) and incubated overnight at RT. Amino-terminally and carboxy-terminally biotinylated A β (1-42) were mixed in a 1:10 ratio with non-biotinylated A β (1-42). The solutions were divided in 90 μ g aliquots. HFIP was removed by evaporation in a Concentrator 5301 (Eppendorf). The pellets were resolved in 10 mM sodium phosphate buffer pH 7.4 by sonification and incubated for seven days at RT for fibril formation. For negative staining, the carbon coated side of each grid (Plano S162 formval/coal film, 200 copper mesh) was incubated with the subsequent sample (20 μ l sample, 3-5 min). The grids were gently washed three times with water to remove the buffer ingredients from the surface (20 μ l ddH_2O). Afterwards the fibrils were stained by uranyl acetate (1 % w/v in ddH_2O , filtered) for 3 min. Residual fluid was removed by a paper tissue. All grids were dried overnight before use. For microscopy a Zeiss Libra 120 TEM was used. The pictures were evaluated with ImageJ.

3.2.19 Atomic force microscopy of A β fibrils

A sample volume of 40 μ l was deposited onto a freshly cleaved mica crystal and left to adhere for 30 min, washed thirty times with 100 μ l drops of pure water, and dried under stream of nitrogen gas. The samples were imaged with a NanoWizard II AFM (JPK Instruments AG, Berlin, Germany) operating in alternating current AFM mode and using Olympus silicon tips on a silicon cantilever (OMCL-160TS-R3) with a typical tip radius of < 7 nm and a spring constant of 26 N/m at a drive frequency of 300 (\pm 100) kHz and a scan rate of 0.3-1 lines per

sec. All data were collected as 512x512 or 1024x1024 pixel images and processed using Gwyddion software 2.22. All images were leveled by mean plane subtraction to correct for tilting of the sample stage and servo range errors. Each scan line in the image was corrected for errors such as streaks, scratches, and noise related to the mica surface. The heights of individual fibrils were measured perpendicular to the fibrillar axis using the extract profile tool in the software “Gwyddion”. Fibril widths and lengths were quantified at half of the maximal heights (Schneider, Larmer *et al.* 1998). In AFM imaging, spatial resolution is limited by artificial broadening known as convolution effect which occurs when observed components are on the same or smaller size scale as the cantilever tip. To account for tip convolution, all measured widths and lengths were corrected for two times the tip size.

3.2.20 Dynamic light scattering

Samples containing $\text{d}_2\text{H}_2\text{O}$ and 312 μM D7RD2 in $\text{d}_2\text{H}_2\text{O}$ were analyzed at 25°C for at least 200 s (10 s sample time) with a scattering angle of 90° with a SpectroSize 300 from Molecular Dimensions. For this a clean quartz cuvette was used. Fitting of the size distributions were performed automatically with the manufacturer software.

4 Results

4.1 Characterization of A β (1-42) with TEM

The C-terminus of A β is crucial for fibril formation. The addition of a biotin tag at the N-terminus or the addition of a biotin tag via a lysine linker at the C-terminus may influence the fibril formation process. Thus, it is necessary to check the impact of C- or N-terminal biotinylation of A β (1-42) on fibril formation. For this purpose, mixtures of A β (1-42) with different amounts of C- or N-terminally biotinylated A β (1-42) were prepared. In detail, the samples contained either 100 % A β (1-42), or 100 % C- or N-terminally biotinylated A β (1-42) or 90 % A β (1-42) and either 10 % C- or N-terminally biotinylated A β (1-42). After preparation, the samples were incubated for 7 d.

During this 7 d period, A β (1-42) was able to aggregate completely into fibrils (Fig. R1: A/B). In contrast, C-terminally biotinylated A β (1-42) was not able to form fibrils (Fig. R1: E), but formed round shaped oligomer-like structures. N-terminally biotinylated A β (1-42) formed bunch-like fibrillar structures (Fig. R1: F). Mixtures containing 90 % A β (1-42) and either 10 % C- or N-terminal biotinylated A β (1-42) were both able to form fibrillar structures that were similar in appearance to fibrils observed with samples containing 100 % A β (1-42) (Fig. R1: C/D). The results indicate that smaller amounts of biotinylated A β (1-42) do not interfere with fibril formation. However, samples containing 100 % C-terminally biotinylated A β (1-42) did not form fibrils. Consequently, C-terminally biotinylated A β (1-42) was used in this work only for monomer preparations.

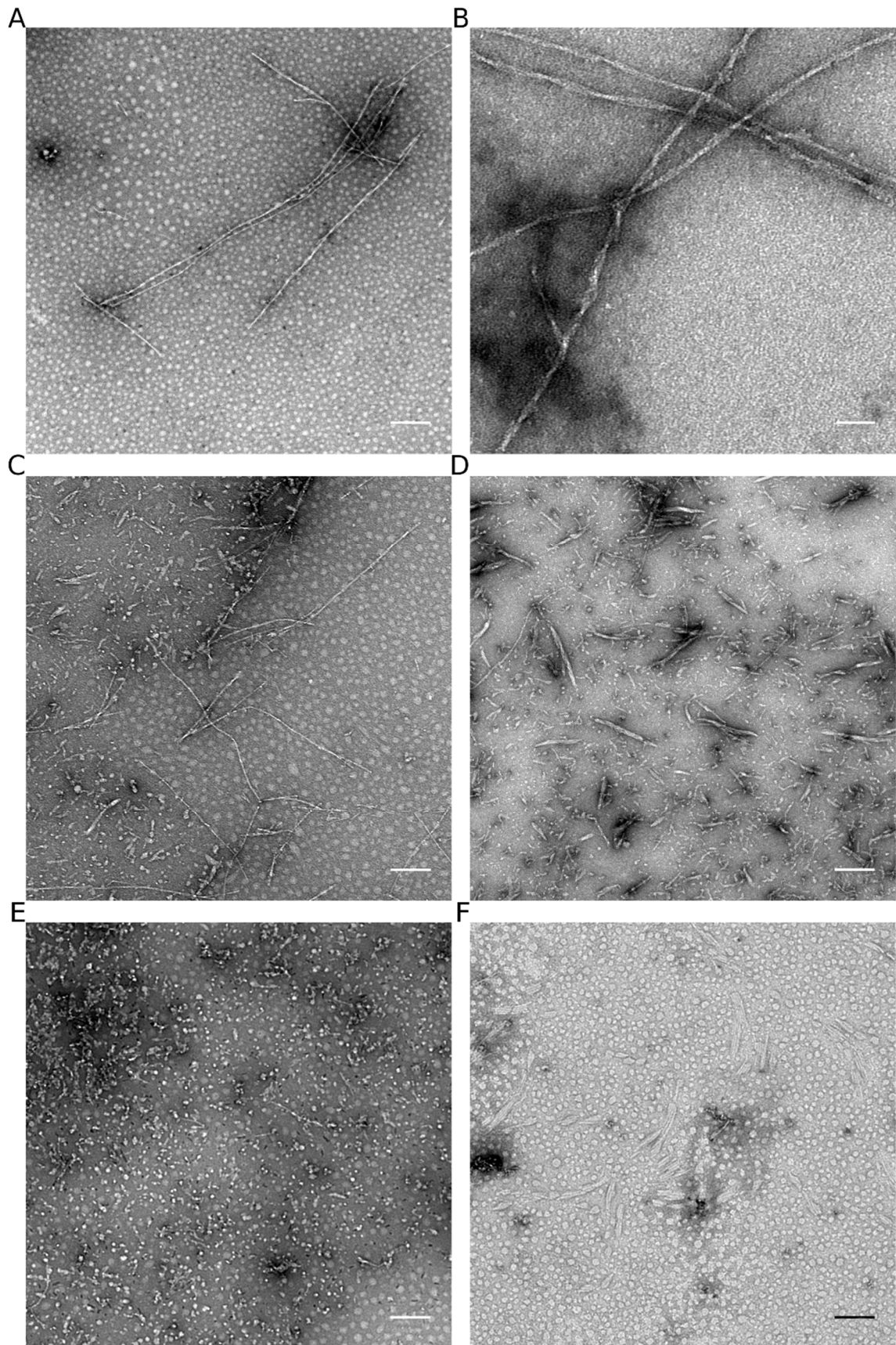


Figure R1: Influence of the biotinylation on the fibrillation of A β . A) and B) A β (1-42), C) 10 % A β (1-42)-Lys-Biotin and 90 % A β (1-42), D) 10 % Biotin-A β (1-42) and 90 % A β (1-42), E) 100 % A β (1-42)-Lys-Biotin, F) 100 % Biotin-A β (1-42). Scale bar: 0.2 μ m.

4.2 Time dependency of A β aggregation

The aggregation process of A β is time dependent. In this work, effort was spent on creating and purifying certain A β assembly states. One method to separate certain assembly states is density gradient centrifugation. To show whether this method is able to resolve A β in a time and size dependent manner, four A β samples were incubated for 0 h, 3 h, 24 h and 7 d. After the incubation period, these samples underwent DGC and SDS-PAGE (0.4 mA per cm²) with Tris/Tricine gels and silver staining (Fig. R2).

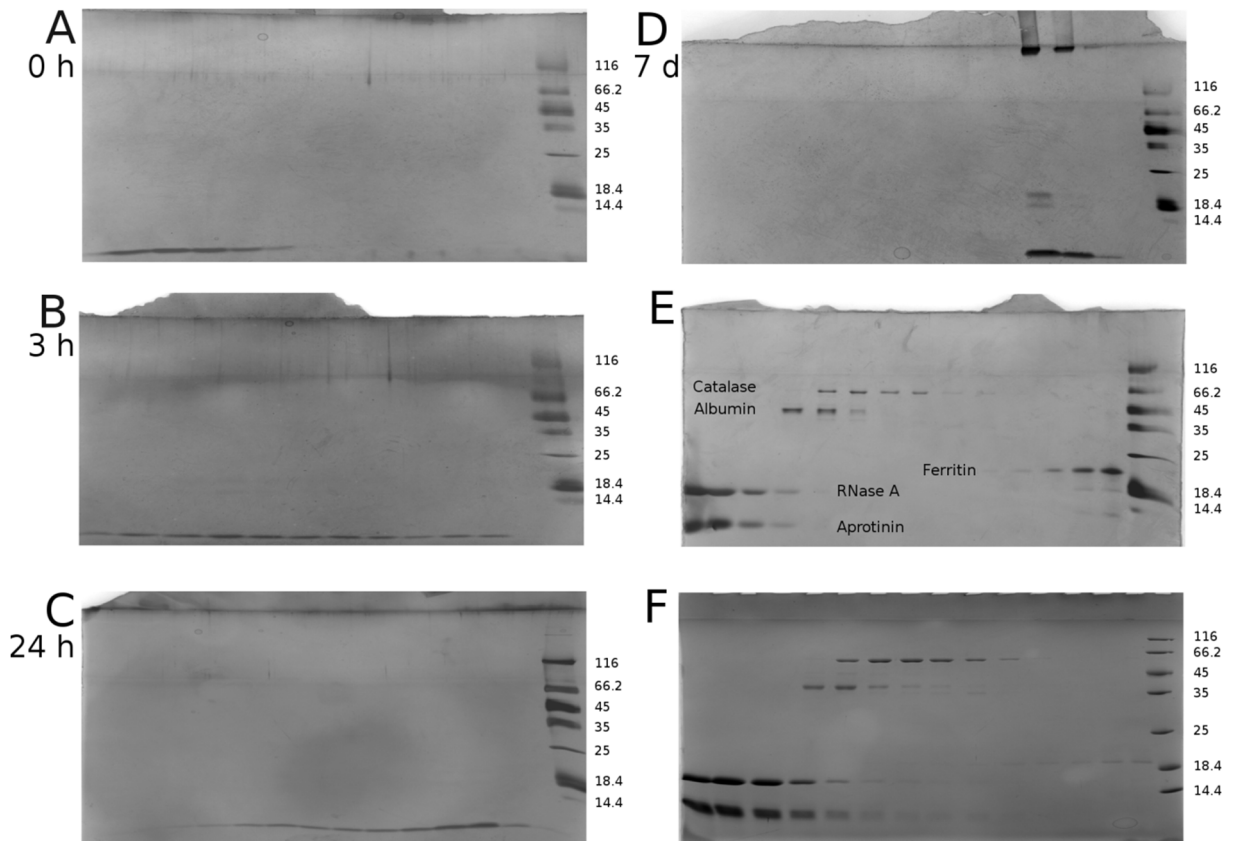


Figure R2: Validation of the density gradient centrifugation with A β . DGC-centrifugation of a A) non-incubated A β sample, B) 3 h incubated A β sample, C) 24 h incubated A β sample, and a D) 7 d incubated A β sample. E) and F) show standard runs with Albumin, Catalase (tetramer), Ferritin (24mer), RNase A and Aprotinin. A)-D) are silver stains with Tris/Tricine gels and F) shows a Coomassie stained gel.

A β is expected to form larger oligomeric species in a time-dependent manner, and thus initially, i.e., 0 h, will be predominantly monomers and progressively over time A β will form oligomeric species, with the end structures appearing as bunch-like fibrils, as observed with TEM after 7 d. Here, an alignment of the incubation time with the size distribution was attempted. With increasing time, the average size of the A β assembly states increased and after day seven the process of fibril formation was complete. The assay was able to show that even without an incubation period there were oligomeric A β species with masses up to 220 kDa (Fig. R2: A). After 3 h, the distribution pattern widened and A β species were found

in every fraction (Fig. R2: B), whereas after 24 h no low molecular weight species were found in the first four fractions (Fig. R2: C). After 7 d of incubation, A β was only found in the last three fractions, which corresponded to a molecular mass of > 440 kDa.

4.3 Characterization of A β (1-42) with AFM

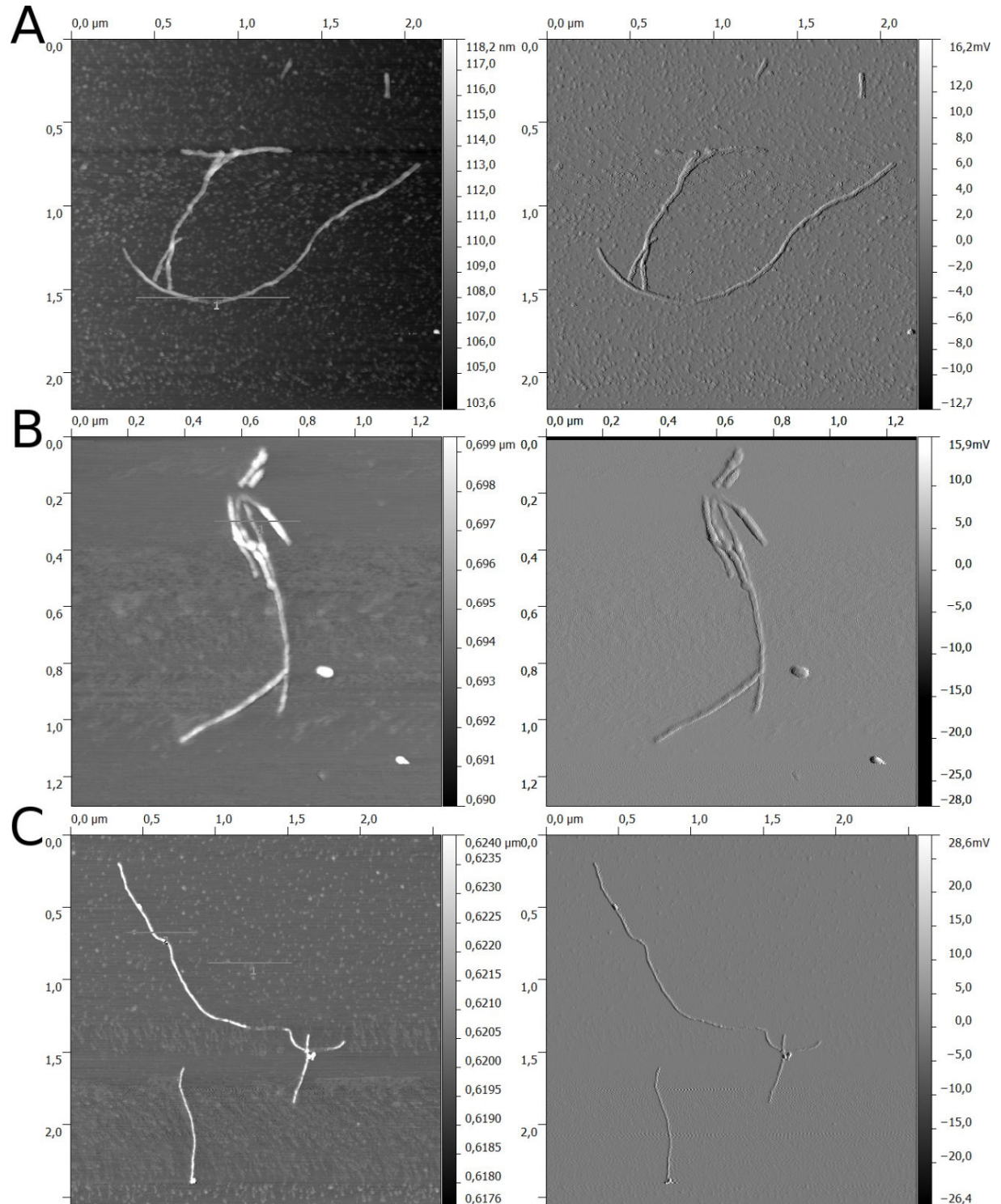


Figure R3: Analysis of A β (1-42) fibrils after DGC by atomic force microscopy. A) The fibrils were created in 10 mM sodium phosphate buffer (pH 7.4) for 24 h and in the case of B/C) separated by density gradient centrifugation to remove smaller A β (1-42) assembly states. Left columns shows maps and the right column the amplitude error map. The height distribution (indicated as bar(s) in the figures in the left column) has been plotted by a histogram (right column).

For SPR studies, the incubation time of A β (1-42) for fibril formation prior to immobilization was 24 h. To prove whether this time is sufficient for fibril or proto-fibril formation, atomic force microscopy (AFM) was applied. Additionally, the possible removal of smaller particles from fibrils by density gradient centrifugation (DGC) was tested. For this, samples containing 90 % A β (1-42) and 10 % N-terminal biotinylated A β (1-42) were incubated for 24 h. After incubation, one sample was purified by DGC and fractions 11-13 were used for further analysis. The other sample was not treated by DGC and used as a reference. Both samples were transferred to a mica surface and finally evaluated by AFM.

The presence of fibrillar species was observed in all samples (Fig. R3: A/B/C). Additionally, smaller non-fibrillar species were found in samples that were not further purified by DGC (Fig. R3/S1: A). In contrast, samples that underwent DGC showed significantly lower amounts and smaller non-fibrillar species (Fig. R3/S1: A vs. B/C).

In conclusion, these experiments showed that a percentage of up to 10 % biotinylated A β (1-42) does not disturb fibril formation, and that an incubation for 24 h is sufficient for fibril/protofibril formation. Finally, with DGC it was possible to reduce the amount of smaller oligomeric assembly states in the fibril preparation. Thus, DGC was applied as a method to reduce the amount of smaller A β species in the fibril preparations of experiments presented below.

4.4 Characterization of A β (1-42) with SPR

For immobilization of different A β (1-42) species a streptavidin-biotin-coupling procedure was chosen, because this approach avoids any requirement to change buffer conditions during A β (1-42) immobilization¹²⁵ and is compatible with many protocols. Due to the strong interaction of streptavidin and biotin, with a dissociation constant K_D of $\sim 10^{-15}$ M¹²⁶, there is virtually no loss of ligand during the experiment. Moreover, streptavidin-biotin-coupling can be used effectively to control the amount of bound ligand simply by varying the concentration of the ligand or the duration of the injection. Fig. R4 shows the experimental setup scheme for the preparation of different A β (1-42) species and their immobilization. Fig. M4 shows sensorgram examples for loading A β (1-42) monomers, oligomers and fibrils onto the chip surface.

Harsh regeneration steps between measurements will likely impair the immobilized A β (1-42) species and therefore such steps must be avoided. As an alternative, very long washing steps have been introduced between separate measurements. To avoid such long periods of washing, the so-called kinetic titration series (here also referred as single cycle kinetics)¹²¹,

where the analyte is injected in increasing concentrations without regeneration steps in-between, is the method of choice. In comparison with classical multi-cycle kinetics, sample consumption and analysis time is reduced and, most importantly, the need for regeneration is eliminated.^{124,127}

For assay development and for checking the quality of the surface characterization of immobilized A β species, the single-chain variable fragment (scFv-IC16) of the antibody IC16 was selected. IC16 was initially selected to target the first 16 amino-acid residues of A β .^{128,129} scFvs are easy to produce and purify, stable at high concentrations for at least weeks, and possess only a single binding site with high specificity for their epitope, thereby avoiding any avidity effects.

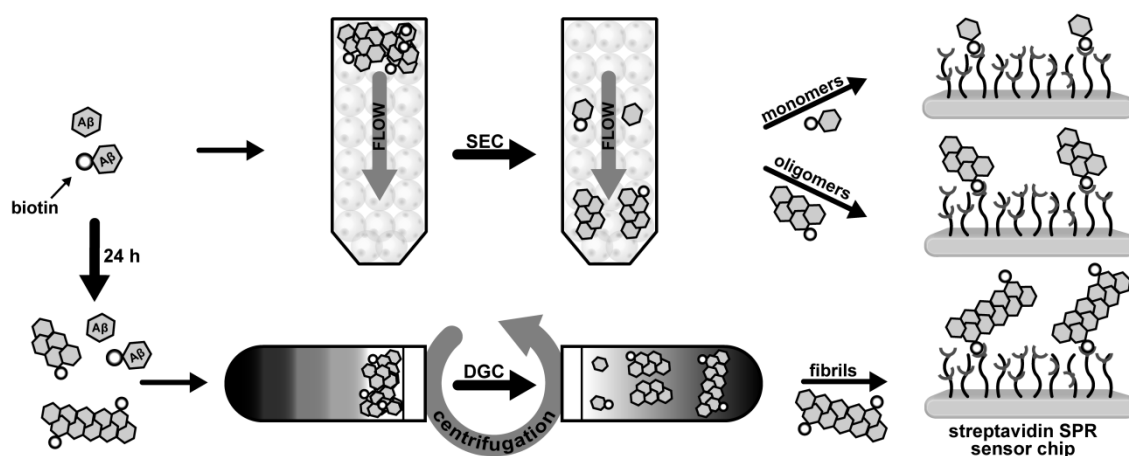


Figure R4: Surface preparation with different A β (1-42) assembly states for surface plasmon resonance (SPR) analysis. Size exclusion chromatography (monomers and oligomers) and density gradient centrifugation (fibrils) ensure highly pure samples for immobilization on sensor surfaces and subsequent SPR measurements.

4.5 Characterization of A β monomers with SPR

To test the specificity of scFv-IC16 to the amino-terminal part of A β , the chosen biotin-streptavidin immobilization procedure should be well-suited. The orientation of A β on the surface can be modulated easily by changing the location of the biotin tag. In theory it should therefore be possible to hide the epitope of scFv-IC16 by fusion of a biotin tag in close proximity. To achieve this, N-terminally biotinylated A β (1-42) monomers (Fig. M4 A) that were purified by size exclusion chromatography (SEC) were immobilized¹²¹. SEC purification ensures the monodispersity of A β monomers. Binding of an anti-A β (1-42) antibody (6E10) demonstrated that A β was successfully immobilized (Fig. R5: B). In contrast, binding of scFv-IC16 to the N-terminally biotinylated A β (1-42) monomer loaded surface could not be detected (Fig. R5: B). In contrast, C-terminally biotinylated A β (1-42) monomers that were

immobilized to the surface was bound by 6E10 and scFv-IC16 (Fig. R5: A). It was concluded that both, N- and C-terminally biotinylated A β monomers were successfully immobilized, but immobilization of N-terminally biotinylated A β (1-42) on the streptavidin-coated sensor chip restricts binding of scFv-IC16. To extract quantitative information from the experimental data of scFv-IC16 and C-terminally biotinylated A β (1-42), the obtained sensorgrams were fitted to a Langmuir 1:1 binding model. Refractive index correction (R_I) was not required because all binding data were double referenced prior to analysis. Fig. R5 and Table R1 show that the resulting fit represents the experimental data very well and yields a K_D of 0.77 μ M. A low χ^2 -value of 4.1 supports this finding. The comparison with steady state affinity analysis revealed an excellent match. With this approach, the K_D determined was equal to 0.97 μ M (χ^2 : 0.38).

Table R1: Overview of the kinetic rates for scFv-IC16 binding to different A β (1-42) assembly states obtained within the single-cycle kinetic SPR experiments. The hash (#) denotes that kinetic rates were determined with a heterogeneous binding model. Standard deviation with number of experiments is given in brackets.

	monomers	monomers [#]	oligomers [#]	fibrils [#]
k_{a1} [a]	$2.27 \cdot 10^4$	$2.16 \cdot 10^4$	$2.66 \cdot 10^4$ ($4.9 \cdot 10^3$; n=4)	$2.96 \cdot 10^4$ ($3.9 \cdot 10^3$; n=3)
k_{d1} [b]	$1.74 \cdot 10^{-2}$	$2.03 \cdot 10^{-2}$	$0.98 \cdot 10^{-2}$ ($1.8 \cdot 10^{-3}$; n=4)	$0.92 \cdot 10^{-2}$ ($1.5 \cdot 10^{-3}$; n=3)
K_{D1} [c]	$7.69 \cdot 10^{-7}$	$9.36 \cdot 10^{-7}$	$3.70 \cdot 10^{-7}$ ($1.4 \cdot 10^{-7}$; n=4)	$3.12 \cdot 10^{-7}$ ($7.5 \cdot 10^{-8}$; n=3)
k_{a2} [a]	-	$4.80 \cdot 10^4$	$1.03 \cdot 10^2$ ($9.2 \cdot 10^1$; n=4)	$4.54 \cdot 10^2$ ($3.7 \cdot 10^2$; n=3)
k_{d2} [b]	-	$4.78 \cdot 10^{-9}$	$5.76 \cdot 10^{-4}$ ($2.9 \cdot 10^{-3}$; n=4)	$1.93 \cdot 10^{-3}$ ($1.0 \cdot 10^{-3}$; n=3)
K_{D2} [c]	-	$9.90 \cdot 10^{-14}$	$5.60 \cdot 10^{-6}$ ($7.9 \cdot 10^{-6}$; n=4)	$4.26 \cdot 10^{-6}$ ($2.2 \cdot 10^{-6}$; n=3)
χ^2	4.1	2.4	3.0	1.2
R_{max1} [d]	36.6	36.2	69.1	89.3
R_{max2} [d]	-	1.6	206.1	143.1

[#]fit to a heterogeneous binding model. Units are: [a] Ms⁻¹, [b] s⁻¹, [c] M, and [d] RU.

4.6 Characterization of A β oligomers with SPR

A β (1-42) oligomers containing 10 % N-terminally biotinylated A β (1-42) were immobilized and checked for successful immobilization of A β with IgG 6E10 and scFv-IC16. To reduce the risk of sample heterogeneity, species different than oligomers were removed by SEC¹²¹. The obtained oligomers were immediately (taking ~10 min for the procedure) immobilized (Fig. M4: A). 6E10 and scFv-IC16 both bound to the A β oligomers on the surface (Fig. R5). Importantly, since N-terminally biotinylated monomers are not recognized by scFv-IC16, it was concluded that the obtained responses are due to scFv-IC16 binding to oligomers. Therefore, scFv-IC16 is a powerful tool for surface characterization and quality control of immobilized A β , and application as a molecular tool for SPR studies with A β in higher aggregation states is conceivable. Antibodies and their respective Fab fragments are often known to recognize both, linear and conformational epitopes. Binding curves were therefore

fit with a heterogeneous ligand binding model. Again, owing to double referencing, a refractive index (RI) correction was not required. Two separate K_D values have been obtained (0.37 μM and 5.60 μM ; χ^2 : 3.0) with affinities differing by one order of magnitude. Use of simpler models increased χ^2 by at least a factor of ten and supports the initial assumption of a second epitope of A β (1-42) oligomers for scFv-IC16. This effect is probably not caused by rebinding effects of the analyte. The total mass of immobilized A β (1-42) oligomers is very comparable with the amount of immobilized A β (1-42) monomers, in which clearly no rebinding could be observed (Fig. R5: A).

4.7 Characterization of A β fibrils with SPR

For immobilization of fibrils, an A β (1-42) mixture with 10 % N-terminally biotinylated A β (1-42) was used. To ensure the absence of lower molecular weight species, density gradient centrifugation (DGC) was applied for separation of fibrils from other oligomeric states and monomers. Iodixanol was used as the gradient medium, because this reagent has several advantages over other potential agents: it is non-ionic, forms self-generated gradients in comparatively short centrifugation times and, most importantly, it is iso-osmotic¹³⁰. This ensures a low influence on protein stability and structure. Nevertheless, AFM was used to analyse the potential influence of Iodixanol on the structural assembly of the prepared fibrils (Fig. R2). The obtained AFM results indicate that fibril formation is not altered by Iodixanol, that the fibrils are virtually identical to A β fibrils previously studied by AFM¹³¹ and that no background signal by lower molecular weight species such as oligomers can be observed. As observed for SEC-purified A β -oligomers, it was possible to immobilize reproducible amounts of the DGC separated A β -fibrils on the surface. The refractive index showed a dramatic jump following sample injection, because of the presence of Iodixanol (Fig. M4: B). Incubation of the flow cell in a continuous flow mode revealed a linear decay of 4 RU (RU: response units; a change of 1 RU corresponds to a mass change of approximately 1 pg per mm²) per hour after 8 h. This decay is assumed to be caused by a small amount of the fibrils dissociating, because similar decays have been observed previously for immobilized fibrils¹³². scFv-IC16 was able to bind to the fibril surface. The binding curves were fit with the identical model used for A β (1-42) oligomers. The resulting dissociation constants for scFv-IC16 binding to A β (1-42) fibrils were determined to be 0.31 μM and 4.26 μM (χ^2 : 1.2, Tab. 1), which are very similar to those obtained for A β oligomers.

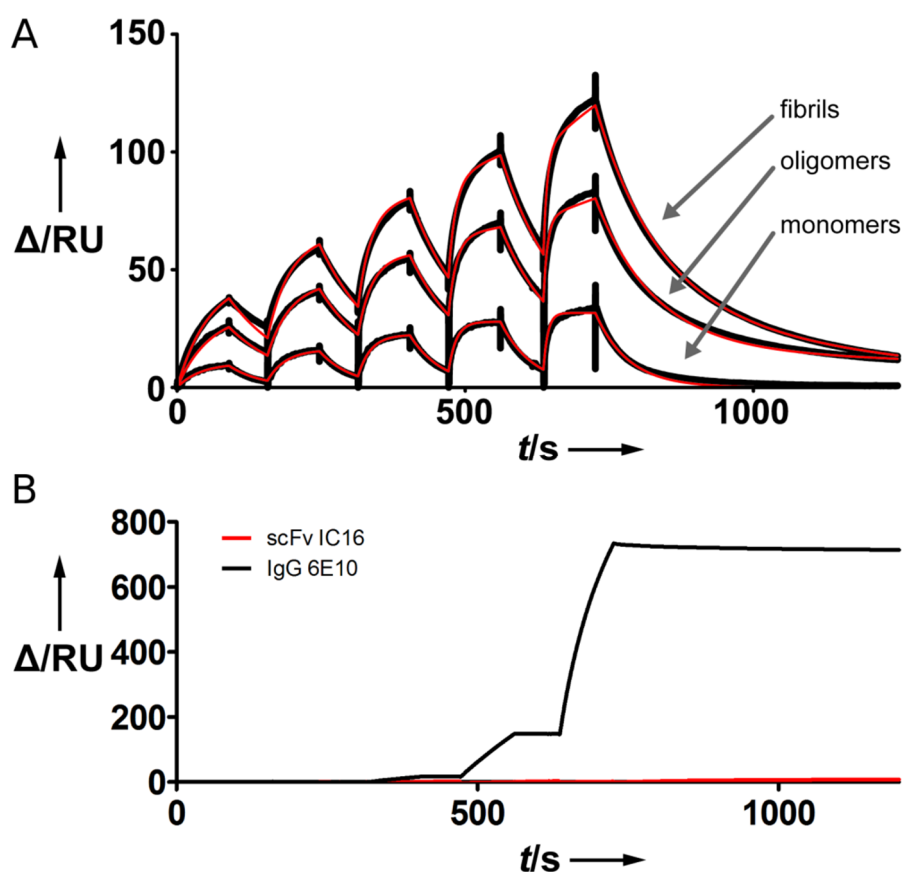


Figure R5: Surface plasmon resonance interactions of scFv-IC16 with A β . A) Interactions of scFv-IC16 with A β -monomers with a biotin tag at the C-terminus and oligomers/fibrils containing a mixture of 10 % N-terminally biotinylated A β (1-42) and 90 % A β (1-42) (immobilized in total: 100 – 200 RU). B) Shows a negative control where scFv-IC16 does not bind to N-terminally biotinylated A β -monomers (immobilized: ~1200 RU), and a positive control using IgG 6E10, which binds to N-terminally biotinylated A β -monomers (1200 RU).

4.8 Characterization of A β monomers with BLI

Biolayer interferometry (BLI) was applied to obtain another validation for the estimated K_D values of the interaction of the scFv-IC16 with A β (1-42) monomers. BLI has become an alternative method to SPR. One advantage of BLI is that the number of sensors can be scaled easily without making the system more error-prone or complex. Theoretically, there is no need to regenerate single sensors, because duplicates of the surface can be easily created by immobilizing an equal amount of ligand on additional sensors. However, this approach has some disadvantages. It is not possible to achieve identical ligand coatings of multiple sensors. Such an approach also increases sensor consumption and it is not guaranteed that the performance of each sensor is equivalent in later measurements. This results in fitting errors, especially if simple models without RI terms are used. Thus, to try to overcome these disadvantages, when compared with SPR, single cycle kinetics using BLI experiments were examined to determine whether this technique is feasible and accurate. Since the software did

not support the evaluation of single cycle kinetics, a script for data export was required. Unfortunately, with the available software it was just possible to fit 1:1 kinetic interactions. This is the reason, why just A β (1-42) monomers have been tested with BLI.

A comparison of parallel sensor kinetics with single cycle kinetics and the quality differences are illustrated in Fig. R6. With the scFv-IC16, the K_D s: 0.18 μ M / χ^2 : 7.17*10⁻⁵ for 0.15 nm ligand, 0.59 μ M / χ^2 : 2.25*10⁻⁴ for 0.41 nm ligand and 0.43 μ M / χ^2 : 9.69*10⁻⁴ for 1.01 nm ligand were obtained for parallel sensor kinetics. As expected the K_D s of the parallel sensor kinetics spread, show relatively high χ^2 , and just one measurement (Fig. R6: E) is close to the expected affinity range. In contrast, the kinetic titration series were showing less deviation and approve the SPR measurements.

Table R2: Comprehensive table of all evaluated fits. Fitting results for the measurements illustrated in Fig. R6. k_a : on-rate constant, k_d : off-rate constant, K_D : dissociation constant (k_d/k_a), RI_1 - RI_5 : baseline drift in nm, χ^2 : chi² in nm².

Fig. R6	k_a (1/Ms)	k_d (1/s)	R_{max} (nm)	K_D (M)	RI	χ^2
A)	3.4*10 ⁴	1.8*10 ⁻²	n.a.	5.4*10 ⁻⁷	0	3.9*10 ⁻⁵
B)	2.7*10 ⁴	1.8*10 ⁻²	n.a.	6.4*10 ⁻⁷	0	6.8*10 ⁻⁵
C)	2.0*10 ⁴	1.4*10 ⁻²	n.a.	7.1*10 ⁻⁷	0	2.4*10 ⁻⁴
D)	7.2*10 ⁴	1.3*10 ⁻²	0.11	1.8*10 ⁻⁷	0	7.2*10 ⁻⁵
E)	2.6*10 ⁴	1.5*10 ⁻²	0.68	5.9*10 ⁻⁷	0	2.3*10 ⁻⁴
F)	3.0*10 ⁴	1.3*10 ⁻²	1.60	4.3*10 ⁻⁷	0	9.7*10 ⁻⁴

With single cycle kinetics, the K_D s: 0.54 μ M / χ^2 : 3.87*10⁻⁵ for 0.15 nm ligand, 0.64 μ M / χ^2 : 6.80*10⁻⁵ for 0.41 nm ligand and 0.71 μ M / χ^2 : 2.44*10⁻⁴ for 1.01 nm ligand were estimated. Clearly for each different amount of ligand tested, the χ^2 -term is at least several fold smaller when compared with the results obtain using parallel sensor kinetics (see Fig. 2: A/B/C vs Fig. 2: D/E/F) and all the estimated K_D s (see Fig. R6 and Tab. R2) are close to the value estimated by SPR.

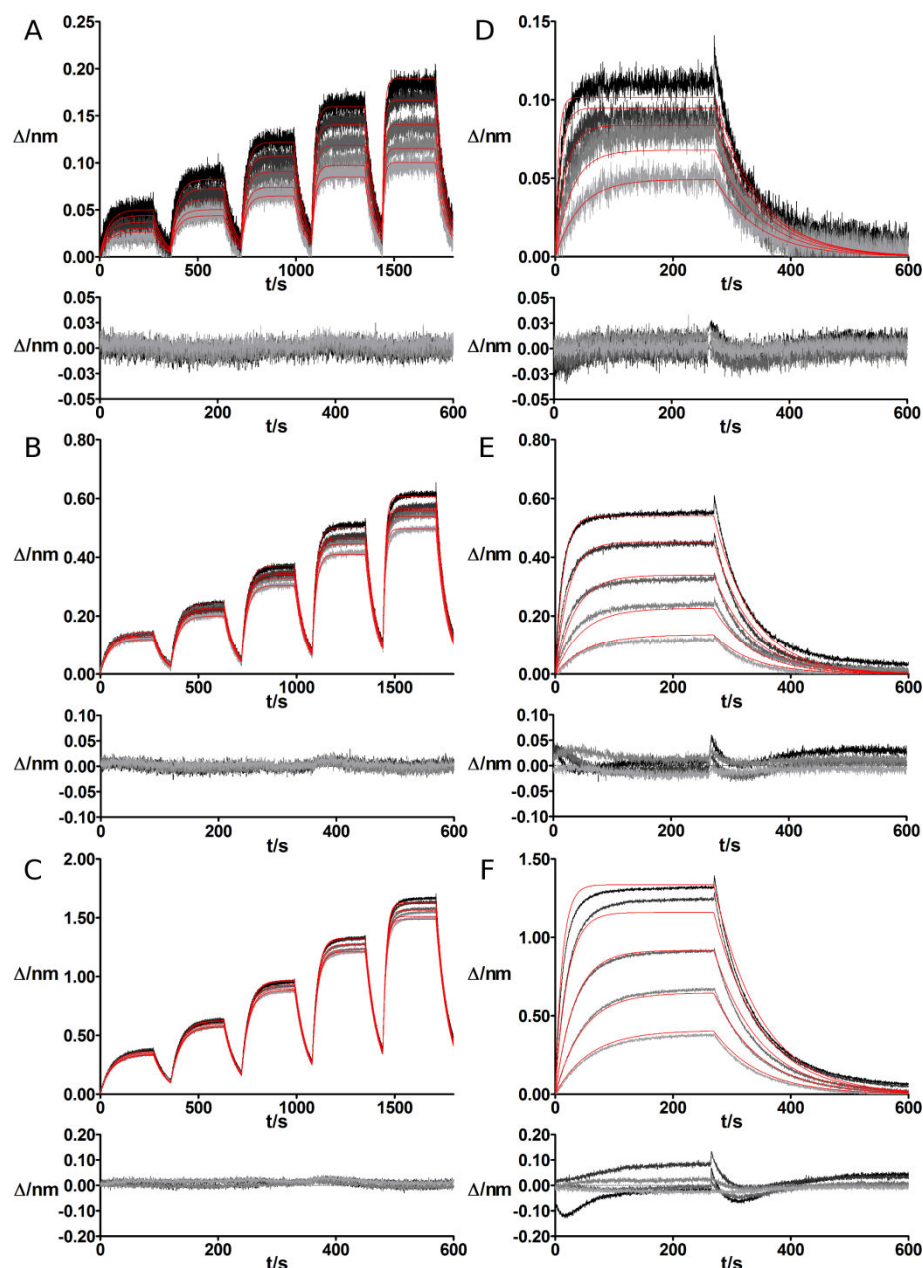


Figure R6: Comparison of multi cycle kinetics and single cycle kinetics with biolayer interferometry using scFv-IC16 as the example. The sensorgrams show the interaction of scFv-IC16 (analyte) with C-terminally biotinylated A β (1-42) (ligand). The amount of ligand was increased from 0.13 nm (A, D), 0.41 nm (B, E) and 1.01 nm (C, F). Applied analyte concentrations were: 2.4, 1.2, 0.6, 0.3 and 0.15 μ M. The fits are indicated by the red lines, whereas the sensorgrams are shown in blue. Each single cycle series was reproduced five times. The residuals of the fits are plotted below the respective sensorgram.

In conclusion, BLI is a suitable technique to estimate binding affinities based on single cycle kinetics and that single cycle kinetics can circumvent drawbacks of the established single-use sensor strategy of the manufacturer. Furthermore, the K_D of the scFv-IC16 in combination with C-terminally biotinylated A β (1-42) monomers was approved.

4.9 pE3-A β oligomer preparation

pE3-A β (3-40) (pE: pyroglutamate) was found to co-aggregate into plaques in Alzheimer's disease. In this experiment, it was shown that production and immobilization of oligomers with pE3-A β (3-40) is possible. Two surfaces were prepared for this experiment. One surface consisted of i) oligomers containing 10 % N-terminally biotinylated A β (1-42) with 90 % A β (1-42) and the other surface consisted of ii) 10 % N-terminally biotinylated A β (1-42) with 90 % pE3-A β (3-40). Since immobilization of the oligomers is via streptavidin-biotin interaction, it is necessary to show whether such oligomers contain pE3-A β (3-40). Consequently, Fab-fragments (Probiobdrug) with specificity for pE3-A β (3-40) were used (*no permission to show data*).

4.10 Characterization of D-peptides

D3 is a peptide selected by mirror image phage display. In the context of the optimization of the properties of D3, there are currently several derived peptides that have been characterized in this work. Some of the peptides contain single or multi amino acid substitutions, whereas others have the same amino acid composition but a rearranged sequence. Additionally it is possible to covalently combine peptides to yield so called "tandem peptides" or to alter the rigidity by cyclisation.

In this work all D3-derivatives were fitted with a heterogeneous ligand binding model, considering two binding sites without R_1 . This will be discussed later (see: Mechanistic explanation of the interaction of D3-derivatives with A β). Fitting with a simple 1:1 binding model increased the χ^2 , and lead to high local deviations of the fit and the sensorgram.

4.10.1 Affinity estimation of direct D3-derivatives

In this chapter, D3 was compared with derivatives that inherited the same amino acid composition as D3. For RD2, the sequence order was changed and for D3D3 or RD2RD2 the number of binding sites was doubled. For this assay, the sensorgrams of these peptides were recorded on surfaces containing either A β (1-42) monomers, oligomers or fibrils.

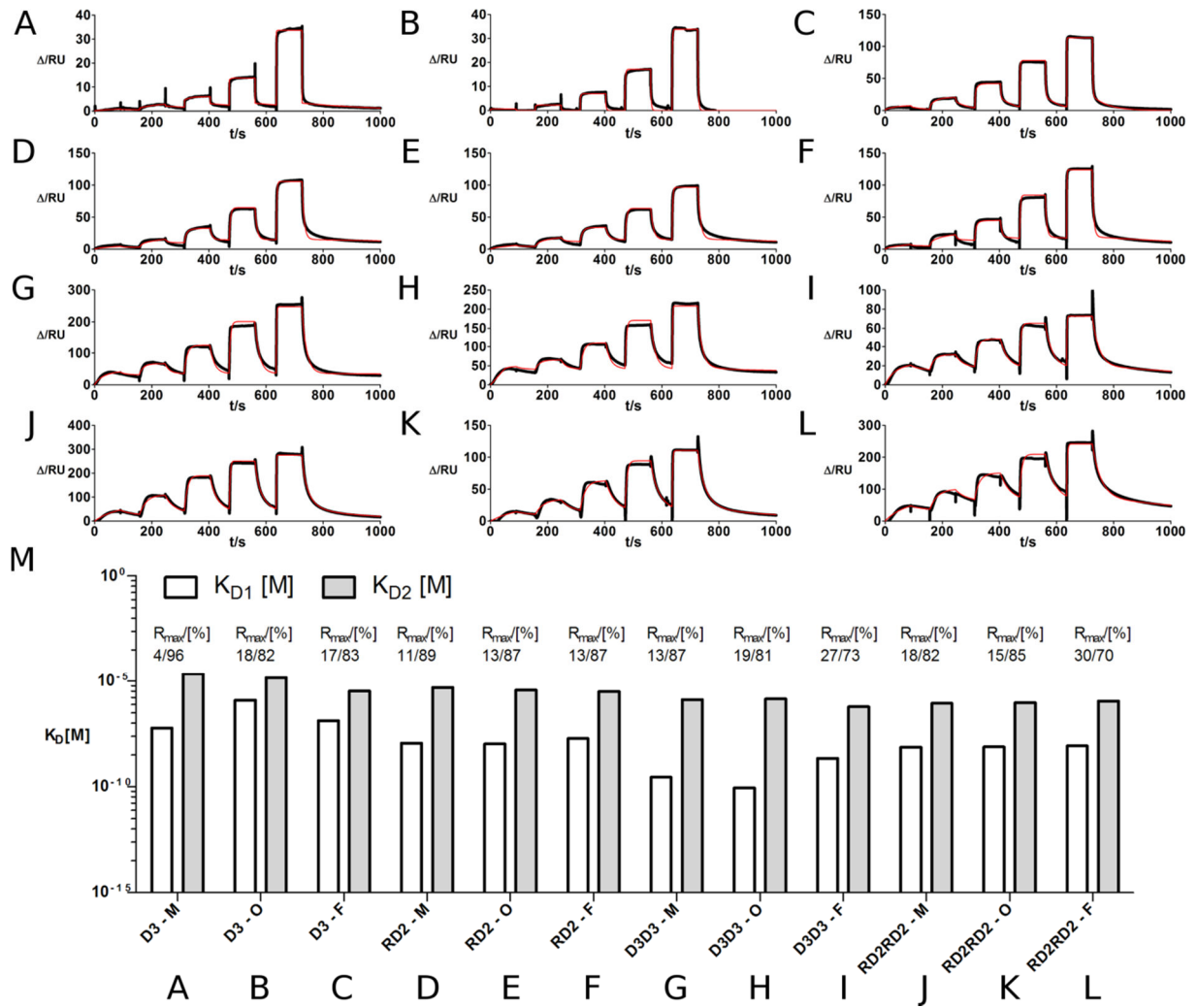


Figure R7: Binding kinetics of D3 and its derivatives to different A β assembly states. A-C Interaction of D3 with A) A β (1-42) monomers, B) oligomers and C) fibrils. D-F interaction of RD2 with D) A β (1-42) monomers, E) oligomers and F) fibrils. G-I interaction of D3D3 with G) A β (1-42) monomers, H) oligomers and I) fibrils. J-L interaction of RD2RD2 with J) A β (1-42) monomers, K) oligomers and L) fibrils. In M), the affinities were plotted for the named peptides and surfaces. For all peptides, two K_{DS} were estimated.

Fitting was possible for all peptides with a heterogeneous ligand model (2 binding sites). Among the monomeric peptides, RD2 presented a higher affinity for both the low and the high affinity sites. For monomers, the difference (K_{D1} and K_{D2}) was: 2.1×10^{-5} M and 5.8×10^{-8} M (D3) vs. 4.8×10^{-6} M and 1.1×10^{-8} M (RD2), for oligomers: 1.4×10^{-5} M and 1.2×10^{-6} M (D3) vs. 3.7×10^{-6} M and 1.0×10^{-8} M (RD2) and for fibrils: 3.3×10^{-6} M and 1.3×10^{-7} M (D3) vs. 3.2×10^{-6} M and 1.9×10^{-8} M (RD2). Differences in affinity for D3 and RD2 against certain A β assembly states were hardly estimable.

Tandem peptides showed a higher affinity than the corresponding monomeric peptides. The difference in affinity between D3D3 and RD2RD2 was low; the low affinity site of RD2RD2 has a higher affinity than the low affinity site of D3D3 against monomers and oligomers (Fig. R7): 1.3×10^{-6} M and 1.4×10^{-6} M (D3D3) vs. 8.7×10^{-7} M and 9.3×10^{-7} M (RD2RD2).

However, the high affinity site of D3D3 has a higher affinity than RD2RD2 for monomers (Fig. R7), oligomers and fibrils: $2.8 \cdot 10^{-10}$ M, $8.9 \cdot 10^{-11}$ M, $2.2 \cdot 10^{-9}$ M (D3D3) vs. $7.3 \cdot 10^{-9}$ M, $7.5 \cdot 10^{-9}$ M, $8.4 \cdot 10^{-9}$ M (RD2RD2).

4.10.2 Single amino acid substitutions

In this chapter it the dependency of the peptide sequence with the affinity was evaluated. For this, five peptides named from DB1 to DB5 were compared with D3 (Fig. R8). The peptides DB1 - DB5 are derived from D3 and characterized by substitutions of single or several amino acids. Changes of the sequence directly alter the affinity to the epitope.

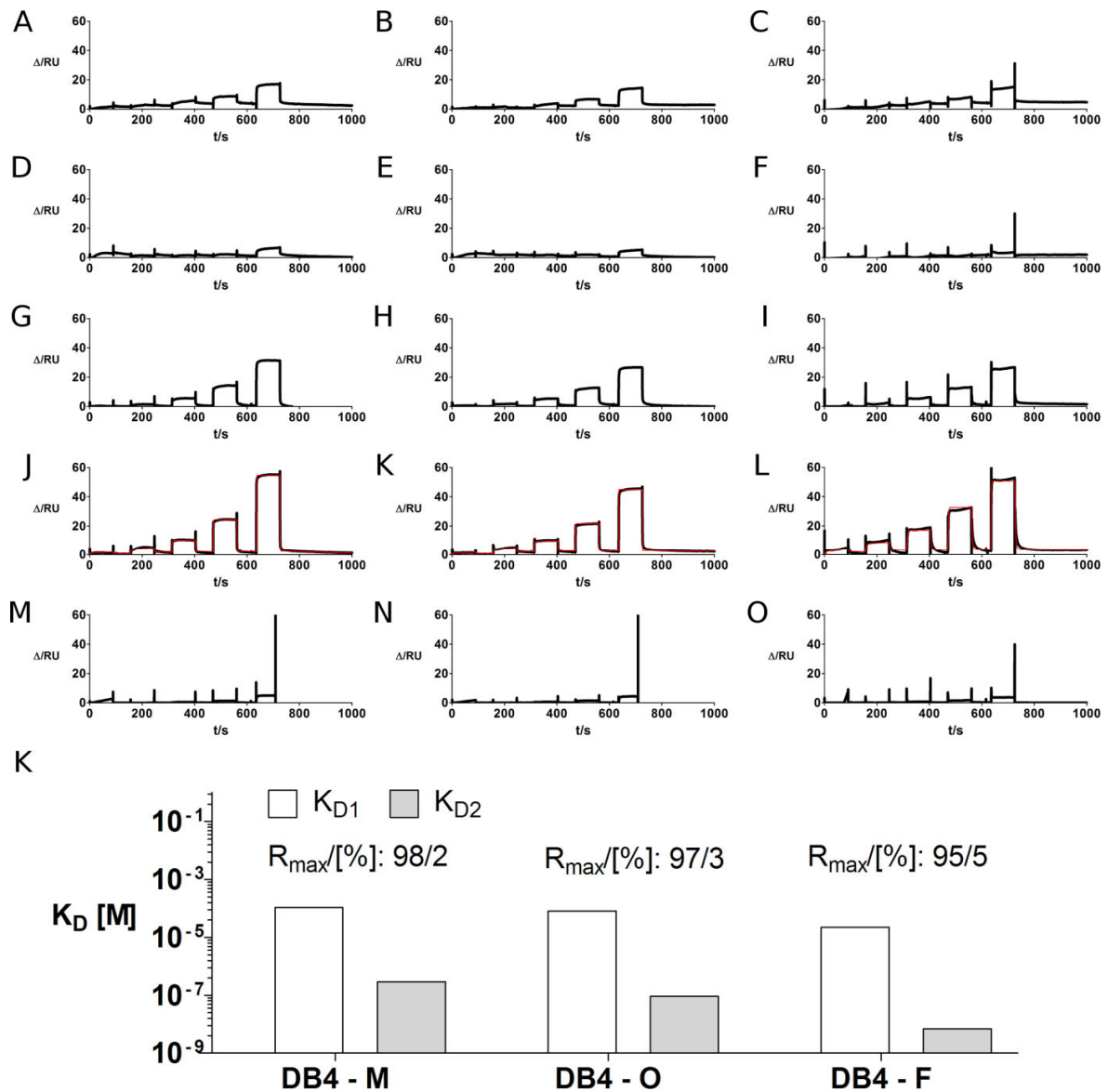


Figure R8: Interaction of the D3 derivatives DB1–5 to different Aβ assembly states. A-C Interaction of DB1 with A) Aβ(1-42) monomers, B) oligomers and C) fibrils. D-F interaction of DB2 with D) Aβ(1-42) monomers, E) oligomers and F) fibrils. G-I interaction of DB3 with G) Aβ(1-42) monomers, H) oligomers and I) fibrils. J-L interaction of DB4 with J) Aβ(1-42) monomers, K) oligomers and L) fibrils. M-O interaction of DB4 with M) Aβ(1-42) monomers, N) oligomers and O) fibrils. In K), the affinities to the indicated surfaces were plotted for DB4. For all peptides, two K_D s were estimated.

The interaction of DB1–DB5 to A β (1-42) monomers, oligomers and fibrils was recorded and evaluated. A kinetic fit for DB1, DB2, DB3 and DB5 was not possible (Fig. R8). For DB4, the sensorgrams showed sufficient curvature and a fit with a heterogeneous ligand model (2 binding sites) was possible. In contrast to D3, the percentage of the contribution of the high affinity site to the total reaction was always < 5 % in the case of monomers, oligomers and fibrils. For monomers, it was < 3 % and could be practically discounted because of the low impact to the total reaction. The low affinity site for each surface type (monomers, oligomers and fibrils) was less affine: DB4: 1.1×10^{-4} M vs. D3: 2.1×10^{-5} M (monomers), DB4: 8.2×10^{-5} M vs. D3: 1.4×10^{-5} M (oligomers), DB4: 2.2×10^{-5} M vs. D3: 3.3×10^{-6} M (fibrils).

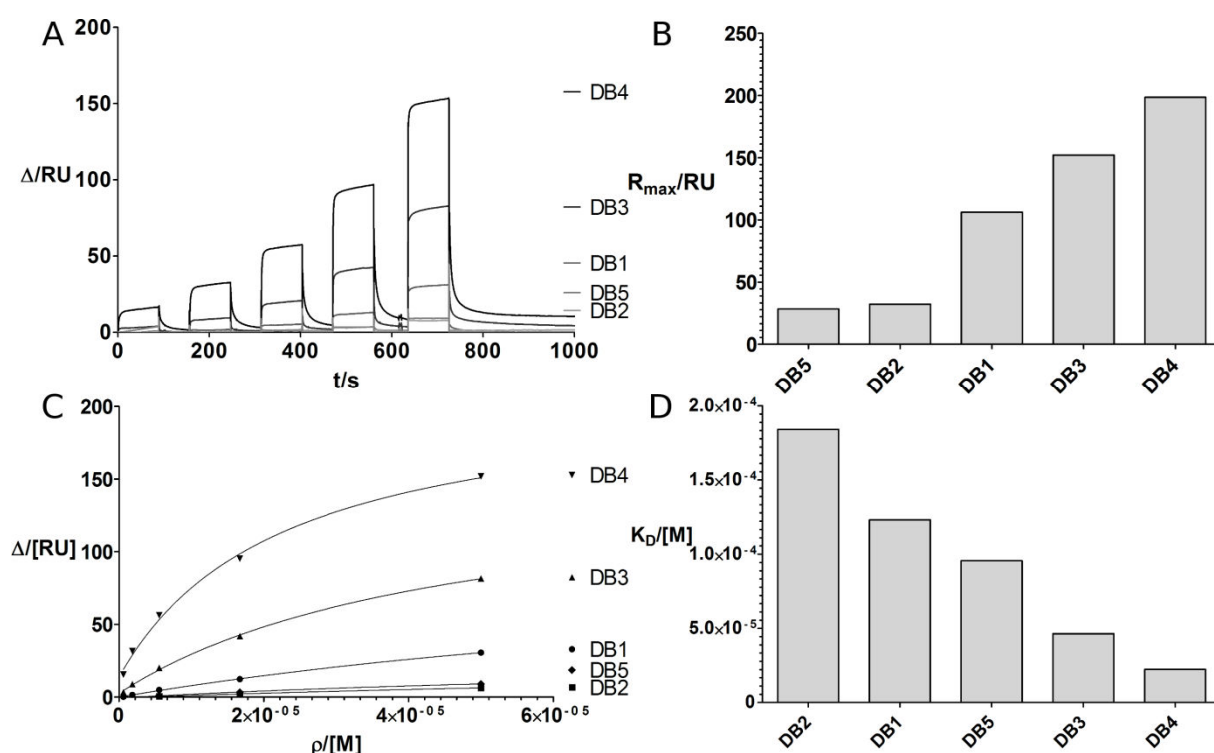


Figure R9: D3 derivatives ordered by affinity, signal amplitude and net-charge. A) Shows the sensorgrams for the peptides DB1–DB5 for A β (1-42) monomers. In B) the calculated R_{\max} values for DB1–DB5 are plotted. In C) the steady state affinity analysis for DB1–DB5 is plotted and in D) the calculated K_D s for DB1–DB5 are plotted.

To evaluate DB1–DB5, the R_{\max} and a K_D based on steady state analysis was estimated. Regarding R_{\max} and the K_D , DB3 and DB4 showed higher responses and affinity than DB1, DB2 and DB5 (Fig. R9). To determine which amino acid substitutions influence the affinity, the R_{\max} and K_D values were used to create an alignment based on the sequence of D3 (Fig. R10).

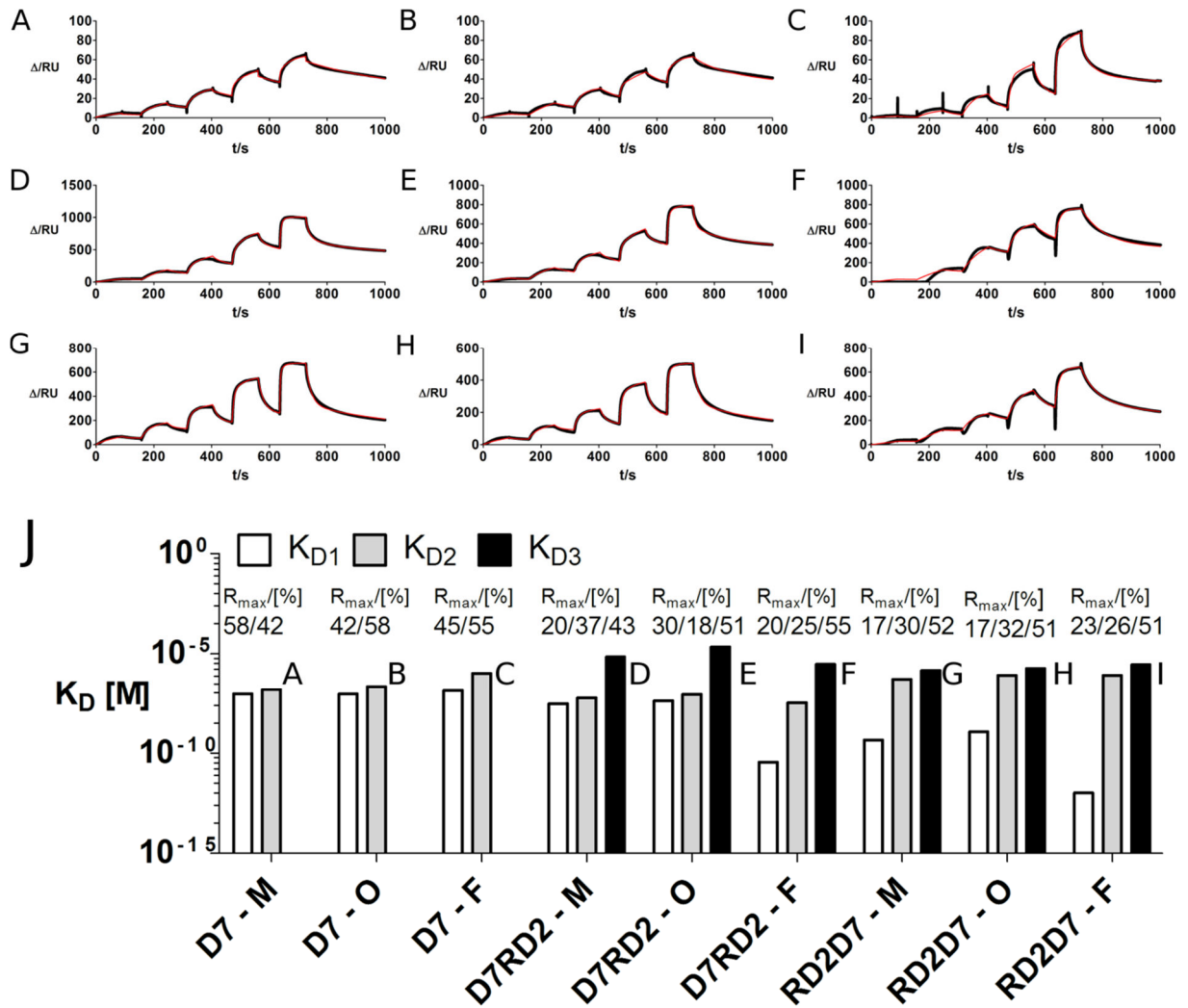


Figure R11: Binding kinetics of D7 and combines with D3 derivatives to different A β assembly states. A-C shows the Interaction of D7 with A) A β (1-42) monomers, B) oligomers and C) fibrils. D-F shows the interaction of D7RD2 with D) A β (1-42) monomers, E) oligomers and F) fibrils. G-I shows the interaction of RD2D7 with G) A β (1-42) monomers, H) oligomers and I) fibrils. In J), the affinities for D7, D7RD2 and RD2D7 were plotted for the named surfaces. The K_D values of D7 were estimated. For D7RD2 and RD2D7 three K_D s have been estimated.

It was possible to show that D7 binds all A β (1-42) surfaces equally well (Fig. R11: A). Fitting was possible for D7 with a heterogeneous ligand model (2 binding sites) as used for RD2. The affinity of D7 towards the surface is comparable with RD2 for both the high and the low affinity sites: D7: $1.5 \cdot 10^{-7}$ M, $9.3 \cdot 10^{-8}$ M (monomers); $2.3 \cdot 10^{-7}$ M, $8.9 \cdot 10^{-8}$ M (oligomers); $1.1 \cdot 10^{-6}$ M, $1.4 \cdot 10^{-7}$ M (fibrils) vs. RD2: $4.8 \cdot 10^{-6}$ M, $1.1 \cdot 10^{-8}$ M (monomers); $3.7 \cdot 10^{-6}$ M, $1.0 \cdot 10^{-8}$ M (oligomers); $3.2 \cdot 10^{-6}$ M, $1.9 \cdot 10^{-8}$ M (fibrils). However, there are differences in the association and dissociation rates. D7 shows in comparison to RD2 a slower dissociation and association rate. Furthermore, in comparison to RD2, D7 has a different distribution pattern of both reactions, which is obvious if one considers the R_{max} values of both sub-reactions. D7 shows a near equal distribution in the range of 42–45 % / 58–55 % for each sub-reaction, whereas RD2 is split into 8–13 % / 92–87 % for each reaction.

A disadvantage of D7 is the lower solubility (~50–100 µM in PBS). Nevertheless, the affinity is in the range of 10^{-7} to 10^{-6} M, thereby suggesting that high solubility is not necessary to achieve equilibrium in a short time frame. Furthermore, because of its high hydrophobicity, D7 is likely to pass the blood-brain-barrier effectively. Nevertheless, one possibility to optimize the solubility and/or affinity of D7 may be to combine this peptide with another binder, such as RD2. In this work, it was possible to prove, that the combination of D7 with RD2, leads to tandem peptides that showed i) an over-proportional increase in signal strength, ii) an increase in binding complexity and iii) an increase in affinity (Fig. R11: B/C). The over-proportional increase in signal strength (i) means that the signal increased by a factor of eight, while the molecular weight roughly increased by the factor of two. This may be due to oligomerization, because of van der Waals forces between D7 domains. For this purpose, one could calculate the surface activity, using the equation¹³³:

$$\text{xi. } RU_{max} = Valency_{Ligand} * \frac{M_{Analyte}}{M_{Ligand}} * RU_{immobilized}$$

Since there are two different binding domains, conclusively for this experiment the equation has to be:

$$\text{from xi. } RU_{max} = 2 * \frac{3231 \text{ kDa}}{4514 \text{ kDa}} * \sim 1200 \text{ RU}$$

The assumption of two distinct binding domains of RD2D7/D7RD2 is based on the idea that both binding sides (RD2 and D7) have 1) different physical properties, 2) show different rate constants and 3) a different distribution pattern of both partial reactions (based on the R_{max}). Following this concept, the maximum theoretical response of RD2D7/D7RD2 to 1200 RU immobilized Aβ(1-42) would be approximately ~1700 RU, if 100 % of the epitope is active. Conclusively, it was not possible to prove the existence of oligomeric RD2D7/D7RD2 with this experiment. For every surface the R_{max} signal was significantly lower than the theoretical maximum. Furthermore, monomeric D7 showed no abnormalities which would indicate oligomerization at these concentrations. Nevertheless, the activity for RD2D7/D7RD2 increased significantly (40 % < activity < 60 %) in comparison to the monomeric peptides D7 or RD2 (< 10 %). Dynamic light scattering measurements of D7RD2 indicate the presence of oligomers of different size (Fig. R12). Unfortunately DLS is not suitable to quantize size distributions within a heterogeneous sample. Using the Rayleigh approximation, the contribution of particles is proportional to $(size)^6$. This means, if the ratio (number of particles per fraction) of two different size fractions (F_1 : 1 nm and F_2 : 10 nm) is equal, the intensity of

bigger fraction is 1,000,000 times higher and thus easily shadows signals of the smaller fractions¹³⁴.

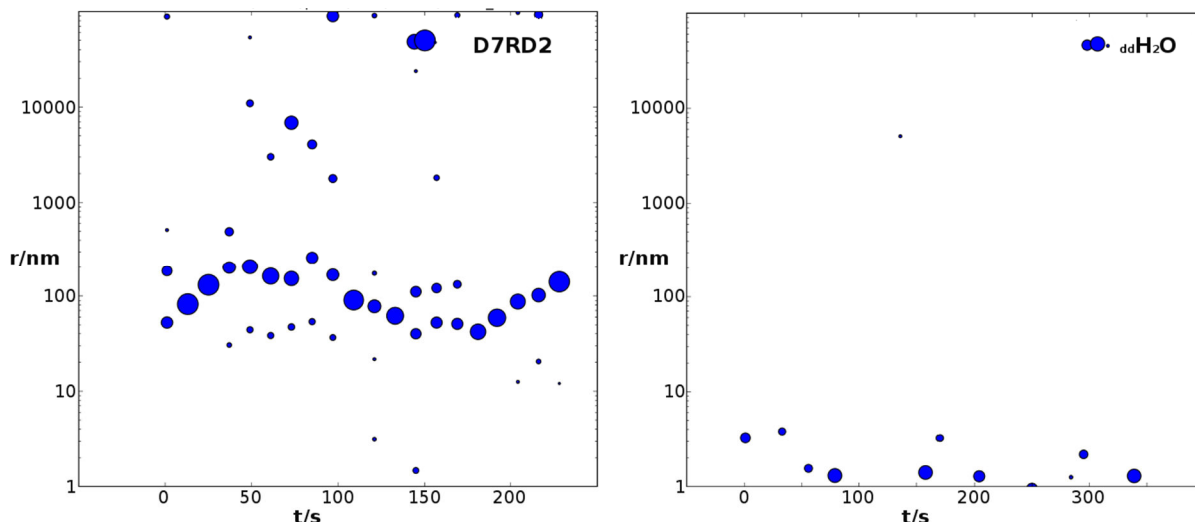


Figure R12: Dynamic light scattering measurement of D7RD2. Plot shows the presence of particles of mainly 100 nm size in the sample containing $\sim 300 \mu\text{M}$ D7RD2. The ddH_2O sample is used for comparison.

The increase in binding complexity (ii) and affinity (iii) is explainable by “avidity”. Avidity happens if there are more than one binding sites, which are independently able to interact with the epitope. Avidity is only influenced by the amount of binding sites, not their target specificity. Well-known examples for avidity are IgGs. Just because of the existence of more than one binding domain, the dissociation times can be increased by orders of magnitude. For scFv-dimers (diabodies), the factor can be up to $40\times$ ¹³⁵.

4.10.4 Characterization of cyclic D3-derivatives

In this chapter, cyclic D3-derivatives have been compared (Fig. R13). All cyclic D3-derivatives were cyclised by linking the C-terminus with the N-terminus (head-to-tail). This approach may increase the resistance of a peptide to digestion, because the termini are traditionally the attack points of enzymes or the proteasome. Additionally, it was shown that cyclisation increases the ability to permeate plasma membranes¹³⁶. Connecting the C- with the N-terminus (head-to-tail) of D3 leads to the peptide cD3z. This has the consequence that one charge disappears. To compensate this, the peptides cD3r and cD3p2k contain an additional arginine or lysine substitution, respectively. The other peptides cD3a and cD3p inherit an additional alanine and proline, respectively. These latter two peptides were used as controls to determine whether an insertion of an additional amino-acid affects affinity. An increase in affinity is not expected though.

For nearly all peptides (one peptide failed) kinetic fits based on a heterogeneous ligand model (2 binding sites) were performed (Fig. R13). Additionally, steady state affinity analyses were performed. In comparison to cD3z the peptides cD3a and cD3p did not show a noticeable increase in affinity for all tested surfaces (Fig. R13: P/Q). cD3r showed for all surfaces tested a higher affinity in comparison to cD3z, for both, the high and the low affinity binding sites: cD3r: 3.0×10^{-6} M, 4.9×10^{-7} M (monomers) vs. cD3z: 4.4×10^{-5} M, 1.6×10^{-6} M (monomers); cD3r: 2.2×10^{-5} M, 6.1×10^{-8} M (oligomers) vs. cD3z: 6.5×10^{-5} M, 3.5×10^{-6} M (oligomers); cD3r: 1.6×10^{-5} M, 6.8×10^{-9} M (fibrils) vs. cD3z: 5.2×10^{-5} M, 1.9×10^{-6} M (fibrils). In comparison to D3, the low affinity site was showing a slightly lower affinity: cD3z: 4.4×10^{-5} M vs. D3: 2.1×10^{-5} M (monomers), cD3z: 6.5×10^{-5} M vs. D3: 1.4×10^{-5} M (oligomers), cD3z: 5.2×10^{-5} M vs. D3: 3.3×10^{-6} M (fibrils). The same was observed for the high affinity site: cD3z: 1.6×10^{-6} M vs. D3: 5.8×10^{-8} M (monomers), cD3z: 3.5×10^{-6} M vs. D3: 1.2×10^{-6} M (oligomers), cD3z: 1.9×10^{-6} M vs. D3: 1.3×10^{-7} M (fibrils). cD3r showed nearly the same affinity as D3 for the low affinity site: cD3r: 3.0×10^{-6} M vs. D3: 2.1×10^{-5} M (monomers), cD3r: 2.2×10^{-5} M vs. D3: 1.4×10^{-5} M (oligomers), cD3r: 1.6×10^{-5} M vs. D3: 3.3×10^{-6} M (fibrils). However, the high affinity site showed higher affinity for oligomers and fibrils (20-fold) and a slightly lower affinity for monomers: cD3r: 4.9×10^{-7} M (monomers) vs. D3: 5.8×10^{-8} M (monomers), cD3r: 6.1×10^{-8} M (oligomers) vs. D3: 1.2×10^{-6} M (oligomers), cD3r: 6.8×10^{-9} M (fibrils) vs. D3: 1.3×10^{-7} M (fibrils). In comparison to other cyclic peptides, cD3p2k showed higher affinity for fibrils.

In this work, it was possible to show that the cyclisation of D3 does not interfere with the binding to A β (1-42) monomers, oligomers or fibrils. Although cD3z lost one amide group because of the head-to-tail connection, the affinity was very similar in comparison to D3. The results using cD3r and cD3p2k showed that the addition of one amino acid can compensate for the loss of the amide group and even enhance the affinity when compared with the results for D3. For cD3a and cD3p, a compensation for the reduced affinity due to the loss of the amide group was not observed and not expected.

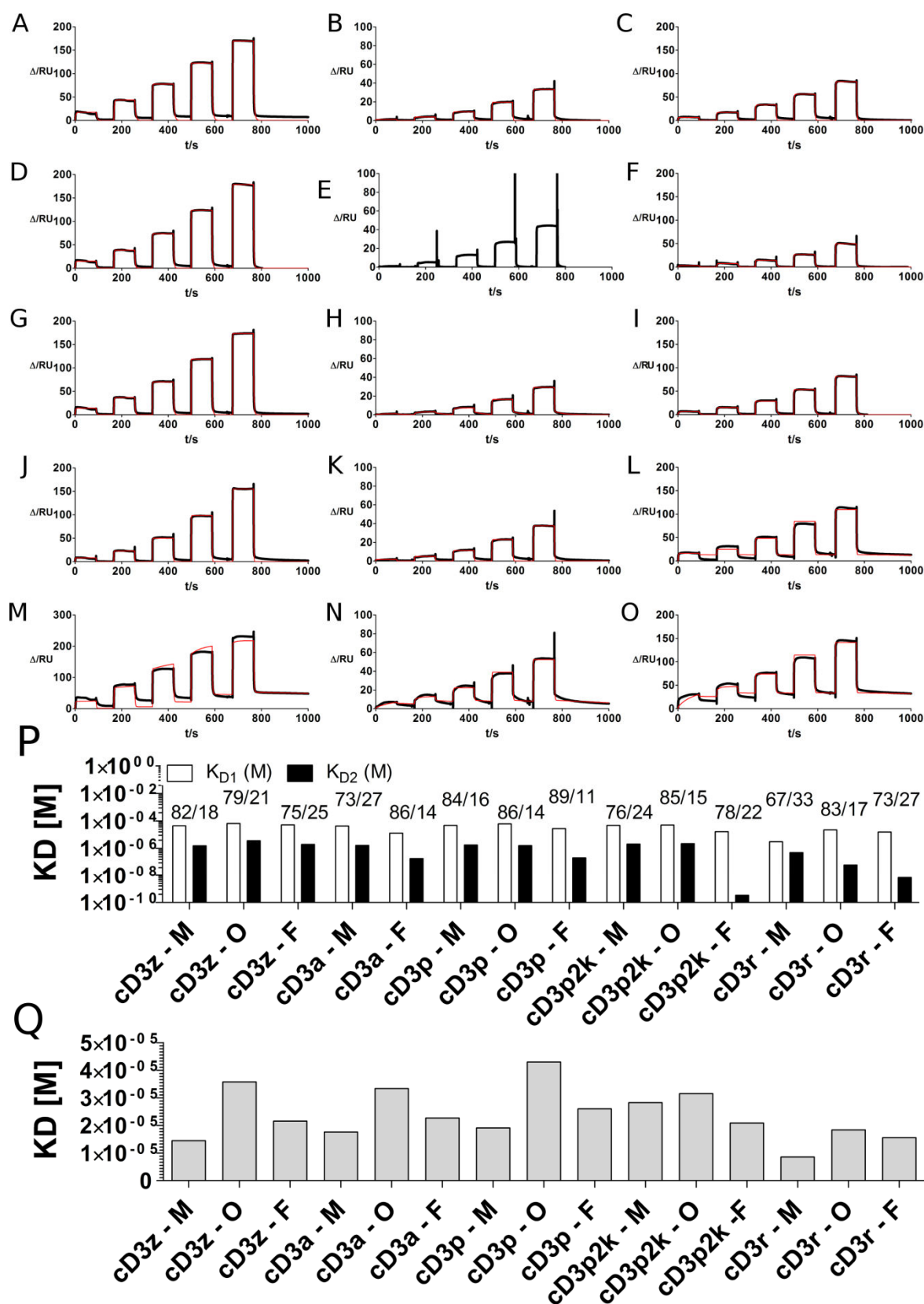


Figure R13: Interactions of cyclic D3 derivatives to different A β assembly states. A-C Interaction of cD3z with A) A β (1-42) monomers, B) oligomers and C) fibrils. D-F interaction of cD3a with D) A β (1-42) monomers, E) oligomers and F) fibrils. G-I interaction of cD3p with G) A β (1-42) monomers, H) oligomers and I) fibrils. J-L interaction of cD3p2k with J) A β (1-42) monomers, K) oligomers and L) fibrils. M-O interaction of cD3r with M) A β (1-42) monomers, N) oligomers and O) fibrils. P) For all peptides, two K_D s were estimated by a heterogeneous ligand model (2 binding sites). The numbers above the bars indicate the R_{max} distribution of both reactions [%]. Q) Analogous to this, the affinities were estimated by steady state affinity analysis.

4.10.5 Interaction of D3 with pE3-A β oligomers and fibrils

After the feasibility of the creation and correct immobilization of oligomers containing pE3-A β (3-40) was proven (*no permission to show*), it was tested, whether D3 is able to interact with pE3-A β (3-40). For this purpose, oligomers and fibrils containing 90 % pE3-A β (3-40) were prepared. A high percentage of pE3-A β (3-40), reduces the signal from the interaction with A β (1-42). Interestingly, the interaction of D3 with such oligomers was just able to be fitted with a heterogeneous ligand model considering 3 binding sites (Fig. R14). Nevertheless, the affinity of each hypothetical binding site was in the range of the interaction of D3 with A β (1-42). The affinities (K_{D1} - K_{D3}) for the interactions with oligomers and fibrils containing 90 % pE3-A β (3-40) were: $4.6 \cdot 10^{-7}$ M, $7.7 \cdot 10^{-5}$ M, $3.5 \cdot 10^{-5}$ M (oligomers) and K_{D1} - K_{D3} : $8.7 \cdot 10^{-9}$ M, $5.4 \cdot 10^{-5}$ M, $1.3 \cdot 10^{-4}$ M (fibrils), which is similar to the affinities (K_{D1} - K_{D2}) of D3 to oligomers and fibrils without pE3-A β (3-40): $1.4 \cdot 10^{-5}$ M, $1.2 \cdot 10^{-6}$ M (oligomers) and $3.3 \cdot 10^{-6}$ M, $1.3 \cdot 10^{-7}$ M (fibrils). Thus, the presence of a pyroglutamate had negligible influence on peptide affinity towards A β .

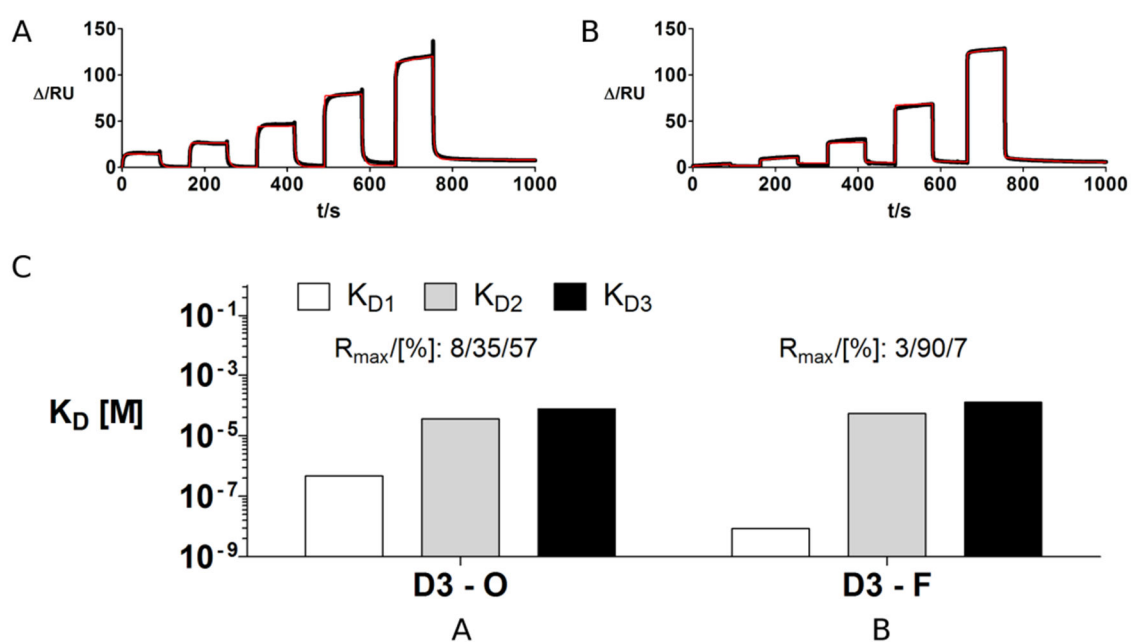


Figure R14: Binding of D3 to A β oligomers and fibrils containing 90 % pE3-A β (3-40). A) Interaction of D3 to oligomers containing pE3-A β (3-40). B) Interaction of D3 to fibrils containing pE3-A β (3-40). C) K_D s of the interaction with oligomers and fibrils containing pE3-A β (3-40), calculated by a kinetic fit based on a 3:1 model.

4.10.6 Thermodynamics of cyclic D3-derivatives

Cyclisation can reduce the entropic term as part of the Gibb's energy⁹⁸, and thus make binding energetically more favourable. This is possible because the degree of freedom is reduced, because the amount of possible folding states is reduced and the molecule becomes

more rigid. With this in mind, the effect of cyclisation may be stronger for longer peptides. In this study the peptides were cyclised covalently by fusing the C- with the N-terminus; another possible way could for example involve the introduction of two cysteines.

Table R4: Thermodynamics in comparison to D3. For the cyclic peptides cD3z and cD3r thermodynamics were estimated by steady state affinity analysis and a kinetic fit based on a 1:1 binding model. Ø: Mean, SD: Standard deviation.

SS-Affinity	cD3z		cD3r		D3	
	Ø	SD	Ø	SD	Ø	SD
ΔH [kJ/mol]	-6.7	0.67	-8.8	0.97	-8.3	1.6
ΔS [J/(K*mol)]	55.0	2.3	60.0	3.3	57.0	5.3

1:1 Kinetics	cD3z		cD3r		D3	
	Ø	SD	Ø	SD	Ø	SD
ΔH [kJ/mol]	-11.0	0.62	-12.0	1.6	-9.8	0.83
ΔS [J/(K*mol)]	52.0	2.1	52.0	5.4	53.0	2.8

To estimate the Gibb's energy and the content of the enthalpy and the entropy in the equation, it is necessary to estimate the binding affinity over a (broad) temperature range. If the interaction requires energy, the value of the Gibb's energy will have a positive sign. Otherwise, if energy is released while both partners bind, the sign will be negative. In the first case, the affinity should increase with temperature, whereas in the second case, the affinity will decrease with temperature. In this experiment, a measurable impact on the entropic term for cyclic D3 derivatives was examined.

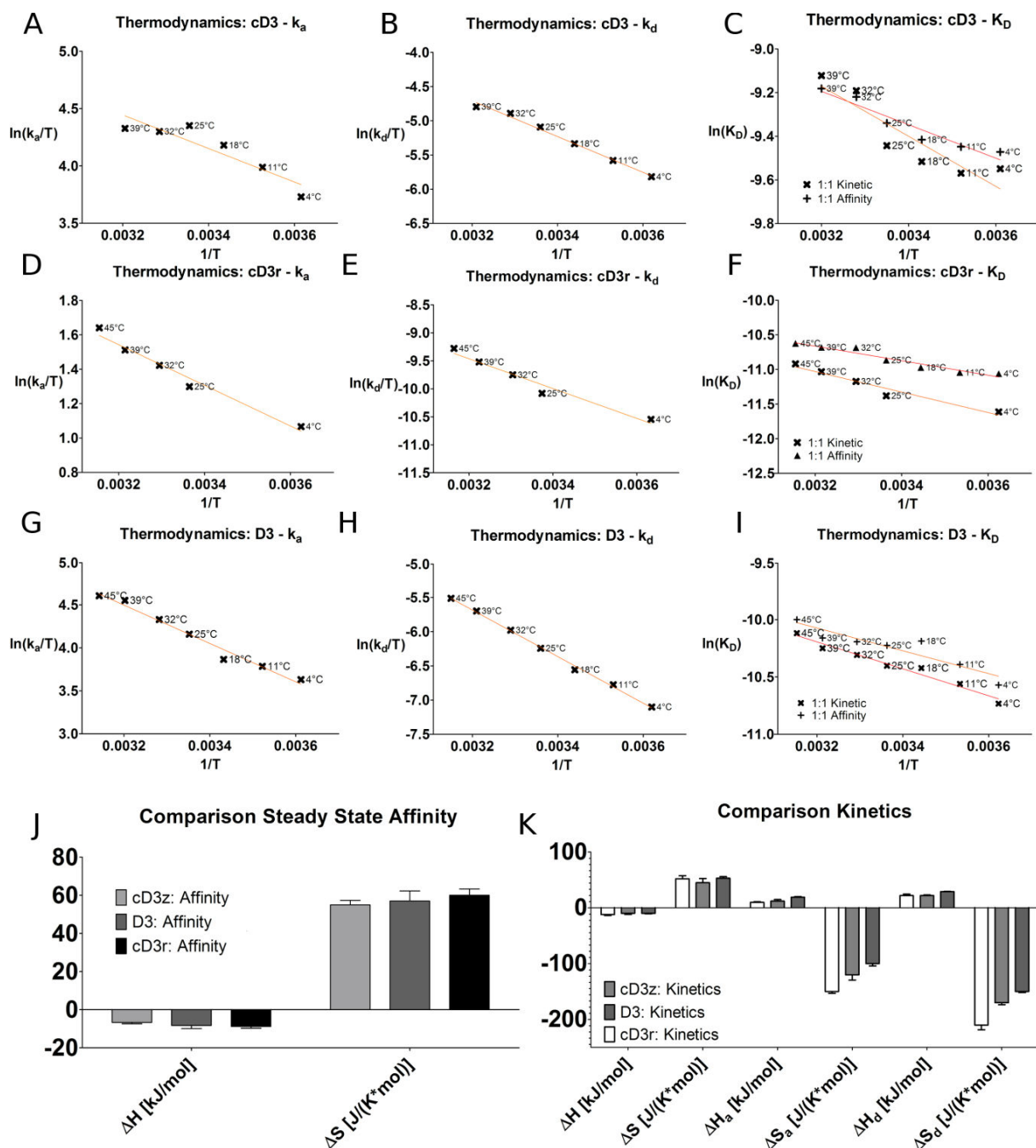


Figure R15: Thermodynamics of D3 derivatives to Aβ(1-42). A) on-rate, B) off-rate and C) K_D of cD3z over the temperature range of 4 to 42°C. E) on-rate, F) off-rate and G) K_D of cD3r over a temperature range of 4 to 42°C. G) on-rate, H) off-rate and I) K_D of D3 over a temperature range of 4 to 42°C. Bar chart of the K_D s of cD3z, cD3r and D3 estimated by J) Fitted binding enthalpy (H) and entropy (S) based on steady-state affinity analysis and K) 1:1 Langmuir kinetics. H_a/S_a and H_d/S_d are calculated by fitting the on- and off-rates.

The sensorgrams of the peptides D3, cD3z and cD3r were fitted by steady state affinity analysis and a 1:1 Langmuir binding model. Both models were compared in Fig. R15 and Tab: R4. For all peptides the enthalpy was negative and if considering the standard deviation, there was no measurable difference among the peptides. In the case of the steady state affinity analysis, the mean enthalpy was -7.9 kJ/mol, with the kinetic fitting model an enthalpy of -10.9 kJ/mol was determined. The entropy values showed even less deviation among the

peptides. Here, the mean entropy was 57.3 J/K*mol with the steady state affinity model and 52.3 J/K*mol for the kinetic fitting model. In conclusion, it was possible to show that the interaction of D3 is an exergonic reaction. However, using SPR analysis it was not possible to confirm whether cyclisation is able to alter the entropic term. An explanation may be that the amount of possible folding states of a 12 amino-acid peptide, such as D3, is too low. The difference in comparison to cyclised D3 derivatives will be too low to estimate with this technique.

4.10.7 Affinity prediction of multivalent D3-derivatives

For many of the characterized peptides, it should be possible to create affinity predictions of hypothetical multivalent D3-derivatives based on the measurements.

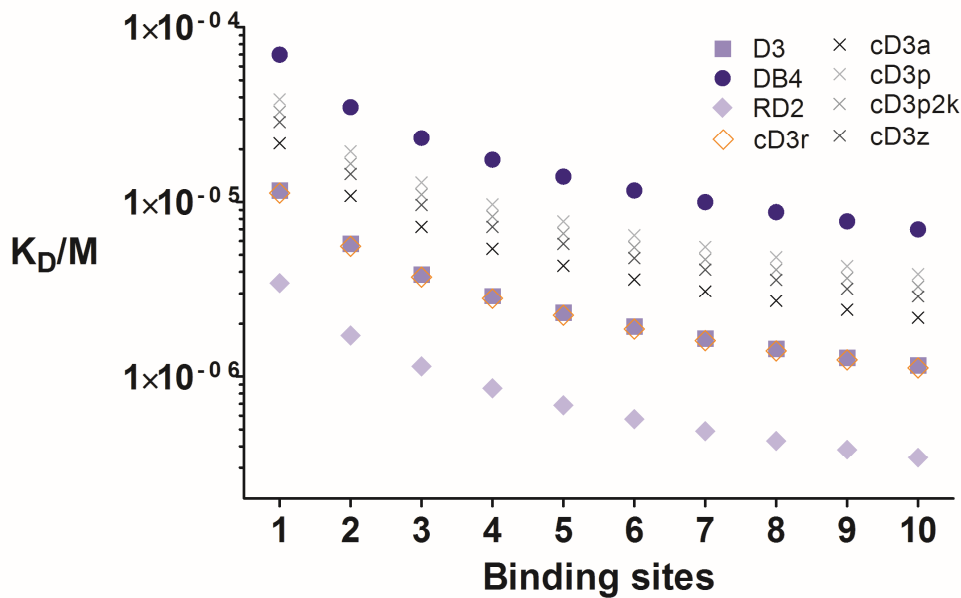


Figure R16: Affinity predictions of D3 derivatives to Aβ(1-42). The theoretically achievable affinity of each peptide was plotted in dependency to the number of binding sites. For this the mean affinity (weighted K_Ds) of the interactions with monomers, oligomers and fibrils (mean) were calculated.

In this work, for all D3-derivates a model with two partial reactions was used for fitting. To keep the predictions simple, both K_Ds were used for calculation of a weighted total K_D (K_w) according to the following simple equation:

xii.
$$K_w = \sum_{i=1}^n \frac{R_{\max_i}}{\sum R_{\max}} * K_{D_i}$$

$\sum R_{\max}$: total R_{\max} for all partial reactions
 R_{\max_i} : response at equilibrium of ..
 K_{D_i} : affinity constant of ..
 .. the current partial reaction (two partial reactions for D3-derivatives).

The so obtained affinities (K_w) for the interactions with monomers, oligomers and fibrils (according to Tab. S1) were averaged (for robustness) and then used to calculate the predicted affinities (Fig. R16 and Tab. R4) based on a model of avidity. For homo-multivalent agents this can be done with the following equation:

$$x. \quad \frac{1}{K_D} = \sum_{i=1}^{\infty} \frac{1}{K_{Di}} \text{ (see introduction)}$$

This approach is not perfect, because secondary effects are not considered, but helps to get an idea of the effectivity of addition of binding sites. For RD2RD2 and D3D3 the estimated, weighted, and averaged K_{DS} were $1.0 \cdot 10^{-6}$ (SD: $0.04 \cdot 10^{-6}$) and $0.9 \cdot 10^{-6}$ (SD: $0.4 \cdot 10^{-7}$) respectively. If considering the standard deviation of the predictions, the match is within the expected range.

Table R4: Affinity predictions of D3 derivatives to A β (1-42). The theoretically achievable affinity of each peptide was calculated in dependency to the number of binding sites (Sites). For this the mean affinity (weighted K_{DS}) of the interactions with monomers, oligomers and fibrils (mean) and standard deviations (SD) were calculated.

Sites	<i>cD3a</i>		<i>cD3p</i>		<i>cD3p2k</i>		<i>cD3r</i>	
	\emptyset	SD	\emptyset	SD	\emptyset	SD	\emptyset	SD
1	$2.2 \cdot 10^{-5}$	$1.5 \cdot 10^{-5}$	$3.9 \cdot 10^{-5}$	$1.5 \cdot 10^{-5}$	$3.3 \cdot 10^{-5}$	$1.6 \cdot 10^{-5}$	$1.1 \cdot 10^{-5}$	$8.2 \cdot 10^{-6}$
2	$1.1 \cdot 10^{-5}$	$7.3 \cdot 10^{-6}$	$1.9 \cdot 10^{-5}$	$7.7 \cdot 10^{-6}$	$1.6 \cdot 10^{-5}$	$7.8 \cdot 10^{-6}$	$5.6 \cdot 10^{-6}$	$4.1 \cdot 10^{-6}$
3	$7.2 \cdot 10^{-6}$	$4.9 \cdot 10^{-6}$	$1.3 \cdot 10^{-5}$	$5.1 \cdot 10^{-6}$	$1.1 \cdot 10^{-5}$	$5.2 \cdot 10^{-6}$	$3.7 \cdot 10^{-6}$	$2.7 \cdot 10^{-6}$
4	$5.4 \cdot 10^{-6}$	$3.7 \cdot 10^{-6}$	$9.7 \cdot 10^{-6}$	$3.8 \cdot 10^{-6}$	$8.2 \cdot 10^{-6}$	$3.9 \cdot 10^{-6}$	$2.8 \cdot 10^{-6}$	$2.1 \cdot 10^{-6}$
5	$4.3 \cdot 10^{-6}$	$2.9 \cdot 10^{-6}$	$7.7 \cdot 10^{-6}$	$3.1 \cdot 10^{-6}$	$6.6 \cdot 10^{-6}$	$3.1 \cdot 10^{-6}$	$2.2 \cdot 10^{-6}$	$1.6 \cdot 10^{-6}$
6	$3.6 \cdot 10^{-6}$	$2.4 \cdot 10^{-6}$	$6.5 \cdot 10^{-6}$	$2.6 \cdot 10^{-6}$	$5.5 \cdot 10^{-6}$	$2.6 \cdot 10^{-6}$	$1.9 \cdot 10^{-6}$	$1.4 \cdot 10^{-6}$
7	$3.1 \cdot 10^{-6}$	$2.1 \cdot 10^{-6}$	$5.5 \cdot 10^{-6}$	$2.2 \cdot 10^{-6}$	$4.7 \cdot 10^{-6}$	$2.2 \cdot 10^{-6}$	$1.6 \cdot 10^{-6}$	$1.2 \cdot 10^{-6}$
8	$2.7 \cdot 10^{-6}$	$1.8 \cdot 10^{-6}$	$4.8 \cdot 10^{-6}$	$1.9 \cdot 10^{-6}$	$4.1 \cdot 10^{-6}$	$1.9 \cdot 10^{-6}$	$1.4 \cdot 10^{-6}$	$1.0 \cdot 10^{-6}$
9	$2.4 \cdot 10^{-6}$	$1.6 \cdot 10^{-6}$	$4.3 \cdot 10^{-6}$	$1.7 \cdot 10^{-6}$	$3.7 \cdot 10^{-6}$	$1.7 \cdot 10^{-6}$	$1.2 \cdot 10^{-6}$	$9.1 \cdot 10^{-7}$
10	$2.2 \cdot 10^{-6}$	$1.5 \cdot 10^{-6}$	$3.9 \cdot 10^{-6}$	$1.5 \cdot 10^{-6}$	$3.3 \cdot 10^{-6}$	$1.6 \cdot 10^{-6}$	$1.1 \cdot 10^{-6}$	$8.2 \cdot 10^{-7}$

Sites	<i>cD3z</i>		<i>D3</i>		<i>DB4</i>		<i>RD2</i>	
	\emptyset	SD	\emptyset	SD	\emptyset	SD	\emptyset	SD
1	$2.9 \cdot 10^{-5}$	$2.3 \cdot 10^{-5}$	$1.2 \cdot 10^{-5}$	$8.7 \cdot 10^{-6}$	$7.0 \cdot 10^{-5}$	$4.5 \cdot 10^{-5}$	$3.4 \cdot 10^{-6}$	$7.6 \cdot 10^{-7}$
2	$1.4 \cdot 10^{-5}$	$1.1 \cdot 10^{-5}$	$5.8 \cdot 10^{-6}$	$4.4 \cdot 10^{-6}$	$3.5 \cdot 10^{-5}$	$2.2 \cdot 10^{-5}$	$1.7 \cdot 10^{-6}$	$3.8 \cdot 10^{-7}$
3	$9.6 \cdot 10^{-6}$	$7.6 \cdot 10^{-6}$	$3.9 \cdot 10^{-6}$	$2.9 \cdot 10^{-6}$	$2.3 \cdot 10^{-5}$	$1.5 \cdot 10^{-5}$	$1.1 \cdot 10^{-6}$	$2.5 \cdot 10^{-7}$
4	$7.2 \cdot 10^{-6}$	$5.7 \cdot 10^{-6}$	$2.9 \cdot 10^{-6}$	$2.2 \cdot 10^{-6}$	$1.7 \cdot 10^{-5}$	$1.1 \cdot 10^{-5}$	$8.6 \cdot 10^{-7}$	$1.9 \cdot 10^{-7}$
5	$5.7 \cdot 10^{-6}$	$4.6 \cdot 10^{-6}$	$2.3 \cdot 10^{-6}$	$1.7 \cdot 10^{-6}$	$1.4 \cdot 10^{-5}$	$8.9 \cdot 10^{-6}$	$6.9 \cdot 10^{-7}$	$1.5 \cdot 10^{-7}$
6	$4.8 \cdot 10^{-6}$	$3.8 \cdot 10^{-6}$	$1.9 \cdot 10^{-6}$	$1.5 \cdot 10^{-6}$	$1.2 \cdot 10^{-5}$	$7.4 \cdot 10^{-6}$	$5.7 \cdot 10^{-7}$	$1.3 \cdot 10^{-7}$
7	$4.1 \cdot 10^{-6}$	$3.3 \cdot 10^{-6}$	$1.7 \cdot 10^{-6}$	$1.2 \cdot 10^{-6}$	$1.0 \cdot 10^{-5}$	$6.4 \cdot 10^{-6}$	$4.9 \cdot 10^{-7}$	$1.1 \cdot 10^{-7}$
8	$3.6 \cdot 10^{-6}$	$2.9 \cdot 10^{-6}$	$1.4 \cdot 10^{-6}$	$1.1 \cdot 10^{-6}$	$8.7 \cdot 10^{-6}$	$5.6 \cdot 10^{-6}$	$4.3 \cdot 10^{-7}$	$9.6 \cdot 10^{-8}$
9	$3.2 \cdot 10^{-6}$	$2.5 \cdot 10^{-6}$	$1.3 \cdot 10^{-6}$	$9.7 \cdot 10^{-7}$	$7.7 \cdot 10^{-6}$	$5.0 \cdot 10^{-6}$	$3.8 \cdot 10^{-7}$	$8.5 \cdot 10^{-8}$
10	$2.9 \cdot 10^{-6}$	$2.3 \cdot 10^{-6}$	$1.2 \cdot 10^{-6}$	$8.7 \cdot 10^{-7}$	$7.0 \cdot 10^{-6}$	$4.5 \cdot 10^{-6}$	$3.4 \cdot 10^{-7}$	$7.6 \cdot 10^{-8}$

5. Discussion

5.1 Surface characterization with scFv-IC16

A comparison of the obtained kinetic rates and overall affinities for scFv-IC16 and A β species revealed that for each A β assembly state (C-terminally biotinylated monomers, 10 % N-terminally biotinylated oligomers and fibrils) there is one interaction component present with nearly identical properties among all three assembly states (Fig. R4 and Tab. R1). The attained association and dissociation rates for the high affinity site of scFv-IC16 binding to A β monomers, oligomers and fibrils are $2.3 \cdot 10^4 \text{ Ms}^{-1}$ and $1.7 \cdot 10^{-2} \text{ s}^{-1}$, $2.7 \cdot 10^4 \text{ Ms}^{-1}$ and $1.0 \cdot 10^{-2} \text{ s}^{-1}$, $3.0 \cdot 10^4 \text{ Ms}^{-1}$ and $0.9 \cdot 10^{-2} \text{ s}^{-1}$, respectively. Based on these rate constants, it is tempting to speculate that the same binding epitope for scFv-IC16 is present in each of the studied A β assembly states. Because this epitope is missing in purely N-terminally biotinylated monomers, but existing for purely C-terminally biotinylated monomers, one can conclude that this epitope contains the very N-terminal residues of A β . Moreover, the affinity of the slower binding reaction of scFv-IC16 binding oligomers and fibrils was nearly one order of magnitude weaker (K_{D2} -values in Tab. R1). Based on this observation it was concluded that A β generates a secondary binding site for scFv-IC16 when forming higher assembly states like oligomer and fibril structures. Remarkably, fitting of sensorgrams obtained with scFv-IC16 binding monomeric A β (1-42) to the heterogeneous ligand binding model, as used for oligomers and fibrils, did not yield a second binding component similar to the oligomer and fibril data. Instead, an unlikely apparent K_D of $9.9 \cdot 10^{-14} \text{ M}$ in concert with an R_{max} value of 1.6 supports the notion that scFv-IC16 binding data for monomers follows a 1:1 Langmuir interaction, which confirms that the A β monomer preparation was extremely homogeneous, and that the secondary binding epitope present in oligomers and fibrils is clearly not a fitting artefact.

Taken together, an approach allowing interaction studies with different homogeneous A β (1-42) assembly states by SPR was established. SEC and DGC purification of A β species prior to streptavidin-biotin coupling ensures sample homogeneity and minimal surface alterations, which are major limitations of SPR experiments involving A β . In addition, a monoclonal antibody-derived scFv was employed for the direct verification of successfully immobilized higher A β assembly states.

5.2 Mechanism for the interaction between D3 and A β (1-42)

In the results, an alignment with D3-derivatives was performed (Fig. R10). Five amino acids of D3 at the positions 3, 5, 7, 9, 10, and 11 were found to influence binding and affinity. In D3, all these amino acids are basic. It was shown that replacing these amino acids with uncharged or acidic amino acids leads to a decrease in binding affinities. Additionally, it was possible to illustrate complementation on these examples.

A closer look at the sequence of A β indicates an accumulation of acidic amino acids at two distinct areas. Because of this, two hypothetical binding sites at the position 1-11 (S1) and 22-23 (S2) are suggested (Fig. D1). It seems reasonable that the interaction of D3-derivatives and A β is stabilized by hydrogen bonds. Because of the spatial distance of ten amino acids between S1 and S2, it seems plausible that a heterogeneous ligand model (considering two binding sites) can be applied for the description of the binding kinetics of all D3-derivatives in this work.

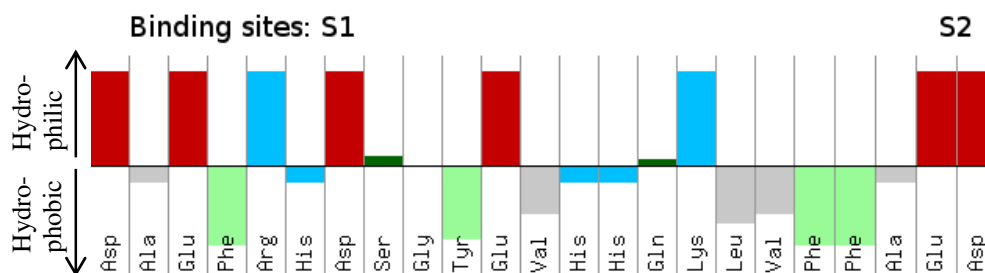


Figure D1: Hydropathy plot of A β (1-23). Acidic amino acids in A β (1-42) are marked in red and distributed in the first 23 amino acids. The hypothetical binding sites are expected at position 1-11 (S1) and at position 22-23 (S2). Color code **Acidic**, **Aromatic**, **Basic**, **Aliphatic**, **Polar**.

Moreover, the fits of all D3-derivatives (Tab. S1) showed a distinct distribution pattern regarding the content of each partial reaction. This is visible on the values of the partial responses $R_{\max 1}$ and $R_{\max 2}$. Remarkably, the high affinity site deviated in all cases between ~10 and ~35 % (based on the total R_{\max}), which is expected using the suggested heterogeneous ligand model with two binding sites.

5.3 Why does RD2 have a higher affinity than D3?

In this work the affinities of RD2 and D3 to A β monomers, oligomers and fibrils have been compared. Results showed a higher affinity for RD2. RD2 possesses an accumulation of basic amino acids at the C-terminus and a cluster of aliphatic amino acids at the N-terminus.

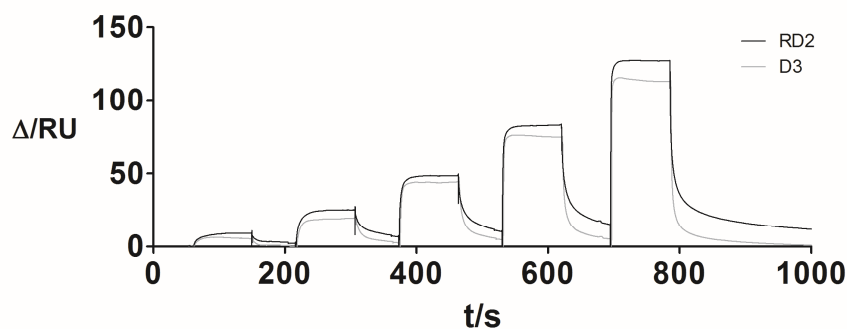


Figure D2: Subsequent injection of RD2 after injection of D3 over a surface coated with A β fibrils. Both peptides consist of the same amino acid composition; however the order of the amino acids differs.

It is possible that RD2 interacts over the neutral N-terminus with another, yet unknown binding locus on A β (1-42). In D3 such interactions are not as well stabilized, because the distribution of the basic amino acids within the sequence is equal. As a consequence, an increased surface activity should be observable for RD2 in comparison to D3. Such behavior will be visible on the R_{\max} values and on the shape of the sensorgram (certainly slower dissociation).

Remarkably, both effects, an increased R_{\max} and a higher affinity, were observed frequently. However, such measurements are only reliable and interpretable in SPR spectroscopy if RD2 is injected directly after D3 has been tested (as in: Fig. D2). Otherwise, secondary effects like dissociation of the immobilized fibrils, impaired surface activity due to aging, and related processes could hide these differences between the two low molecular weight agents. If this model is really true, such interactions may be impaired with non-ionic detergence, e.g. Surfactant P20. However, this was not tested explicitly in the thesis, because high molecular assembly states such as A β fibrils may get destabilized in such buffer conditions.

5.4 How is D3 overcoming the plasma membrane?

The ability of peptides to permeate through membranes decreases with increasing mass. However, properties like the presence of basic clusters have been found to influence the uptake of the compound into the cell very efficiently by plasma-membrane pore formation¹³⁷⁻¹⁴⁰. A famous example is the HIV-1 related protein Tat^{137,138,140}. This mechanism could be driven by the guanide groups and yields an explanation of D3's ability to overcome the blood-brain barrier^{141,142}. A comparison between the protein Tat and D3/RD2 is given in Fig. D3. There are similarities in other regions too, but the highest similarity occurs in the basic cluster, which mediates Tat's functionality to mediate membranes.

Tat :	53	RQRRRAH
D3 :	1	RPRTLH
		* * * *

Tat :	52	RRQRR
RD2 :	8	RRRRR
		* * * *

Figure D3: Alignment of D3/RD2 with HIV-1 protein Tat. Both peptides have a high similarity to one highly charged cluster of the virus protein Tat.

This is interesting, because usually the ability of a drug to permeate membranes scales roughly with its solubility in fat, but decreases rapidly with the hydrophilicity. Additionally, drugs with a higher hydrophobicity are more likely the target of enzymes, which decreases their bioavailability¹⁴³. D3 is a peptide and thus passes the gastrointestinal tract efficiently. Additionally, D3 combines a high solubility ($\gg 10$ mM) and enzymatic stability with the ability to pass plasma membranes likely due to an arginine driven mechanism.

5.5 Multivalency in D-peptides

In this work it was possible to demonstrate, that dimerization of peptides increases always the affinity to A β (Tab. S1). Unfortunately, fitting with a 1:1 Langmuir binding model yielded high fitting errors (more than 20 % of the R_{\max}) and may not correctly describe the interaction with the ligand (see: *Mechanism for the interaction of D3 with A β*). A comparison of estimated and predicted K_D , based on the interaction of the peptides D3, RD2 and their tandem peptides with A β is given in Tab. R4 and Fig. R16. In comparison to D3, the predicted K_D of RD2 was closer to the estimated one.

If the interaction of D3 is driven mainly by the arginine residues, differences between the peptides D3 and RD2 would be expected. In the case of D3, the basic amino acids are more or less equally distributed in the sequence. RD2 possesses an accumulation of basic amino acids at the C-terminus, and thus RD2RD2 may behave as having two binding sites with less cooperativity in comparison with D3D3.

5.6 Combinations with the A β binding site D7

D7 (sequence: “htrfeyyvvhms”) contains three tyrosines and one phenylalanine, which renders this peptide hydrophobic and reduces solubility in water. RD2 has a condensation of charges at its C-terminus (sequence: “ptlhthnrrrrr”) and is very hydrophilic. The combination of RD2 with D7 seemed to cause an increase in affinity to A β . The R_{\max}

increased by the factor of ~8, the mass however, just doubled. This observation could be caused by i) oligomerization or ii) micelle like formation¹⁴⁴ and/or as a consequence of the iii) presence of two different binding sites.

Regarding the hypothesis i), D7RD2 and RD2D7 may form oligomers. However, the solubility of D7 is much lower and neither binding kinetics, nor R_{\max} indicate the presence of oligomers for concentrations up to 12.5 μM . Nevertheless oligomer formation seems possible, because hydrophobic regions of RD2D7 and D7RD2 are longer in comparison with D7. For RD2D7, the arginine rich region is in the center of the peptide and thus a different performance in comparison to D7RD2 would be expected.

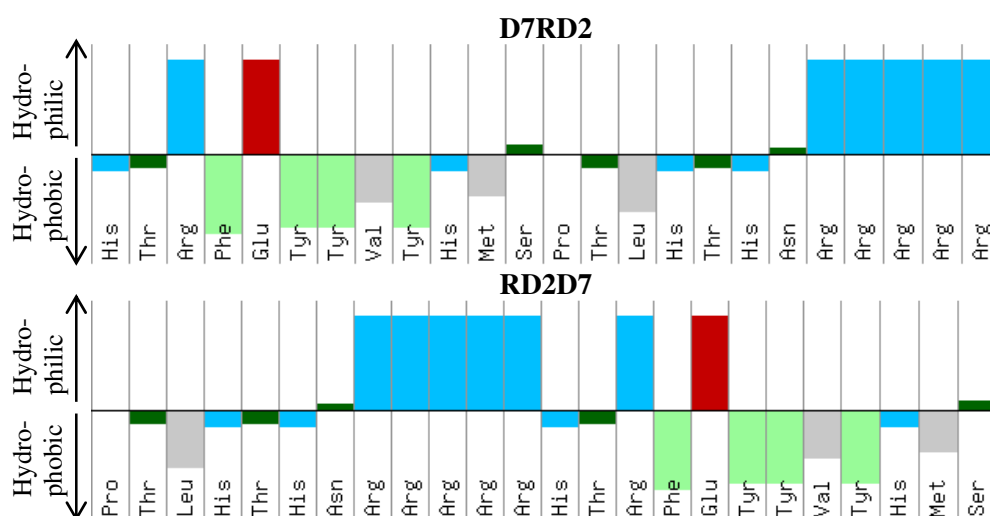


Figure D4: Hydropathy plot of D7RD2 and RD2D7. Both peptides contain the same composition of binding sites, but a different arrangement. Color code **Acidic**, **Aromatic**, **Basic**, **Aliphatic**, **Polar**.

Thus, both peptides, D7RD2 and RD2D7 were expected to show a difference in K_D . Indeed, the kinetic fits showed a noticeable difference in the K_D . A prediction for micelle formation would be that interactions with the dextran matrix should be greatly increased. Dextran possesses hydroxyl groups and the cluster of basic amino acids in both, RD2D7 and D7RD2, should interact with different affinities towards the dextran matrix. However, unspecific binding with the matrix was similar for both peptides. In conclusion, micelle formation is very unlikely, but oligomer formation may be present. Oligomer formation of the analyte obfuscates affinity estimation. Because of avidity the estimated K_D s would be smaller than the true affinities for the monomeric peptide. Furthermore, sample heterogeneity increases the complexity of the kinetics. The most certain indicator of oligomer formation would be an R_{\max} value which is higher than possible for non-aggregated RD2D7 or D7RD2. For RD2D7 and D7RD2 the R_{\max} values increased drastically in comparison to RD2 or D7, but remained lower than the theoretical maximum. This is an indicator but not a proof of peptide oligomerization.

DLS measurements provide evidence of oligomeric species, but do not allow the accurate quantification of them. However, this would facilitate the evaluation of the fits.

With two different binding sites for one epitope, one could increase the agent concentration at the target as long as there are no steric hindrances (for small peptides they would be low in comparison to IgGs). In the case of radiotherapy it would be possible to create higher local radiation dosages with less side-effect. The short half-life time of peptides in the body would be an additional advantage. Unfortunately, the combination with D7 led to oligomer formation, as determined by DLS measurements.

5.7 Cyclisation of D-peptides

Cyclisation of compounds was intended to make interactions energetically more favorable by decreasing the entropy. Cyclisation of peptides removed one net charge. It was possible to demonstrate that compensation of the removed charge by insertion of an arginine could increase the affinity to A β .

Estimation of thermodynamic properties showed that enthalpy and entropy of linear and cyclic D3-derivatives are similar. However it was not possible to demonstrate a decrease in entropy. One possibility is that there really is no decrease in entropy. Another explanation is that the fitting error increased with the temperature. This is reasonable because the affinity decreases with increasing temperature, as the interaction is exergonic. This leads to a reduction of sensorgram curvature. The easiest alternative for estimating thermodynamics would be application of ITC, because this technique is not dependent on the size of the interactants. Unfortunately, for ITC both A β and D3 have to be in solution at high concentrations (mM range). However, A β is hard to solubilize and forms oligomeric particles spontaneously. Use of soluble fragments like A β (1-16) to A β (1-28) would overcome the low solubility, but raises new questions regarding comparability with A β (1-42).

5.8 Peptides as drugs and optimization strategies for D3

In the following sections, some brief suggestions to enhance the properties of peptide based drug candidates like D3 and its derivatives are given and discussed. In general, optimization should enhance existing properties without impairing existing advantages. This is the reason why some strategies are preferred in comparison with others in the following sections.

5.8.1 Is adding binding sites useful?

Predictions of polyvalent D3-derivatives seem possible, as comparisons with D3- or RD2-tandem peptides revealed and allow estimation of the binding affinity. One option of peptide

optimization is to rapidly increase the affinity by adding additional binding sites. However it is questionable whether multimerization makes D-peptides more effective for AD therapy. This is because of mainly three reasons. i) The dependency of the K_D to the number of binding sites is proportional only under ideal conditions. Secondary effects which perturb this interaction are e.g. rotational and translational entropy, which shows a weak correlation with the mass, the conformational entropy of linkers (if present) and the effects of cooperativity between binding sites (if present)¹⁰¹. ii) The biggest advantage of peptide drugs in comparison to proteins is their size. Because of this, synthesis is possible and makes production scalable and cost effective. The addition of binding sites reduces this advantage, because the efficiency of synthesis and purification decays with the length.

5.8.2 How to enhance the plasma half-life time?

Because peptides are known for fast renal clearance (in the timescale of minutes), one should focus on optimization of the half-life time of D3-derivatives¹⁴⁵. Renal tissue contains glomeruli with a pore size of around 8 nm, which corresponds to a cut-off size of approximately 5 kDa. Most particles below 5 kDa are cleared very fast¹⁴⁵. In contrast, proteins with sizes above 50-70 kDa remain efficiently in the bloodstream¹⁴⁵. However, there are some exceptions, some peptides with long half-life times are able to interact with huge plasma proteins.

Consequently, the easiest way to optimize the half-life time would be to increase the size. This could be achieved by linking to polymers like i) PEG, ii) plasma proteins with long half-life times, or iii) binding domains of serum albumins¹⁴⁵. Linking to lipophilic groups such as iv) triglycerides is a common procedure to increase the membrane permeability of small molecules and for peptide drugs it could increase the size which would be beneficial for the half-life time. Unfortunately, for D3-derivatives this would remove some of the positive properties, such as solubility and may cause micelle formation. Adding a PEG-tag would not reduce solubility, but the chance of the compound to permeate membranes might suffer. The same problem might appear when D3 is linked to a large protein. The best might be coupling to a (small < 20 amino acids) albumin binding domain¹⁴⁶. This would keep the compound small, soluble, the ability to permeate membranes would be maintained, and it ensures a prolonged plasma half-life time.

5.9 Future perspective of peptide design

Within this work, the main mechanisms of the interaction of D3 and related peptides with A β were evaluated and discussed. Here, I will give the sequence of an optimized D3-derivative.

Previous work revealed the consensus sequence “DICLPRWGCLW” for an albumin binding L-peptide¹⁴⁶. For compatibility with the existing D-peptide system it is necessary to translate this sequence into a D-peptide sequence with preserved arrangement of side chains. To achieve this, the sequence can be translated into a retro-inverso D-peptide sequence. The idea was already explained in the introduction and preserves elements of the structure (see: Fig. I3). The result is the D-peptide sequence “wlcgwrplcid”. This peptide has the same arrangement of side chains. Unfortunately, the direction of the C- and N-terminus is inverted. However, literature indicates that the impact of this circumstance is neglectable for peptides in this length scale¹⁴⁷.

A more critical point in peptide design is the production efficiency. The aim is to keep the peptide as small as possible, which is important for properties like trans-membrane transport too. Consequently, the suggested binding site “wlcgwrplcid” could be tagged to the gently truncated RD2(3-12) sequence “hthnrrrrr”. The result is demonstrated in Fig. D5. The suggested peptide may have a better plasma half-life time. Additionally, the affinity to A β could be increased by additional interaction potential through the N-terminal aliphatic region. Similar was observed already when comparing RD2 with D3.

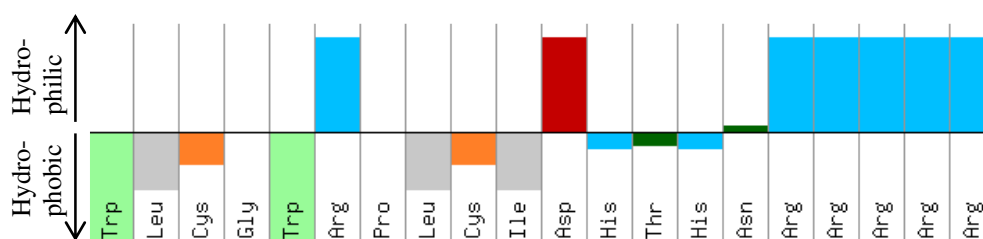


Figure D5: Hydropathy plot of a 20 amino acid D-peptide for AD therapy. This example consists of a truncated RD2 binding site and the retro-inverso sequence of a serum albumin consensus sequence. Color code **Acidic**, **Aromatic**, **Basic**, **Aliphatic**, **Polar**, **Cysteine**.

Obviously, the pharmacokinetics of this suggested peptide will change. In the organism, there will be an equilibrium reaction of binding and dissociation from the serum albumins. The affinity of the peptide to the serum albumins will have a direct impact on the i) half-life time and the ii) availability for the main target A β . Only the free (unbound) peptide will be able to pass the blood brain barrier and bind extracellular A β .

Future work is necessary to elucidate the necessity of a linker or the introduction of additional amino acids between or around the two binding sites. Moreover, the affinity of the albumin binding site should be well tuned, considering the points i) and ii).

6. Summary

The market for peptide based drugs is continuously growing because peptides can be produced in a scalable and cost efficient way, and may offer a possibility for treatment of Alzheimer's disease (AD). Peptides fulfill versatile roles in nature. Often they act as signal or transmitter molecules. A drawback of L-peptides is their propensity for degradation. In contrast, D-peptides possess enhanced enzymatic stability. In this work, D-peptides for AD therapy were characterized by SPR spectroscopy with the aim of property and sequence optimization.

Homogenous purification and immobilization of different A β species is crucial for *in-vitro* SPR experiments. TEM and AFM micrographs proved the feasibility of the applied purification protocols for the selected A β species. For characterization of the SPR sensor surfaces, the monovalent analyte scFv-IC16 was chosen. scFv-IC16 was able to prove the existence of oligomeric/fibrillar A β species after immobilization. Results of scFv-IC16 indicate the existence of an additional binding site for oligomeric and fibrillar A β species. The D-peptide D3 is able to bind all immobilized A β (1-42) species such as monomers, oligomers, fibrils and pE3-A β (3-40) oligomers and fibrils with similar affinity. Important spots in the sequence of D3, which alter the affinity to A β have been localized by alignments of D3-derivatives. Despite the fact that the D-peptide RD2 possesses the same AA-composition as D3, it showed a higher affinity to all tested A β (1-42) species. In comparison to the monovalent peptides D3 and RD2, the corresponding tandem peptides D3D3/RD2RD2 (and their permutations) showed an increased affinity to all A β (1-42) species. This observation was congruent with the suggested model of avidity used for affinity prediction of such tandem peptides. The interaction of the D-peptide D7 with A β displayed in comparison to D3 or RD2 a different association and dissociation pattern. In contrast to the expectations, the RD2/D7 tandem peptides showed a greatly enhanced surface activity and increased interaction complexity. These observations are explainable by oligomerization (*but not precipitation*) of the tandem peptides with each other.

7. Zusammenfassung

Peptide spielen in der Natur vielfältige Rollen und dienen beispielsweise als Signal- oder Transmittermoleküle. Einer der Vorteile von Peptiden im Vergleich zu Proteinen ist ihre einfache und skalierbare Produktion. Nicht zuletzt deswegen werden Peptide verstärkt als Medikamente eingesetzt. Mittlerweile ist auch der Einsatz zur Behandlung von Morbus Alzheimer (AD) denkbar, da einige Peptide in der Lage sind die Bluthirnschranke zu überwinden. Allerdings werden L-Peptide leicht enzymatisch abgebaut. D-Peptide sind im Vergleich stabiler. In dieser Arbeit wurden D-Peptide mit SPR-Spektroskopie mit dem Ziel der Sequenz- und Eigenschaftsoptimierung charakterisiert.

Die homogene Aufreinigung und Immobilisierung von A β -Monomeren, -Oligomeren und – Fibrillen für SPR-Spektroskopie ist von entscheidender Bedeutung für die Verlässlichkeit von *in-vitro* Assays. TEM und AFM Aufnahmen untermauern die Notwendigkeit der verwendeten Aufreinigungsprotokolle. Die so hergestellten Sensoroberflächen wurden mit scFv-IC16 charakterisiert. Dadurch war es möglich höhermolekulare A β (1-42)-Spezies nachzuweisen und von A β (1-42)-Monomeren zu unterscheiden. Momentan wird die Rolle von pE3-A β -Oligomeren bei AD diskutiert. Eine Möglichkeit der Herstellung und Immobilisierung von pE3(3-40)-A β -Oligomeren/Fibrillen wurde demonstriert. D3 war in der Lage alle untersuchten A β (1-42)-Spezies und pE3-A β (3-40)-Oligomere/Fibrillen mit vergleichbarer Affinität binden kann. Durch Alignements von D3-Derivaten konnten Bereiche in der Sequenz von D3 und A β (1-42) ausfindet gemacht werden, die die Affinität der Interaktion beeinflussen. Im Vergleich zu D3, zeigt RD2 eine höhere Affinität zu allen untersuchten A β (1-42)-Spezies, obwohl die AA-Zusammensetzung beider Peptide identisch ist. Die Tandempeptide D3D3/RD2RD2 zeigten im Vergleich zu D3 bzw. RD2 eine erhöhte Affinität gegenüber allen untersuchten A β (1-42)-Spezies. Diese Beobachtung entspricht dem verwendeten Modell zur Berechnung der Affinität basierend auf Avidität. Die Interaktion von D7 und A β (1-42) besitzt im Vergleich zu D3 oder RD2 andere Assoziations- und Dissoziationsverläufe. Die abgeleiteten Tandempeptide auf Basis von D7 und RD2 wiesen eine deutlich stärker erhöhte Oberflächenaktivität auf, als bei anderen Tandempeptiden festgestellt wurde. Dieser Effekt war nur durch die Oligomerisierung der Tandempeptide untereinander erklärbar.

8. Literature

- 1 Halpert, B. P. Development of the term "senility" as a medical diagnosis. *Minnesota medicine* **66**, 421-424 (1983).
- 2 Terry, R. D. The pathogenesis of Alzheimer disease: an alternative to the amyloid hypothesis. *Journal of neuropathology and experimental neurology* **55**, 1023-1025 (1996).
- 3 Berchtold, N. C. & Cotman, C. W. Evolution in the Conceptualization of Dementia and Alzheimer's Disease: Greco-Roman Period to the 1960s. *Neurobiology of Aging* **19**, 173-189, doi:[http://dx.doi.org/10.1016/S0197-4580\(98\)00052-9](http://dx.doi.org/10.1016/S0197-4580(98)00052-9) (1998).
- 4 Mahendra, B. *Dementia: A survey of the syndrome of dementia*. (MTP Press Limited, 1987).
- 5 Magner, L. N. *A History of Medicine*. (Taylor & Francis, 1992).
- 6 Venzmer, G. *Five Thousand Years of Medicine*. (Taplinger, 1972).
- 7 Bernal, J. D. *Science in History: Volume 1 : the Emergence of Science*. (C.A. Watts & Company Limited, 1969).
- 8 Shakespeare, W. & Harbage, A. *The complete works*. (The Viking Press, 1977).
- 9 Barrough, P. *The Methode of Phisicke: Conteyning the Causes, Signes, and Cures of Inward Diseases in Mans Body from the Head to the Foote : where Unto is Added, the Forme and Rule of Making Remedies and Medicines, which Our Phisitians Commonly Use at this Day, with the Proportion, Quantitie, & Names of Ech Medicine*. (Vautroullier, 1583).
- 10 MACALPINE, R. A. H. & Macalpine, I. *Three Hundred Years of Psychiatry, 1535-1860. A History Presented in Selected English Texts. [Edited By] R. Hunter ... I. Macalpine. [With Illustrations]*. (Oxford University Press, 1963).
- 11 Pinel, P. *A Treatise on Insanity: In which are Contained the Principles of a New and More Practical Nosology of Maniacal Disorders Than Has Yet Been Offered to the Public*. (W. Todd, 1806).
- 12 Berrios, G. E. in *Dementia* (eds Alistair Burns & Raymond Levy) Ch. 1, 5-19 (Springer US, 1994).
- 13 Forstl, H. & Howard, R. Recent studies on dementia senilis and brain disorders caused by atheromatous vascular disease: by A. Alzheimer, 1898. *Alzheimer disease and associated disorders* **5**, 257-264 (1991).
- 14 Hachinski, V. Binswanger's disease: neither Binswanger's nor a disease. *Journal of the neurological sciences* **103**, 1 (1991).
- 15 Mast, H., Tatemichi, T. K. & Mohr, J. P. Chronic brain ischemia: the contributions of Otto Binswanger and Alois Alzheimer to the mechanisms of vascular dementia. *Journal of the neurological sciences* **132**, 4-10 (1995).
- 16 Schneider, R. & Wiczorek, V. Historical aspects of neurosciences. Otto Binswanger (1852-1929). *Journal of the neurological sciences* **103**, 61-64 (1991).
- 17 Marinesco, G. *Sur les lésions et la pathogénie de l'épilepsie dite essentielle, par MM. les Drs Paul Blocq et Georges Marinesco*.
- 18 Schiller, F. *Founders of Neurology*. (Charles C Thomas, 1970).
- 19 Amor, S. *et al.* Inflammation in neurodegenerative diseases--an update. *Immunology* **142**, 151-166, doi:10.1111/imm.12233 (2014).
- 20 Golde, T. E. & Miller, V. M. Proteinopathy-induced neuronal senescence: a hypothesis for brain failure in Alzheimer's and other neurodegenerative diseases. *Alzheimer's research & therapy* **1**, 5, doi:10.1186/alzrt5 (2009).
- 21 Golde, T. E., Eckman, C. B. & Younkin, S. G. Biochemical detection of A β isoforms: implications for pathogenesis, diagnosis, and treatment of Alzheimer's disease.

- Biochimica et Biophysica Acta (BBA) - Molecular Basis of Disease* **1502**, 172-187, doi:[http://dx.doi.org/10.1016/S0925-4439\(00\)00043-0](http://dx.doi.org/10.1016/S0925-4439(00)00043-0) (2000).
- 22 Pesiridis, G. S., Lee, V. M. & Trojanowski, J. Q. Mutations in TDP-43 link glycine-rich domain functions to amyotrophic lateral sclerosis. *Human molecular genetics* **18**, R156-162, doi:10.1093/hmg/ddp303 (2009).
 - 23 Narhi, L. *et al.* Both familial Parkinson's disease mutations accelerate alpha-synuclein aggregation. *The Journal of biological chemistry* **274**, 9843-9846 (1999).
 - 24 Suzuki, H. *et al.* ALS-linked P56S-VAPB, an aggregated loss-of-function mutant of VAPB, predisposes motor neurons to ER stress-related death by inducing aggregation of co-expressed wild-type VAPB. *Journal of neurochemistry* **108**, 973-985, doi:10.1111/j.0022-3042.2008.05857.x (2009).
 - 25 Rajagopalan, S. & Andersen, J. K. Alpha synuclein aggregation: is it the toxic gain of function responsible for neurodegeneration in Parkinson's disease? *Mechanisms of ageing and development* **122**, 1499-1510 (2001).
 - 26 Lindholm, D., Wootz, H. & Korhonen, L. ER stress and neurodegenerative diseases. *Cell death and differentiation* **13**, 385-392 (2006).
 - 27 Takeda, K., Kaisho, T. & Akira, S. Toll-like receptors. *Annual review of immunology* **21**, 335-376, doi:10.1146/annurev.immunol.21.120601.141126 (2003).
 - 28 McDermott, M. F. & Tschopp, J. From inflammasomes to fevers, crystals and hypertension: how basic research explains inflammatory diseases. *Trends in molecular medicine* **13**, 381-388, doi:10.1016/j.molmed.2007.07.005 (2007).
 - 29 Mond, J. J., Lees, A. & Snapper, C. M. T cell-independent antigens type 2. *Annual review of immunology* **13**, 655-692, doi:10.1146/annurev.iy.13.040195.003255 (1995).
 - 30 Mond, J. J., Vos, Q., Lees, A. & Snapper, C. M. T cell independent antigens. *Current opinion in immunology* **7**, 349-354 (1995).
 - 31 Glenner, G. G. Amyloid deposits and amyloidosis. The beta-fibrilloses (first of two parts). *The New England journal of medicine* **302**, 1283-1292, doi:10.1056/NEJM198006053022305 (1980).
 - 32 Garcia, K. C., Teyton, L. & Wilson, I. A. Structural basis of T cell recognition. *Annual review of immunology* **17**, 369-397, doi:10.1146/annurev.immunol.17.1.369 (1999).
 - 33 Jankowsky, J. L. *et al.* Persistent amyloidosis following suppression of Abeta production in a transgenic model of Alzheimer disease. *PLoS medicine* **2**, e355, doi:10.1371/journal.pmed.0020355 (2005).
 - 34 Bacskaï, B. J. *et al.* Imaging of amyloid-beta deposits in brains of living mice permits direct observation of clearance of plaques with immunotherapy. *Nature medicine* **7**, 369-372, doi:10.1038/85525 (2001).
 - 35 Prada, C. M. *et al.* Antibody-mediated clearance of amyloid-beta peptide from cerebral amyloid angiopathy revealed by quantitative in vivo imaging. *The Journal of neuroscience : the official journal of the Society for Neuroscience* **27**, 1973-1980, doi:10.1523/JNEUROSCI.5426-06.2007 (2007).
 - 36 Bence, N. F., Sampat, R. M. & Kopito, R. R. Impairment of the ubiquitin-proteasome system by protein aggregation. *Science* **292**, 1552-1555, doi:10.1126/science.292.5521.1552 (2001).
 - 37 Venkatraman, P., Wetzel, R., Tanaka, M., Nukina, N. & Goldberg, A. L. Eukaryotic proteasomes cannot digest polyglutamine sequences and release them during degradation of polyglutamine-containing proteins. *Molecular cell* **14**, 95-104 (2004).
 - 38 Yamamoto, A., Lucas, J. J. & Hen, R. Reversal of neuropathology and motor dysfunction in a conditional model of Huntington's disease. *Cell* **101**, 57-66, doi:10.1016/S0092-8674(00)80623-6 (2000).
 - 39 Li, J. *et al.* Enhancement of proteasomal function protects against cardiac proteinopathy and ischemia/reperfusion injury in mice. *The Journal of clinical investigation* **121**, 3689-3700, doi:10.1172/JCI45709 (2011).

- 40 Janeway, C. A., Jr. How the immune system recognizes invaders. *Scientific American* **269**, 72-79 (1993).
- 41 Hayflick, L. The Limited in Vitro Lifetime of Human Diploid Cell Strains. *Experimental cell research* **37**, 614-636 (1965).
- 42 Campisi, J. & d'Adda di Fagagna, F. Cellular senescence: when bad things happen to good cells. *Nature reviews. Molecular cell biology* **8**, 729-740, doi:10.1038/nrm2233 (2007).
- 43 Korsak, K., Dolatshad, N. F., Silva, A. T. & Saffrey, M. J. Ageing of enteric neurons: oxidative stress, neurotrophic factors and antioxidant enzymes. *Chemistry Central journal* **6**, 80, doi:10.1186/1752-153X-6-80 (2012).
- 44 Cantuti-Castelvetri, I. *et al.* Somatic mitochondrial DNA mutations in single neurons and glia. *Neurobiol Aging* **26**, 1343-1355, doi:10.1016/j.neurobiolaging.2004.11.008 (2005).
- 45 Ridge, P. G., Ebbert, M. T. W. & Kauwe, J. S. K. Genetics of Alzheimer's Disease. *BioMed Research International* **2013**, 13, doi:10.1155/2013/254954 (2013).
- 46 Patterson, C. *et al.* Diagnosis and treatment of dementia: 1. Risk assessment and primary prevention of Alzheimer disease. *CMAJ : Canadian Medical Association journal = journal de l'Association medicale canadienne* **178**, 548-556, doi:10.1503/cmaj.070796 (2008).
- 47 Thinakaran, G. & Koo, E. H. Amyloid precursor protein trafficking, processing, and function. *The Journal of biological chemistry* **283**, 29615-29619, doi:10.1074/jbc.R800019200 (2008).
- 48 Cruts, M. & Van Broeckhoven, C. Molecular genetics of Alzheimer's disease. *Annals of medicine* **30**, 560-565 (1998).
- 49 Choy, R. W., Cheng, Z. & Schekman, R. Amyloid precursor protein (APP) traffics from the cell surface via endosomes for amyloid beta (Abeta) production in the trans-Golgi network. *Proceedings of the National Academy of Sciences of the United States of America* **109**, E2077-2082, doi:10.1073/pnas.1208635109 (2012).
- 50 Kim, J. *et al.* Biogenesis of gamma-secretase early in the secretory pathway. *The Journal of cell biology* **179**, 951-963, doi:10.1083/jcb.200709012 (2007).
- 51 Le Roy, C. & Wrana, J. L. Clathrin- and non-clathrin-mediated endocytic regulation of cell signalling. *Nature reviews. Molecular cell biology* **6**, 112-126, doi:10.1038/nrm1571 (2005).
- 52 Wu, F. & Yao, P. J. Clathrin-mediated endocytosis and Alzheimer's disease: an update. *Ageing research reviews* **8**, 147-149, doi:10.1016/j.arr.2009.03.002 (2009).
- 53 Takeda, A. *et al.* In Alzheimer's disease, heme oxygenase is coincident with Alz50, an epitope of tau induced by 4-hydroxy-2-nonenal modification. *Journal of neurochemistry* **75**, 1234-1241 (2000).
- 54 Busciglio, J., Lorenzo, A., Yeh, J. & Yankner, B. A. beta-amyloid fibrils induce tau phosphorylation and loss of microtubule binding. *Neuron* **14**, 879-888 (1995).
- 55 Sutherland, C. What Are the bona fide GSK3 Substrates? *International journal of Alzheimer's disease* **2011**, 505607, doi:10.4061/2011/505607 (2011).
- 56 Melov, S. *et al.* Mitochondrial oxidative stress causes hyperphosphorylation of tau. *PLOS ONE* **2**, e536, doi:10.1371/journal.pone.0000536 (2007).
- 57 Duran, M. C., Chan, H. L. & Timms, J. F. Identification of oxidative stress-induced tyrosine phosphorylated proteins by immunoprecipitation and mass spectrometry. *Methods Mol Biol* **527**, 33-45, ix, doi:10.1007/978-1-60327-834-8_3 (2009).
- 58 Russell, R. C., Yuan, H. X. & Guan, K. L. Autophagy regulation by nutrient signaling. *Cell research* **24**, 42-57, doi:10.1038/cr.2013.166 (2014).
- 59 Morgan, D. O. Principles of CDK regulation. *Nature* **374**, 131-134, doi:10.1038/374131a0 (1995).

- 60 Canman, C. E. *et al.* Activation of the ATM kinase by ionizing radiation and phosphorylation of p53. *Science* **281**, 1677-1679 (1998).
- 61 Wagner, E. F. & Nebreda, A. R. Signal integration by JNK and p38 MAPK pathways in cancer development. *Nature reviews. Cancer* **9**, 537-549, doi:10.1038/nrc2694 (2009).
- 62 Wang, J. Z., Xia, Y. Y., Grundke-Iqbal, I. & Iqbal, K. Abnormal hyperphosphorylation of tau: sites, regulation, and molecular mechanism of neurofibrillary degeneration. *Journal of Alzheimer's disease : JAD* **33 Suppl 1**, S123-139, doi:10.3233/JAD-2012-129031 (2013).
- 63 Porter, A. G. & Janicke, R. U. Emerging roles of caspase-3 in apoptosis. *Cell death and differentiation* **6**, 99-104, doi:10.1038/sj.cdd.4400476 (1999).
- 64 Jo, J. *et al.* Abeta(1-42) inhibition of LTP is mediated by a signaling pathway involving caspase-3, Akt1 and GSK-3beta. *Nature neuroscience* **14**, 545-547, doi:10.1038/nn.2785 (2011).
- 65 Hernandez, F., Gomez de Barreda, E., Fuster-Matanzo, A., Lucas, J. J. & Avila, J. GSK3: a possible link between beta amyloid peptide and tau protein. *Experimental neurology* **223**, 322-325, doi:10.1016/j.expneurol.2009.09.011 (2010).
- 66 Beurel, E. & Jope, R. S. The paradoxical pro- and anti-apoptotic actions of GSK3 in the intrinsic and extrinsic apoptosis signaling pathways. *Progress in neurobiology* **79**, 173-189, doi:10.1016/j.pneurobio.2006.07.006 (2006).
- 67 Li, H. L. *et al.* Phosphorylation of tau antagonizes apoptosis by stabilizing beta-catenin, a mechanism involved in Alzheimer's neurodegeneration. *Proceedings of the National Academy of Sciences of the United States of America* **104**, 3591-3596, doi:10.1073/pnas.0609303104 (2007).
- 68 Wang, H. H. *et al.* Tau overexpression inhibits cell apoptosis with the mechanisms involving multiple viability-related factors. *Journal of Alzheimer's disease : JAD* **21**, 167-179, doi:10.3233/JAD-2010-091279 (2010).
- 69 Fath, T., Eidenmuller, J. & Brandt, R. Tau-mediated cytotoxicity in a pseudohyperphosphorylation model of Alzheimer's disease. *The Journal of neuroscience : the official journal of the Society for Neuroscience* **22**, 9733-9741 (2002).
- 70 Stoothoff, W. H. & Johnson, G. V. Hyperosmotic stress-induced apoptosis and tau phosphorylation in human neuroblastoma cells. *Journal of neuroscience research* **65**, 573-582 (2001).
- 71 Fasulo, L., Ugolini, G. & Cattaneo, A. Apoptotic effect of caspase-3 cleaved tau in hippocampal neurons and its potentiation by tau FTDP-mutation N279K. *Journal of Alzheimer's disease : JAD* **7**, 3-13 (2005).
- 72 Marin, N. *et al.* Beta-amyloid-induced activation of caspase-3 in primary cultures of rat neurons. *Mechanisms of ageing and development* **119**, 63-67 (2000).
- 73 Harada, J. & Sugimoto, M. Activation of caspase-3 in beta-amyloid-induced apoptosis of cultured rat cortical neurons. *Brain research* **842**, 311-323 (1999).
- 74 Snyder, E. M. *et al.* Regulation of NMDA receptor trafficking by amyloid-beta. *Nature neuroscience* **8**, 1051-1058, doi:10.1038/nn1503 (2005).
- 75 Hernandez, C. M., Kaye, R., Zheng, H., Sweatt, J. D. & Dineley, K. T. Loss of alpha7 nicotinic receptors enhances beta-amyloid oligomer accumulation, exacerbating early-stage cognitive decline and septohippocampal pathology in a mouse model of Alzheimer's disease. *The Journal of neuroscience : the official journal of the Society for Neuroscience* **30**, 2442-2453, doi:10.1523/JNEUROSCI.5038-09.2010 (2010).
- 76 Movsesyan, V. A., Stoica, B. A. & Faden, A. I. MGLuR5 activation reduces beta-amyloid-induced cell death in primary neuronal cultures and attenuates translocation

- of cytochrome c and apoptosis-inducing factor. *Journal of neurochemistry* **89**, 1528-1536, doi:10.1111/j.1471-4159.2004.02451.x (2004).
- 77 Renner, M. *et al.* Deleterious effects of amyloid beta oligomers acting as an extracellular scaffold for mGluR5. *Neuron* **66**, 739-754, doi:10.1016/j.neuron.2010.04.029 (2010).
- 78 Michalon, A. *et al.* Chronic pharmacological mGlu5 inhibition corrects fragile X in adult mice. *Neuron* **74**, 49-56, doi:10.1016/j.neuron.2012.03.009 (2012).
- 79 Nussbaum, J. M. *et al.* Prion-like behaviour and tau-dependent cytotoxicity of pyroglutamylated amyloid-beta. *Nature* **485**, 651-655, doi:10.1038/nature11060 (2012).
- 80 Tekirian, T. L., Yang, A. Y., Glabe, C. & Geddes, J. W. Toxicity of pyroglutaminated amyloid beta-peptides 3(pE)-40 and -42 is similar to that of A beta1-40 and -42. *Journal of neurochemistry* **73**, 1584-1589 (1999).
- 81 Pivtoraiko, V. N. *et al.* Cortical pyroglutamate amyloid-beta levels and cognitive decline in Alzheimer's disease. *Neurobiol Aging*, doi:10.1016/j.neurobiolaging.2014.06.021 (2014).
- 82 Becker, A. *et al.* Glutaminyl cyclase-mediated toxicity of pyroglutamate-beta amyloid induces striatal neurodegeneration. *BMC neuroscience* **14**, 108, doi:10.1186/1471-2202-14-108 (2013).
- 83 Lison, H. *et al.* Disrupted cross-laminar cortical processing in beta amyloid pathology precedes cell death. *Neurobiology of disease* **63**, 62-73, doi:10.1016/j.nbd.2013.11.014 (2014).
- 84 Morawski, M. *et al.* Glutaminyl cyclase in human cortex: correlation with (pGlu)-amyloid-beta load and cognitive decline in Alzheimer's disease. *Journal of Alzheimer's disease : JAD* **39**, 385-400, doi:10.3233/JAD-131535 (2014).
- 85 Freir, D. B. *et al.* Interaction between prion protein and toxic amyloid beta assemblies can be therapeutically targeted at multiple sites. *Nature communications* **2**, 336, doi:10.1038/ncomms1341 (2011).
- 86 Forloni, G., Scip, A., Borsello, T. & Balducci, C. The neurodegeneration in Alzheimer disease and the prion protein. *Prion* **7**, 60-65, doi:10.4161/pri.23286 (2013).
- 87 Chen, S., Yadav, S. P. & Surewicz, W. K. Interaction between human prion protein and amyloid-beta (Abeta) oligomers: role OF N-terminal residues. *The Journal of biological chemistry* **285**, 26377-26383, doi:10.1074/jbc.M110.145516 (2010).
- 88 Abramov, A. Y., Canevari, L. & Duchen, M. R. Beta-amyloid peptides induce mitochondrial dysfunction and oxidative stress in astrocytes and death of neurons through activation of NADPH oxidase. *The Journal of neuroscience : the official journal of the Society for Neuroscience* **24**, 565-575, doi:10.1523/JNEUROSCI.4042-03.2004 (2004).
- 89 Lashuel, H. A., Hartley, D., Petre, B. M., Walz, T. & Lansbury, P. T., Jr. Neurodegenerative disease: amyloid pores from pathogenic mutations. *Nature* **418**, 291, doi:10.1038/418291a (2002).
- 90 Demuro, A., Smith, M. & Parker, I. Single-channel Ca(2+) imaging implicates Abeta1-42 amyloid pores in Alzheimer's disease pathology. *The Journal of cell biology* **195**, 515-524, doi:10.1083/jcb.201104133 (2011).
- 91 Lee, J. *et al.* Role of the fast kinetics of pyroglutamate-modified amyloid-beta oligomers in membrane binding and membrane permeability. *Biochemistry* **53**, 4704-4714, doi:10.1021/bi500587p (2014).
- 92 Chinnery, P. F., Samuels, D. C., Elson, J. & Turnbull, D. M. Accumulation of mitochondrial DNA mutations in ageing, cancer, and mitochondrial disease: is there a common mechanism? *Lancet* **360**, 1323-1325, doi:10.1016/S0140-6736(02)11310-9 (2002).

- 93 WATCHING PEPTIDE DRUGS GROW UP. *Chemical & Engineering News Archive* **83**, 17-24, doi:10.1021/cen-v083n011.p017 (2005).
- 94 Current Pharmaceutical Design. *Bentham Science Publishers* **5**, 66 (1990).
- 95 Chong, P., Sia, C., Tripet, B., James, O. & Klein, M. Comparative immunological properties of enantiomeric peptides. *Lett Pept Sci* **3**, 99-106, doi:10.1007/bf00126739 (1996).
- 96 Gainza, P. *Wikipedia*, 1 (2010).
- 97 Sun, N., Funke, S. A. & Willbold, D. Mirror image phage display--generating stable therapeutically and diagnostically active peptides with biotechnological means. *Journal of biotechnology* **161**, 121-125, doi:10.1016/j.jbiotec.2012.05.019 (2012).
- 98 Horton, D. A., Bourne, G. T. & Smythe, M. L. Exploring privileged structures: the combinatorial synthesis of cyclic peptides. *Journal of computer-aided molecular design* **16**, 415-430 (2002).
- 99 Szilard, L. über die Entropieverminderung in einem thermodynamischen System bei Eingriffen intelligenter Wesen. *Z. Physik* **53**, 840-856, doi:10.1007/bf01341281 (1929).
- 100 Morton, T. A., Myszka, D. G. & Chaiken, I. M. Interpreting complex binding kinetics from optical biosensors: a comparison of analysis by linearization, the integrated rate equation, and numerical integration. *Analytical biochemistry* **227**, 176-185, doi:10.1006/abio.1995.1268 (1995).
- 101 Krishnamurthy, V. M., Estroff, L. A. & Whitesides, G. M. in *Fragment-based Approaches in Drug Discovery* 11-53 (Wiley-VCH Verlag GmbH & Co. KGaA, 2006).
- 102 Murphy, K. M. *et al. Janeway Immunologie*. (Spektrum Akademischer Verlag, 2009).
- 103 Wood, R. W. On a Remarkable Case of Uneven Distribution of Light in a Diffraction Grating Spectrum. *Proceedings of the Physical Society of London* **18**, 269 (1902).
- 104 Wood, R. W. XXVII. Diffraction gratings with controlled groove form and abnormal distribution of intensity. *Philosophical Magazine Series 6* **23**, 310-317, doi:10.1080/14786440208637224 (1912).
- 105 Bohm, D. & Pines, D. A Collective Description of Electron Interactions. I. Magnetic Interactions. *Physical Review* **82**, 625-634 (1951).
- 106 Pines, D. & Bohm, D. A Collective Description of Electron Interactions: II. Individual Particle Aspects of the Interactions. *Physical Review* **85**, 338-353 (1952).
- 107 Bohm, D. & Pines, D. A Collective Description of Electron Interactions: III. Coulomb Interactions in a Degenerate Electron Gas. *Physical Review* **92**, 609-625 (1953).
- 108 Pines, D. A Collective Description of Electron Interactions: IV. Electron Interaction in Metals. *Physical Review* **92**, 626-636 (1953).
- 109 Powell, C. J. & Swan, J. B. Effect of Oxidation on the Characteristic Loss Spectra of Aluminum and Magnesium. *Physical Review* **118**, 640-643 (1960).
- 110 Otto, A. Excitation of nonradiative surface plasma waves in silver by the method of frustrated total reflection. *Z. Physik* **216**, 398-410, doi:10.1007/bf01391532 (1968).
- 111 Kretschmann, E. & Raether, H. Radiative decay of nonradiative surface plasmons excited by light. *Z. Naturforsch. A* **23**, 2135, doi:citeulike-article-id:3901347 (1968).
- 112 Kretschmann, E. Die Bestimmung optischer Konstanten von Metallen durch Anregung von Oberflächenplasmaschwingungen. *Z. Physik* **241**, 313-324, doi:10.1007/bf01395428 (1971).
- 113 Pockrand, I., Swalen, J. D., Gordon II, J. G. & Philpott, M. R. Surface plasmon spectroscopy of organic monolayer assemblies. *Surface Science* **74**, 237-244, doi:http://dx.doi.org/10.1016/0039-6028(78)90283-2 (1978).
- 114 Oh, B. K., Kim, Y. K., Park, K. W., Lee, W. H. & Choi, J. W. Surface plasmon resonance immunosensor for the detection of Salmonella typhimurium. *Biosensors & bioelectronics* **19**, 1497-1504, doi:10.1016/j.bios.2003.12.009 (2004).

- 115 Lofas, S. & Johnsson, B. A novel hydrogel matrix on gold surfaces in surface plasmon resonance sensors for fast and efficient covalent immobilization of ligands. *Journal of the Chemical Society, Chemical Communications*, 1526-1528, doi:10.1039/c39900001526 (1990).
- 116 Lofas, S. Dextran modified self-assembled monolayer surfaces for use in biointeraction analysis with surface plasmon resonance. *Pure and Applied Chemistry* **629**, 829-834, doi:citeulike-article-id:1281991 (1995).
- 117 Freeberg, B. photo contest. *High School Photo Winner's Showcase* (2011).
- 118 Akimoto, T., Sasaki, S., Ikebukuro, K. & Karube, I. Effect of incident angle of light on sensitivity and detection limit for layers of antibody with surface plasmon resonance spectroscopy. *Biosensors & bioelectronics* **15**, 355-362 (2000).
- 119 Quinn, J. G. *et al.* Development and Application of Surface Plasmon Resonance-Based Biosensors for the Detection of Cell-Ligand Interactions. *Analytical biochemistry* **281**, 135-143, doi:<http://dx.doi.org/10.1006/abio.2000.4564> (2000).
- 120 Andrade, C., Abdalla, D. S. P., Oliveira, M. D., Faulin, T. & Hering, V. *Biosensors for Detection of Low-Density Lipoprotein and Its Modified Forms*. (INTECH Open Access Publisher, 2011).
- 121 Johansson, A. S. *et al.* Physiochemical characterization of the Alzheimer's disease-related peptides A beta 1-42Arctic and A beta 1-42wt. *The FEBS journal* **273**, 2618-2630, doi:10.1111/j.1742-4658.2006.05263.x (2006).
- 122 Wood, S. J., Maleeff, B., Hart, T. & Wetzel, R. Physical, morphological and functional differences between ph 5.8 and 7.4 aggregates of the Alzheimer's amyloid peptide Abeta. *Journal of molecular biology* **256**, 870-877, doi:10.1006/jmbi.1996.0133 (1996).
- 123 Nagel-Steger, L. *et al.* Modulation of aggregate size- and shape-distributions of the amyloid-beta peptide by a designed beta-sheet breaker. *European biophysics journal : EBJ* **39**, 415-422, doi:10.1007/s00249-009-0416-2 (2010).
- 124 Karlsson, R., Katsamba, P. S., Nordin, H., Pol, E. & Myszka, D. G. Analyzing a kinetic titration series using affinity biosensors. *Analytical biochemistry* **349**, 136-147, doi:10.1016/j.ab.2005.09.034 (2006).
- 125 Amijee, H. *et al.* The N-methylated peptide SEN304 powerfully inhibits Abeta(1-42) toxicity by perturbing oligomer formation. *Biochemistry* **51**, 8338-8352, doi:10.1021/bi300415v (2012).
- 126 Green, N. M. Avidin. 1. The Use of (14-C)Biotin for Kinetic Studies and for Assay. *The Biochemical journal* **89**, 585-591 (1963).
- 127 Glück, J. M., Koenig, B. W. & Willbold, D. Nanodiscs allow the use of integral membrane proteins as analytes in surface plasmon resonance studies. *Analytical biochemistry* **408**, 46-52, doi:10.1016/j.ab.2010.08.028 (2011).
- 128 Dornieden, S. *et al.* Characterization of a single-chain variable fragment recognizing a linear epitope of abeta: a biotechnical tool for studies on Alzheimer's disease? *PLOS ONE* **8**, e59820, doi:10.1371/journal.pone.0059820 (2013).
- 129 Muller-Schiffmann, A. *et al.* Combining independent drug classes into superior, synergistically acting hybrid molecules. *Angewandte Chemie* **49**, 8743-8746, doi:10.1002/anie.201004437 (2010).
- 130 Ford, T., Graham, J. & Rickwood, D. Iodixanol: a nonionic iso-osmotic centrifugation medium for the formation of self-generated gradients. *Analytical biochemistry* **220**, 360-366, doi:10.1006/abio.1994.1350 (1994).
- 131 Stine, W. B., Jr. *et al.* The nanometer-scale structure of amyloid-beta visualized by atomic force microscopy. *Journal of protein chemistry* **15**, 193-203 (1996).
- 132 Cannon, M. J., Williams, A. D., Wetzel, R. & Myszka, D. G. Kinetic analysis of beta-amyloid fibril elongation. *Analytical biochemistry* **328**, 67-75, doi:10.1016/j.ab.2004.01.014 (2004).

- 133 GE-Healthcare. Biacore T200 Software Handbook. *GE Healthcare Bio-Sciences AB* (2010).
- 134 Instruments, M. A Basic Guide to Particle Characterization. *Malvern Instruments Limited Manual* (2012).
- 135 Holliger, P., Prospero, T. & Winter, G. "Diabodies": small bivalent and bispecific antibody fragments. *Proceedings of the National Academy of Sciences of the United States of America* **90**, 6444-6448 (1993).
- 136 Rezai, T., Yu, B., Millhauser, G. L., Jacobson, M. P. & Lokey, R. S. Testing the conformational hypothesis of passive membrane permeability using synthetic cyclic peptide diastereomers. *Journal of the American Chemical Society* **128**, 2510-2511, doi:10.1021/ja0563455 (2006).
- 137 Brooks, H., Lebleu, B. & Vives, E. Tat peptide-mediated cellular delivery: back to basics. *Advanced drug delivery reviews* **57**, 559-577, doi:10.1016/j.addr.2004.12.001 (2005).
- 138 Salomone, F. *et al.* A novel chimeric cell-penetrating peptide with membrane-disruptive properties for efficient endosomal escape. *Journal of controlled release : official journal of the Controlled Release Society* **163**, 293-303, doi:10.1016/j.jconrel.2012.09.019 (2012).
- 139 Sun, D., Forsman, J., Lund, M. & Woodward, C. E. Effect of arginine-rich cell penetrating peptides on membrane pore formation and life-times: a molecular simulation study. *Physical chemistry chemical physics : PCCP* **16**, 20785-20795, doi:10.1039/c4cp02211d (2014).
- 140 Vives, E., Brodin, P. & Lebleu, B. A truncated HIV-1 Tat protein basic domain rapidly translocates through the plasma membrane and accumulates in the cell nucleus. *The Journal of biological chemistry* **272**, 16010-16017 (1997).
- 141 Liu, H., Funke, S. A. & Willbold, D. Transport of Alzheimer disease amyloid-beta-binding D-amino acid peptides across an in vitro blood-brain barrier model. *Rejuvenation research* **13**, 210-213, doi:10.1089/rej.2009.0926 (2010).
- 142 van Groen, T., Kadish, I., Funke, S. A., Bartnik, D. & Willbold, D. Treatment with D3 removes amyloid deposits, reduces inflammation, and improves cognition in aged AbetaPP/PS1 double transgenic mice. *Journal of Alzheimer's disease : JAD* **34**, 609-620, doi:10.3233/JAD-121792 (2013).
- 143 Alavijeh, M. S., Chishty, M., Qaiser, M. Z. & Palmer, A. M. Drug metabolism and pharmacokinetics, the blood-brain barrier, and central nervous system drug discovery. *NeuroRx : the journal of the American Society for Experimental NeuroTherapeutics* **2**, 554-571, doi:10.1602/neurorx.2.4.554 (2005).
- 144 Trent, A., Marullo, R., Lin, B., Black, M. & Tirrell, M. Structural properties of soluble peptide amphiphile micelles. *Soft Matter* **7**, 9572-9582, doi:10.1039/c1sm05862b (2011).
- 145 Pollaro, L. & Heinis, C. Strategies to prolong the plasma residence time of peptide drugs. *MedChemComm* **1**, 319-324, doi:10.1039/c0md00111b (2010).
- 146 Dennis, M. S. *et al.* Albumin binding as a general strategy for improving the pharmacokinetics of proteins. *The Journal of biological chemistry* **277**, 35035-35043, doi:10.1074/jbc.M205854200 (2002).
- 147 Taylor, M. *et al.* Development of a proteolytically stable retro-inverso peptide inhibitor of beta-amyloid oligomerization as a potential novel treatment for Alzheimer's disease. *Biochemistry* **49**, 3261-3272, doi:10.1021/bi100144m (2010).

9. Supporting Information

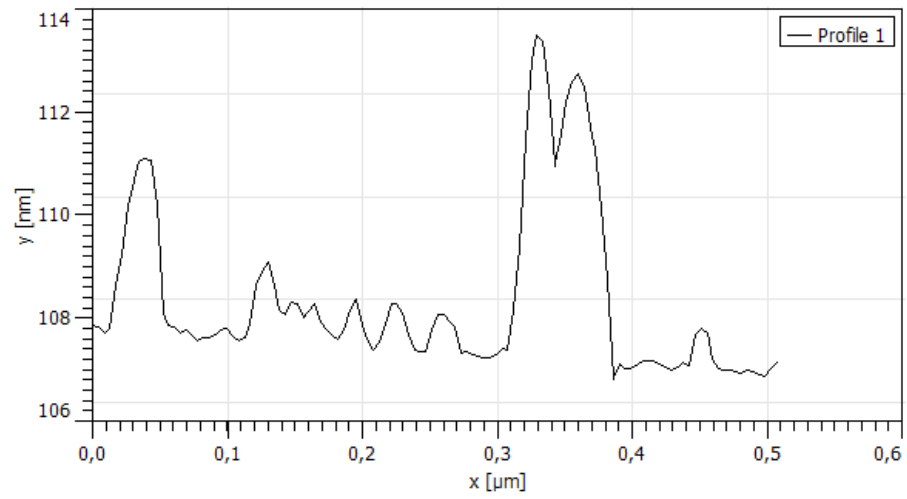
Table S1: Comprehension of the binding kinetics. k_a : binding velocity in Ms^{-1} , k_d : dissociation velocity in s^{-1} , K_D : k_d/k_a in M, R_{max} : Maximum response at equilibrium, χ^2 : Error of the fit.

	k_{a1}	k_{d1}	k_{a2}	k_{d2}	K_{D1}	K_{D2}	$R_{\text{max}1}$	$R_{\text{max}2}$	χ^2
cD3a - F	1.3×10^6	2.3×10^{-1}	1.6×10^5	2.0×10^0	1.3×10^{-5}	1.8×10^{-7}	75.8	12.3	0.5
cD3a - M	5.5×10^4	2.4×10^0	2.3×10^5	3.7×10^{-1}	4.3×10^{-5}	1.7×10^{-6}	161.8	58.9	13.6
cD3p - F	7.3×10^4	2.0×10^0	3.3×10^5	6.8×10^{-2}	2.8×10^{-5}	2.0×10^{-7}	88.2	8.6	2
cD3p - M	4.6×10^4	2.1×10^0	2.0×10^5	3.5×10^{-1}	4.7×10^{-5}	1.8×10^{-6}	159.8	57.9	4.7
cD3p - O	3.0×10^4	1.8×10^0	1.7×10^4	2.6×10^{-2}	6.1×10^{-5}	1.6×10^{-6}	38	3.8	0.3
cD3p2k - F	7.7×10^4	1.3×10^0	1.2×10^6	4.3×10^{-4}	1.7×10^{-5}	3.4×10^{-10}	109.1	13.5	11.5
cD3p2k - M	2.3×10^4	1.1×10^0	6.7×10^7	1.4×10^2	4.7×10^{-5}	2.1×10^{-6}	168.8	33.2	6.9
cD3p2k - O	1.2×10^4	6.3×10^{-1}	4.7×10^9	1.0×10^4	5.1×10^{-5}	2.2×10^{-6}	42.9	7.2	1.4
cD3r - F	3.5×10^4	2.3×10^{-4}	6.9×10^4	1.1×10^0	1.6×10^{-5}	6.8×10^{-9}	120.6	34	14.8
cD3r - M	5.9×10^2	2.9×10^{-4}	2.0×10^5	6.2×10^{-1}	3.0×10^{-6}	4.9×10^{-7}	168.7	53	60.7
cD3r - O	3.1×10^4	6.8×10^{-1}	2.5×10^4	1.5×10^{-3}	2.2×10^{-5}	6.1×10^{-8}	51	9.1	2.2
cD3z - F	1.1×10^4	5.6×10^{-1}	2.0×10^6	3.9×10^0	5.2×10^{-5}	1.9×10^{-6}	28.7	77.7	4
cD3z - M	4.2×10^4	1.8×10^0	1.5×10^5	2.3×10^{-1}	4.4×10^{-5}	1.6×10^{-6}	68.2	138.3	34.6
cD3z - O	8.4×10^5	3.0×10^0	1.1×10^4	6.9×10^{-1}	6.5×10^{-5}	3.5×10^{-6}	39.7	7.5	0.9
D3D3 - F	7.4×10^4	4.4×10^{-2}	5.9×10^5	1.3×10^{-3}	5.9×10^{-7}	2.2×10^{-9}	55.4	20.4	2.9
D3D3 - M	5.3×10^5	1.5×10^{-4}	4.8×10^4	6.2×10^{-2}	1.3×10^{-6}	2.8×10^{-10}	233.8	35.6	32.2
D3D3 - O	7.0×10^4	9.6×10^{-2}	5.5×10^8	4.9×10^{-2}	1.4×10^{-6}	8.9×10^{-11}	184.6	42.1	25.3
D3 - F	1.4×10^5	1.8×10^{-2}	2.0×10^5	6.6×10^{-1}	3.3×10^{-6}	1.3×10^{-7}	114.2	23.3	1.5
D3 - M	6.2×10^4	3.6×10^{-3}	1.1×10^7	2.3×10^2	2.1×10^{-5}	5.8×10^{-8}	82.1	3.4	0.5
D3 - O	3.0×10^4	4.1×10^{-1}	1.1×10^7	1.3×10^1	1.4×10^{-5}	1.2×10^{-6}	50.3	10.9	0.6
D7 - F	2.1×10^8	2.2×10^2	1.6×10^3	2.2×10^{-4}	1.1×10^{-6}	1.4×10^{-7}	53.3	44.5	2.7
D7 - M	1.0×10^5	9.3×10^{-3}	2.4×10^3	3.6×10^{-4}	1.5×10^{-7}	9.3×10^{-8}	37.4	27.5	1.3
D7 - O	6.6×10^4	1.5×10^{-2}	4.5×10^3	4.0×10^{-4}	2.3×10^{-7}	8.9×10^{-8}	14.7	19.2	0.5
DB4 - F	1.7×10^4	3.9×10^{-1}	1.7×10^4	1.2×10^{-4}	2.2×10^{-5}	7.1×10^{-9}	68.4	3.5	2.4
DB4 - M	1.5×10^4	1.6×10^0	9.9×10^3	2.9×10^{-3}	1.1×10^{-4}	3.0×10^{-7}	165.1	2.5	0.4
DB4 - O	3.6×10^4	3.0×10^0	7.4×10^3	6.8×10^{-4}	8.2×10^{-5}	9.2×10^{-8}	111.5	2.9	0.3
RD2 - F	9.2×10^4	2.9×10^{-1}	8.9×10^4	1.7×10^{-3}	3.2×10^{-6}	1.9×10^{-8}	131	19.4	6.9
RD2 - M	2.9×10^4	1.4×10^{-1}	5.6×10^4	6.2×10^{-4}	4.8×10^{-6}	1.1×10^{-8}	124.7	15.4	4
RD2 - O	8.0×10^4	8.2×10^{-4}	2.9×10^4	1.1×10^{-1}	3.7×10^{-6}	1.0×10^{-8}	104.6	15.9	4.4
RD2RD2 - F	3.0×10^4	3.3×10^{-2}	1.9×10^5	1.6×10^{-3}	1.1×10^{-6}	8.4×10^{-9}	180.1	76.4	35.3
RD2RD2 - M	3.8×10^5	2.8×10^{-3}	4.4×10^4	3.8×10^{-2}	8.7×10^{-7}	7.3×10^{-9}	157.7	33.9	21.8
RD2RD2 - O	5.0×10^4	4.6×10^{-2}	4.7×10^5	3.5×10^{-3}	9.3×10^{-7}	7.5×10^{-9}	100	17.4	7.7
D3RD2 - M	3.9×10^4	7.6×10^{-2}	1.5×10^6	1.2×10^{-3}	1.9×10^{-6}	8.1×10^{-10}	105	8	8.5
D3RD2 - O	3.7×10^5	8.3×10^{-4}	4.2×10^4	7.2×10^{-2}	2.3×10^{-9}	1.7×10^{-6}	13.5	127.5	7.7
RD2D3 - M	6.0×10^8	3.7×10^{-1}	4.3×10^4	6.1×10^{-2}	6.2×10^{-10}	1.4×10^{-6}	13.6	92.8	14.3
RD2D3 - O	4.2×10^4	4.7×10^{-2}	6.0×10^5	8.8×10^{-4}	1.1×10^{-6}	1.5×10^{-9}	113.9	17.4	10.7

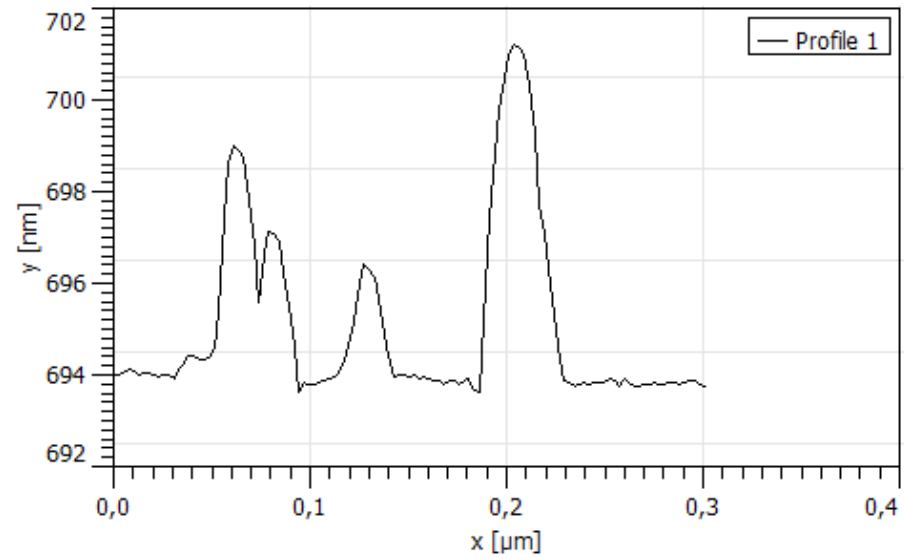
Table S1: Comprehension of the binding kinetics. k_a : binding velocity in Ms^{-1} , k_d : dissociation velocity in s^{-1} , K_D : k_d/k_a in M, R_{max} : Maximum response at equilibrium, χ^2 : Error of the fit.

	k_{a1}	k_{d1}	K_{D1}	$R_{\text{max}1}$	χ^2
D7RD2 - M	$6.70 \cdot 10^5$	$3.90 \cdot 10^{-2}$	$5.90 \cdot 10^{-8}$	241	62.5
D7RD2 - O	$3.90 \cdot 10^3$	$1.60 \cdot 10^{-4}$	$4.20 \cdot 10^{-8}$	360	39.9
D7RD2 - F	$1.50 \cdot 10^4$	$5.10 \cdot 10^{-4}$	$3.40 \cdot 10^{-8}$	212	330
RD2D7 - M	$1.20 \cdot 10^5$	$5.30 \cdot 10^{-5}$	$4.50 \cdot 10^{-10}$	125	46.5
RD2D7 - O	$4.20 \cdot 10^3$	$3.60 \cdot 10^{-3}$	$8.40 \cdot 10^{-7}$	176	26.7
RD2D7 - F	$1.40 \cdot 10^5$	$1.40 \cdot 10^{-7}$	$1.00 \cdot 10^{-12}$	170	111
	k_{a2}	k_{d2}	K_{D2}	$R_{\text{max}2}$	
D7RD2 - M	$5.90 \cdot 10^3$	$1.80 \cdot 10^{-4}$	$3.00 \cdot 10^{-8}$	442	
D7RD2 - O	$1.20 \cdot 10^5$	$1.10 \cdot 10^{-2}$	$8.80 \cdot 10^{-8}$	219	
D7RD2 - F	$1.50 \cdot 10^4$	$5.40 \cdot 10^{-7}$	$3.60 \cdot 10^{-11}$	172	
RD2D7 - M	$5.90 \cdot 10^3$	$3.10 \cdot 10^{-3}$	$5.30 \cdot 10^{-7}$	219	
RD2D7 - O	$9.30 \cdot 10^4$	$1.10 \cdot 10^{-4}$	$1.10 \cdot 10^{-9}$	96	
RD2D7 - F	$2.70 \cdot 10^3$	$2.20 \cdot 10^{-3}$	$8.30 \cdot 10^{-7}$	190	
	k_{a3}	k_{d3}	K_{D3}	$R_{\text{max}3}$	
D7RD2 - M	$2.00 \cdot 10^4$	$1.40 \cdot 10^{-1}$	$7.00 \cdot 10^{-6}$	508	
D7RD2 - O	$7.80 \cdot 10^3$	$1.80 \cdot 10^{-1}$	$2.30 \cdot 10^{-5}$	607	
D7RD2 - F	$4.30 \cdot 10^3$	$1.30 \cdot 10^{-2}$	$3.00 \cdot 10^{-6}$	463	
RD2D7 - M	$3.90 \cdot 10^4$	$5.70 \cdot 10^{-2}$	$1.50 \cdot 10^{-6}$	377	
RD2D7 - O	$3.10 \cdot 10^4$	$5.70 \cdot 10^{-2}$	$1.80 \cdot 10^{-6}$	279	
RD2D7 - F	$7.30 \cdot 10^3$	$2.10 \cdot 10^{-2}$	$2.90 \cdot 10^{-6}$	367	

A



B



C

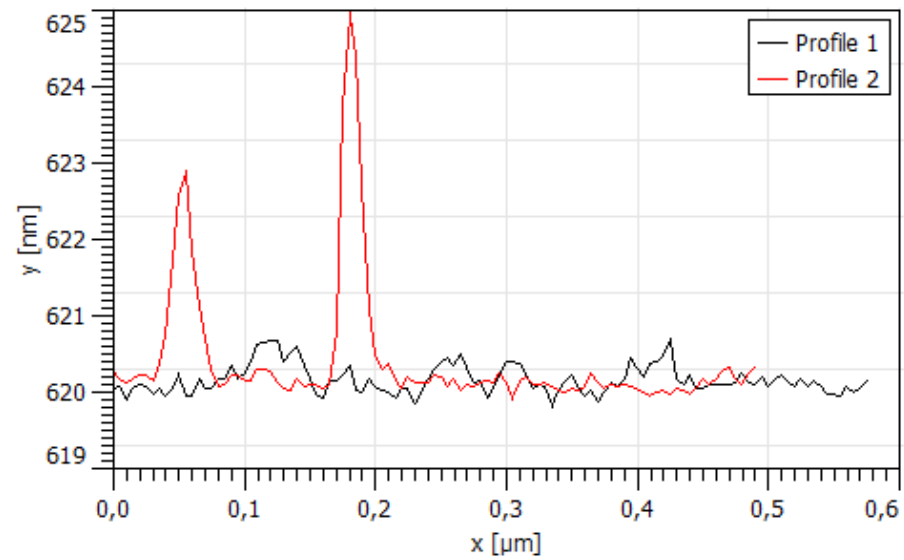


Figure S1: Height plots of the A β fibrils from Fig. R3. A), B), C) corresponds to Fig. R3 A), B) and C).

Publications and presentations

Accepted papers:

- i. Kinetic Titration Series with Biolayer Interferometry. Daniel Frenzel, Dieter Willbold. PLOS ONE
- ii. Immobilization of Homogeneous Monomeric, Oligomeric and Fibrillar A β Species for Reliable SPR Measurements. Daniel Frenzel and Julian M. Glück, Oleksandr Brener, Philipp Oesterhelt, Luitgard Nagel-Steger, Dieter Willbold. PLOS ONE
- iii. Amyloid aggregation inhibitory mechanism of arginine-rich D-peptides. O. Olubiyi, D. Frenzel, D. Bartnik, J.M. Glück, O. Brener, L. Nagel-Steger, S.A. Funke, D. Willbold and B. Strodel. Curr. Med. Chem.

Poster presentations:

- i. Design and development of an SPR-assay that quantifies the interaction of various abeta-binding agents with abeta monomers, oligomers and fibrils. 12th Symposium on Alzheimer Therapy in Stockholm

Danksagung

Ich möchte in erster Linie Dieter Willbold für die Bereitstellung des Projekts, die fachliche Hilfestellung, die hervorragende Laborausstattung und vor allem für seine Unterstützung und Geduld bei der Verfassung der Publikationen danken.

Weiterhin möchte ich Julian Glück für seine Unterstützung bei der Planung und Durchführung der Experimente, seiner Hilfe beim Anfertigen der ersten Publikation und für seine motivierenden Ansprachen während der Einlernphase danken.

Außerdem gebührt Max Michel mein Dank. Er konnte mir nicht nur bei Fragen zum Thema Proteinaufreinigung hilfreich zur Seite stehen, auch hat er sich hingebungsvoll um die Flüssigchromatographie gekümmert. Das hat sehr vielen Mitarbeitern die Versuche gerettet.

Nicht zuletzt möchte ich mich bei Andrew Dingley bedanken, der vermutlich viele Stunde für das Korrekturlesen aufgeopfert hat, um die Arbeit zu verbessern.

Zuletzt möchte ich mich bei meinen Eltern bedanken, die immer an mich geglaubt haben. Ob zu Recht, weiß ich leider noch nicht.

Eidesstattliche Erklärung

Ich erkläre hiermit, diese Arbeit selbstständig angefertigt zu haben. Es wurden nur die in der Arbeit benannten Quellen und Hilfsmittel benutzt. Wörtlich oder sinngemäß übernommenen Gedanken habe ich als solches kenntlich gemacht.

Datum, Ort

Unterschrift

Curriculum vitae

Daniel Frenzel

Husarenstr. 9
69121 Heidelberg, Germany
Mobile: 0176-81646678
Mail: dgdanielf@gmail.com



Personal information

Date of birth:	30.08.1987
Nationality	German

Education

11/2011 - 12/2014 Forschungszentrum Jülich	PhD Thesis: Optimization and characterization of D-peptides for treatment of Alzheimer's disease
10/2009 - 10/2011 University of Bayreuth	Master - Biochemistry and Molecular Biology Thesis: „Mitochondrial dynamics and cytotoxicity in a yeast model for amyotrophic lateral sclerosis“
10/2006 - 09/2009 University of Bayreuth	Bachelor – Biology Thesis: “Does increased production of FtsH enhance the sporulation frequency”
08/1998 - 07/2006 Martin-Rinckart-Gymnasium	Grammar school

Internships

09/2010 - 11/2010 University of Bayreuth	Microinjections of „Chromosomal Passenger Complex“-components in <i>Xenopus laevis</i> stage VI oocytes
08/2008 - 09/2008 Paul-Gerhardt-Stift Lutherstadt Wittenberg	Microbial evaluation of blood cultures
04/2008 – 08/2009 Chair for applied informatics IV University of Bayreuth	Application development with Qt4 and OpenGL in C++

Skills:

Cell biology:	Molecular Cloning, Cell Culture, Microinjections, <i>E. coli</i> , <i>B. subtilis</i> , <i>S. cerevisiae</i> , SH-SY5Y, HEK, HeLA, Autoradiography, FACS
Biochemistry:	Protein Purification, Liquid Chromatography, Immunohistochemistry, DNA-Chips, PCR, Sequencing, Immunohistochemistry, <i>In-vitro</i> Translation, (Mirror Image) Phage Display
Biophysics:	Surface-Plasmon-Resonance-Spectroscopy (SPR), Thermophoresis, Biolayer Interferometry (BLI), ITC
Microscopy:	Atomic force microscopy (AFM), Fluorescence microscopy (+confocal, +tiff), Transmission electron microscopy (TEM)

IT-Skills:

Programming languages:	C/C++, CUDA
Scripting languages:	Python, Bash, JavaScript, HTML
Operating systems:	Linux (Debian/OpenSuse), Windows
Toolkits:	GUI-design with Qt3/4/5, GTK and wxWidgets, Parallelization with OpenMP, Image analysis with OpenCV, CMake
Misc.:	MS Office, LibreOffice and Graphpad, SQL, JSON

Publications and Conferences:

PLOS ONE:	Immobilization of homogeneous monomeric, oligomeric and fibrillar A β species for reliable SPR measurements
PLOS ONE:	Kinetic titration series with biolayer interferometry
Current Medicinal Chemistry:	Amyloid aggregation inhibitory mechanism of arginine-rich D-peptides.
12 th Symposium on Alzheimer Therapy Stockholm	„Design and development of an SPR-assay that quantifies the interaction of various abeta-binding agents with abeta monomers, oligomers and fibrils.“
Book review, Packt Publishing	„Mastering Beaglebone Robotics“

Projects:

C++-Library:	ANNetGPGPU - Neural network library with GPU support code.google.com/p/annetgpgpu
Linux/Arduino/Embedded:	RPiCopter – Firmware for controlling quadcopters via WiFi/3G (AP based on Debian): code.google.com/p/rpicopter Experiences with Arduino based hardware (ATMega), Linux kernel driver development: github.com/BeaglePilot/BeagleBone-Black-MS5611-Driver

Languages and Certificates:

Fluent:	English
Native:	German
Graduate school certificates:	Dealing with Intercultural Challenges, Projektleiterkurs nach § 15 Abs. 2 S. 1 Nr. 3 GenTS, Leadership skills

aus dem Institut für
der Heinrich-Heine-Universität Düsseldorf

Gedruckt mit der Genehmigung der
Mathematisch-Naturwissenschaftlichen Fakultät der
Heinrich-Heine-Universität Düsseldorf

Referent: Dieter Willbold

Korreferent(en): Georg Groth

Tag der mündlichen Prüfung: 16.12.2014